Analyzing reproductive growth dynamics of greenhouse-grown strawberries based on environment and eco-physiological functions

小野, 信太朗

KYUSHU UNIVERSITY

Analyzing reproductive growth dynamics of greenhouse-grown strawberries based on environment and eco-physiological functions

Doctor Thesis by

Shintaro Ono

The Laboratory of Agricultural Meteorology,

Bioproduction Environmental Sciences,

Agro-environmental Sciences,

Graduate School of Bioresource and Bioenvironmental Sciences,

Kyushu University

December 2023

Contents

Preface

Background

The strawberry (*Fragaria* × *ananassa* Duch.) is a widely cultivated horticultural crop in temperate, subtropical, and Mediterranean climates (Menzel, 2021), and currently, strawberry plants are predominantly cultivated in the greenhouse (Neri *et al*., 2012; Samtani *et al*., 2019), where various environmental control technologies have been developed to achieve high yield (Lu *et al*., 2015) with a focus on enhancing photosynthetic rate, which is an essential physiological function of crops closely linked to yield (Long *et al*., 2006). For example, Hidaka *et al*. (2016) reported that supplemental lighting with elevated CO_2 concentration and temperature accelerated flowering and resulted in significant increase in fruit yield. Furthermore, in recent years, new technologies, which also focus on reducing energy consumption, have been reported (Yoneda *et al*., 2020; Hidaka *et al*., 2022). For more accurate utilization of these technologies, the establishment of predictive tools for reproductive growth dynamics throughout the cultivation period is required.

While many row crops and vegetable crops are typically harvested once at the end of the growing season, strawberry fruits are usually harvested every 3 to 4 days. Furthermore, considering that there are multiple high yield waves occurring throughout cultivation period (MacKenzie and Chandler, 2009) and that the unit price fluctuates significantly depending on the timing (Wu *et al*., 2015), the significance of reproductive growth dynamics prediction for environmental control and consequently the optimization of yield is substantial. In light of these situations, statistical predictive models based on correlations with environmental conditions (Lobell *et al*., 2006; Pathak *et al*., 2016) and machine learning (Khoshnevisan *et al*., 2014) have been developed and reported. However, the reproductive growth dynamics of strawberries involves many eco-physiological functions (*e.g*., the relationship between fruit growth and the

rate of translocation of photosynthetic products from leaves to fruits as reported by Hidaka *et al*., 2019). Consequently, it is necessary to consider not only environment but also eco-physiological functions to construct a more universal and accurate predictive model for reproductive growth dynamics, while such examples are currently lacking.

Objectives and summary of this thesis

In this thesis, the objective is to analyze the reproductive growth dynamics (*i.e*., flowering and harvest after fruit maturation) in greenhouse-grown strawberries, based on not only environment but also eco-physiological functions (such as photosynthesis). To achieve this, I addressed the following three matters. Summary is presented in Fig. P.1.

In chapter 1, As measuring photosynthetic rate throughout the cultivation period was not practical, I investigated whether leaf photosynthetic rate was limited by environmental stresses on sunny days for more accurately estimating photosynthetic rate of greenhouse-grown strawberries. Furthermore, the diurnal variations in the factors of photosynthesis reduction were analyzed, considering the changes in greenhouse environmental conditions and leaf water potential from sunrise to sunset. The content of this chapter was published as Yokoyama and Ono *et al*. (2023 co-first) in *Photosynthetica*.

In chapter 2, I hypothesized that cumulative photosynthetic rate, which combines information on multiple environmental factors and eco-physiological functions, could be more useful as an index for predicting days from flowering to harvesting compared to cumulative light intensity and temperature, which have been conventionally used for indices. To test this, I measured the daily environmental conditions and dates of reproductive growth events of approximately 2,700 fruits (*e.g*., flowering, fruit set, and harvesting). Additionally, building upon the results from chapter 1, I estimated the photosynthetic rate while considering limitation by environmental stresses. Finally, the variability of cumulative values among each index from

flowering to harvesting were statistically compared. The content of this chapter was published as Ono *et al*. (2023) in *The Journal of Horticultural Science and Biotechnology*.

In chapter 3, I analyzed the relationship between daily flowering dynamics of the first inflorescence, which directly correlates with harvesting dynamics during the most lucrative period, and the history of environmental factors and leaf photosynthetic rate. To conduct these, I daily obtained the environments inside the greenhouse, photosynthetic rate, and flowering dynamics throughout the three cultivation periods. The content of this chapter is currently being prepared for submission.

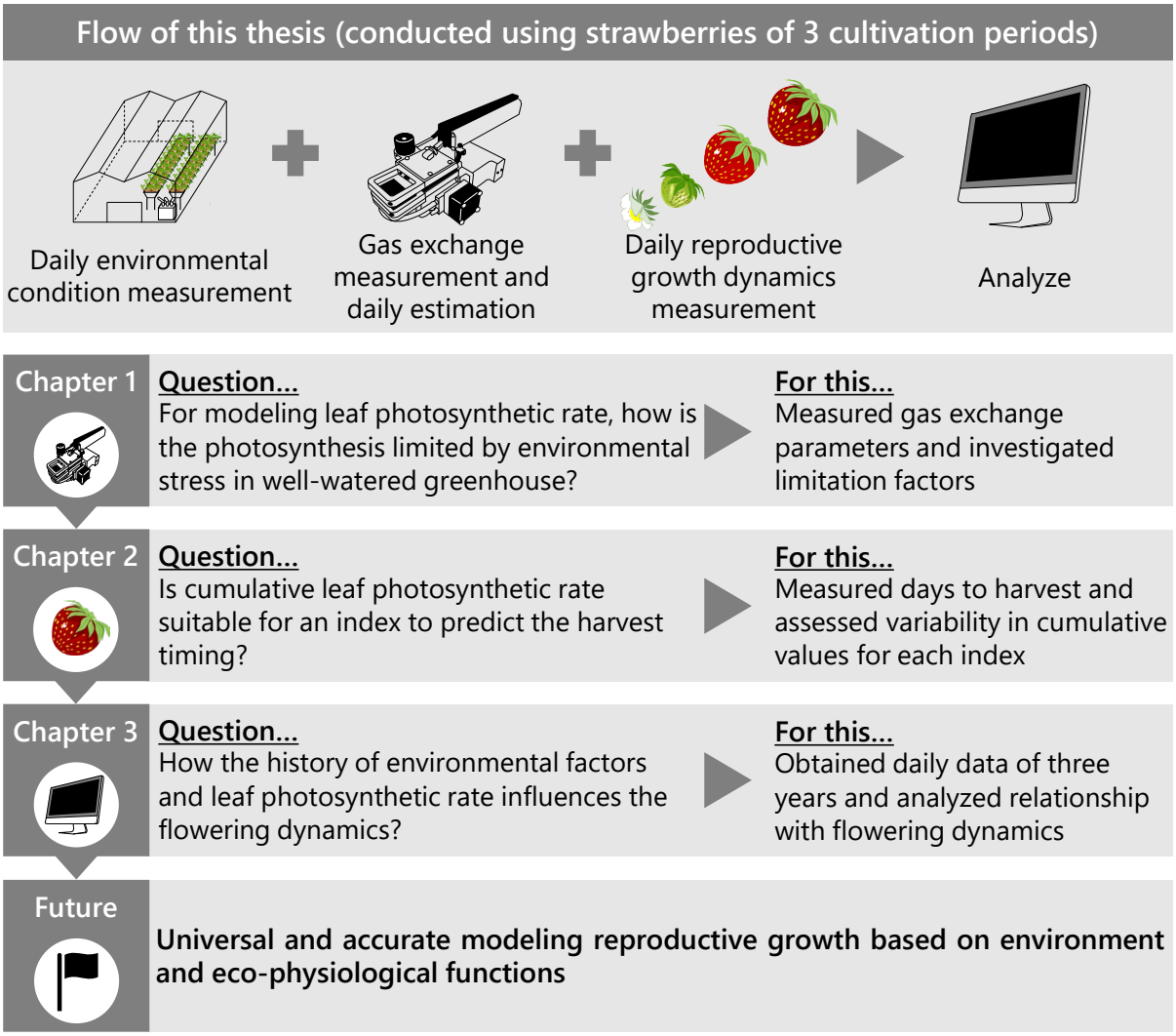

Figure P.1 Schematic diagram of summary of this study.

Chapter 1

For modeling leaf photosynthetic rate, how is the photosynthesis limited by environmental stress in well-watered greenhouse?

1.1. Introduction

On sunny days, plants actively engage in photosynthesis; however, despite sufficient solar radiation, the photosynthetic rate often decreases around midday. Under strong solar radiation, a decrease in photosynthetic rate around midday, known as midday depression of photosynthesis (hereafter midday depression), is frequently observed (Roessler and Monson 1985; Raschke and Resemann 1986; Ayari *et al*., 2000; Muraoka *et al*., 2000; Pelletier *et al*., 2016). Notably, identifying the environmental factors limiting the photosynthetic rate is essential for preventing crop yield loss caused by a decrease in photosynthesis.

Owing to the high solar heat load, environmental conditions in greenhouse often become unfavorable for photosynthesis, especially on sunny days in warmer climate regions (He *et al*., 2007; López *et al*., 2012). As the photosynthetic process consists of diffusion of CO_2 from the atmosphere to the carboxylation site, which was thought to be largely regulated by stomatal functioning and activity of biochemical process at the carboxylation site (Wilson *et al*., 2000), the regulation of photosynthesis by environmental factors has been investigated in greenhouse-grown crops in relation to stomatal and biochemical limitations (Ayari *et al*., 2000; Fan *et al*., 2010; Yuan *et al*., 2016; Rodrigues *et al*., 2018; Sarabi *et al*., 2019). Common environmental stresses in greenhouse agriculture include high light and temperature stresses, which inhibit the activity of photosynthetic enzymes and electron transport chains and induce biochemical limitations (He *et al*., 2007; Hu *et al*., 2009; Fan *et al*., 2010; Szymańska *et al*.,

2017; Lu *et al*., 2017). Although high light and temperature conditions are the primary contributors to biochemical limitations, they can indirectly increase stomatal limitation. The transpiration rate is elevated under high light and temperature conditions to suppress an increase in leaf temperature. If water uptake from the roots is insufficient to compensate for water loss via transpiration, plants close their stomata to prevent further water loss (Robinson and Bower 1988). In addition, an increase in temperature results in an elevated vapor pressure deficit (*VPD*), which increases stomatal limitation by inducing stomatal closure (Lu *et al*., 2015; Zhang *et al*., 2015, Yuan *et al*., 2016). Depending on stress severity, water stress increases stomatal and non-stomatal limitations. Under mild water stress conditions, stomatal limitation is the predominant factor for the decrease in photosynthetic rate, whereas non-stomatal limitation increases under severe water stress conditions (Yuan *et al*., 2016; Song *et al*., 2020). These studies showed that different photosynthetic limitations (*e.g.,* stomatal or biochemical limitations) regulate photosynthesis depending on the environmental conditions. As the environmental conditions inside the greenhouse change dynamically throughout the day, photosynthetic limiting factors would also change throughout the day. Moreover, rather than a single physiological factor, multiple concurrently operating factors can limit the photosynthetic rate. Therefore, to understand how environmental factors limit the photosynthetic rate, diurnal changes in the relative proportions of photosynthetic limitation factors require evaluation.

Quantitative limitation analysis, which was proposed by Jones (1985) and further extended by Wilson *et al*., (2000) and Grassi and Magnani (2005), is one of the common methods for investigating dynamic changes in photosynthetic limitations. Traditionally, the constraints imposed by environmental stress on photosynthesis have been analyzed in terms of stomatal and biochemical limitation (*i.e.,* maximum carboxylation rate) (Wilson *et al*., 2000), whereas Grassi and Magnani (2005) showed the importance of including mesophyll conductance in the analysis. Since then, quantitative limitation analysis has often been used under field conditions to examine the changes in relative proportions of photosynthetic

limitations (*i.e.,* stomatal, mesophyll, and biochemical limitations) under limited soil–water conditions over relatively long periods (Grassi and Magnani 2005; Galle *et al*., 2009; Grassi *et al*., 2009; Flexas *et al*., 2009; Egea *et al*., 2011; Zhu *et al*., 2021). However, this quantitative analysis was infrequently used to examine greenhouse-grown horticultural crops (Chen *et al*., 2014; Zhang *et al*., 2021). Because the environmental conditions inside a greenhouse differ from those outside in the field, changes in photosynthetic limitations and their proportion to reductions in photosynthetic rate would differ from previous field-based studies conducted under water stress. For example, Grassi *et al*. (2009) reported that diffusional limitation (*i.e.,* stomatal and mesophyll limitations) was the dominant limiting factor for photosynthesis under water stress conditions, whereas the proportion of biochemical limitation was higher when water stress was less severe. Because greenhouse-grown horticultural crops are generally well-watered, biochemical limitation would play a greater role in the photosynthetic regulation of greenhouse-grown crops than it would in studies conducted under water stress.

In this chapter, I examined how different photosynthetic limitations (*i.e.,* stomatal, mesophyll, and biochemical limitations) regulate leaf photosynthetic rate in response to diurnal changes under greenhouse environment conditions. I hypothesized that diffusional limitations (*i.e.,* stomatal and mesophyll) have a relatively smaller proportion than biochemical limitations in well-watered greenhouse-grown strawberry. To achieve this, the gas exchange and chlorophyll fluorescence of greenhouse-grown strawberries were measured on a diurnal scale for three days under varying environmental conditions, followed by quantitative limitation analysis to evaluate the diurnal changes in photosynthetic limitations.

1.2. Materials and methods

1.2.1. Plant materials and growth conditions

Strawberry nurseries (*Fragaria* × *ananassa* Duch. cv. Fukuoka S6) were grown in a greenhouse (37 m long × 9 m wide × 4.5 m high) located at the National Agricultural and Food Research Organization (Kyushu Okinawa Agricultural Research Center, Japan; 33°18.4′ N, 130°32.8′ E). The nurseries, which were selected from mother stocks, were planted in plastic pots filled with a 3:5:2 (v:v:v) mixture of peat moss, coconut shell, and charcoal on June 11, 2020. A nutrient solution (OK F-1, OAT Agrio Co., Ltd., Tokyo, Japan; electrical conductivity = 0.6 dS m^{-1}) was supplied at a rate of 300 mL d^{-1} / plant at 9:00, 11:00, 13:00, 15:00, and 17:00 each day. To induce anthesis, nutrient supplementation was stopped between mid-August and mid-September; thus, only water was supplied during this period. Flower buds differentiated on the first inflorescence until mid-September, and other growth conditions were set as described by Hidaka *et al*., (2019). On October 1, 2020, 288 plants were transplanted on cultivation beds (15 m long × 30 cm wide × 80 cm high) and filled with the culture soil (Good Soil, Kaneya Co., Ltd., Aichi, Japan) in a greenhouse (20 m long × 8 m wide × 4 m high) located at Ito Plant Experiment Fields & Facilities, Faculty of Agriculture, Kyushu University, Fukuoka, Japan (33°35.5′ N, 130°12.9′ E), with 20 cm intervals between plants and inter-row spacing of 15 cm (Fig. 1.1). The plants were supplied with a nutrient solution (same as that described above) at a rate of 200 to 300 mL d^{-1}/plant depending on the temperature inside the greenhouse, at 1-h intervals during daytime (6:00–18:00). The greenhouse was equipped with an oil heater (HK2027TEV, NEPON Inc., Tokyo, Japan) and a ventilation system comprising roof and side-wall windows to keep the temperature between 8°C and 22°C. In addition, to prevent excessive high temperature and drying inside the greenhouse, the fine mist cooling system (the mist nozzle diameter, 0.15 mm; dynamic injection pump flow rate, 1.5 L min^{-1}; Green.com Inc., Tokyo, Japan) was operated for 2 min at 15-min intervals from 10:00 to 16:00 only on sunny

days. Flowers were pollinated by bees.

Inside the greenhouse, the environmental conditions such as photosynthetic photon flux density (PPFD), temperature (T_a), and relative humidity (*RH*) were measured using a quantum sensor (PAR-02D, Prede Co., Ltd., Tokyo, Japan) and temperature/humidity sensor (HMP60, Vaisala, Helsinki, Finland), respectively. A single set of meteorological sensors was placed around the center of the greenhouse between plant rows at a height of 1.2 m (near the canopy top; Fig. 1.1). Data were measured at 5-s intervals, and 10-min means were logged in a programmable data logger (CR-1000, Campbell Scientific Inc., Logan, USA). The vapor pressure deficit (*VPD*) inside the greenhouse was calculated from T_a and *RH*. In addition, the outside solar radiation (*I*) at the same interval was obtained from a meteorological station (pyranometer: CHF-SE20-JM, Climatec Inc., Tokyo, Japan) located about 120 m away from the greenhouse used in the experiment.

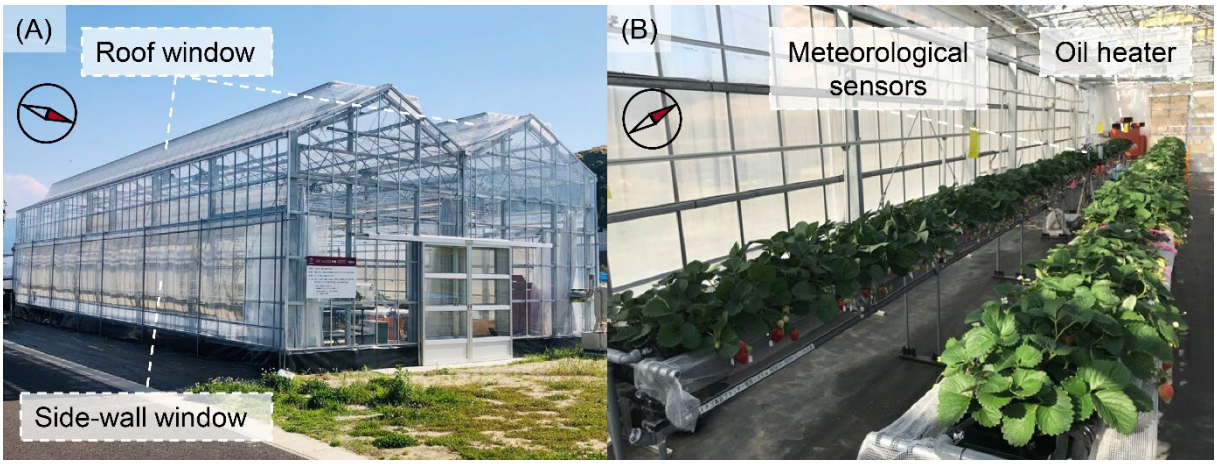

Figure 1.1 Photographs of the exterior (A) and interior (B) of the greenhouse used in the experiment.

1.2.2. Measurements of photosynthetic parameters and leaf water potential

Diurnal changes in photosynthetic parameters (light-saturated photosynthetic rate A_{nmax}, stomatal conductance to water vapor g_{sw}, and chlorophyll fluorescence) under light-saturated conditions were measured using a portable gas exchange system (LI-6400, LI-COR, Lincoln, NE, USA) equipped with a leaf chamber fluorometer (LI-6400-40, LI-COR, Lincoln, NE, USA) on May 22, 23, and 30, 2021, which were relatively sunny days. This measurement was conducted to evaluate the diurnal changes in mesophyll conductance (g_m) using the variable *J* method (Harley *et al*., 1992) and maximum carboxylation rate based on CO_2 concentration at the carboxylation site using the one-point method (De Kauwe *et al*., 2016; Fig. 1.2). The measurements were conducted on randomly selected fully expanded sun leaves from 6:30 am to 18:00 pm at an interval of about 30 min under light-saturating PPFD of 1500 μmol m^{-2} s^{-1} with a CO_2 concentration of 400 μmol mol^{-1}. In addition, the temperature and vapor pressure deficit inside the chamber were allowed to follow ambient conditions.

From the fluorescence measurements, the effective quantum yield of PSII photochemistry (Φ_{PSII}) was determined as follows:

$$\Phi_{PSII} = F'_m - F_s/F'_m, \quad (1.1)$$

where F_s is the steady-state fluorescence yield at a PPFD of 1500 μmol m^{-2} s^{-1} and F'_m is the maximum fluorescence measured with a light-saturating pulse. Then, the electron transport rate (*ETR*) was calculated as follows:

$$ETR = \alpha \cdot \beta \cdot \Phi_{PSII} \cdot \mathrm{PPFD}, \quad (1.2)$$

where α is the leaf absorptance, which was assumed to be 0.85 (Evans and Loreto, 2000), and β is the portioning of absorbed quanta between PSI and PSII, which was assumed to be 0.5 (Laisk and Loreto, 1996).

Diurnal changes in leaf water potential (Ψ_w) were also measured along with the gas exchange measurements every two hours from 6:00 to 18:00 ($n = 3$ for each measurement point).

Ψ_w was measured using a pressure chamber (Pump-up Chamber, PMS Instruments, Albany, OR, USA). The measurements of Ψ_w were made on a different plant used for the gas exchange measurements to avoid any effects by sampling leaves for the Ψ_w measurement.

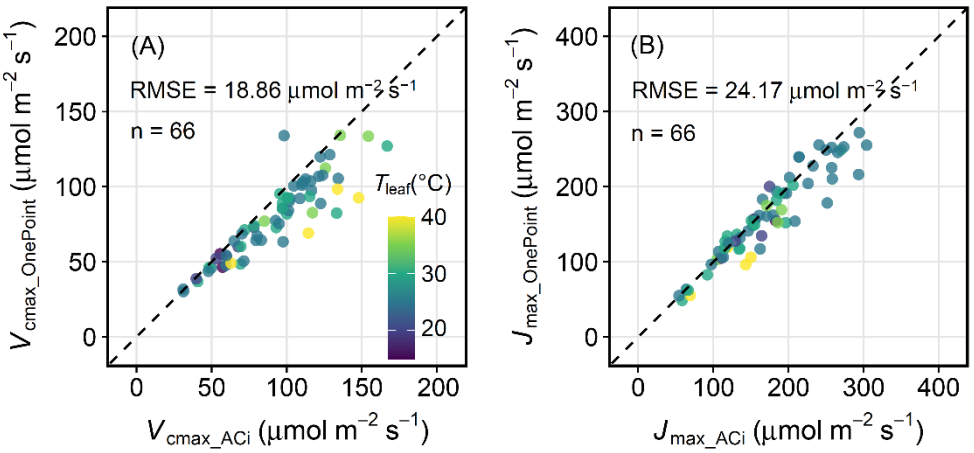

Figure 1.2 Relationship between the maximum carboxylation rate (V_{cmax}) obtained by A–C_i curve method and by one point method (A) and between maximum electron transport rate (J_{max}) obtained by A–C_i curve method and by one point method (B). These relationships were obtained using strawberry leaves grown in the same greenhouse as this experiment. The dashed line and plot color denote a one-to-one relationship and leaf temperature (T_{leaf}), respectively.

1.2.3. Assessing the risk of intercellular CO_2 concentration miscalculations

To derive a reliable value of the maximum carboxylation rate based on CO_2 concentration at the carboxylation site and g_m, an accurate measurement of intercellular CO_2 concentration (C_i; *i.e.,* accurate measurement of A_{nmax} and g_{sw}) is important (Pons *et al*., 2009). The effect of cuticular transpiration on g_{sw} calculation is negligible when transpiration through the stomata is sufficiently large relative to cuticular transpiration. However, when g_{sw} becomes lower under high evaporative demand conditions, g_{sw} could be overestimated due to a relative increase in cuticular transpiration, resulting in an error in C_i value (*e.g.,* Boyer *et al*., 1997; Márquez *et al*., 2021). Thus, I recalculated C_i to account for the effect of cuticular transpiration. Cuticular conductance was determined using the method of Sack *et al*. (2003). Briefly,

strawberry leaves were dried on a laboratory bench for 2–4 h, and the leaves were weighed at intervals of 1–5 min. Leaf temperature (T_{leaf}), temperature, and relative humidity were measured by the infrared thermography camera (FLIR i5, IRIE SHOKAI Co., Ltd., Tokyo, Japan) and the temperature–humidity recorder (TR-72Ui, T&D Co., Nagano, Japan), respectively, and used to calculate leaf-to-air *VPD*. Cuticular transpiration was estimated from the slope of the decline in leaf weight and then normalized by the leaf area. The leaf area was estimated from the measured leaf's picture using *ImageJ v. 1.53* software. Finally, cuticular conductance was evaluated by dividing cuticular transpiration by leaf-to-air *VPD*. Moreover, to avoid errors, CO_2 leakage in the gas exchange measurement was corrected, as described by Flexas *et al*. (2007a).

Because patchy stomatal closure could cause an error in C_i when plants are subjected to stress conditions, I checked the reliability of the measured C_i value based on the C_i–g_{sw} relationship, as described by Grassi *et al*. (2009). Owing to the sharp increase in C_i for g_{sw} values less than 0.05 mol m^{-2} s^{-1} (Fig. 1.3), data below this threshold were omitted from the estimation of photosynthetic parameters.

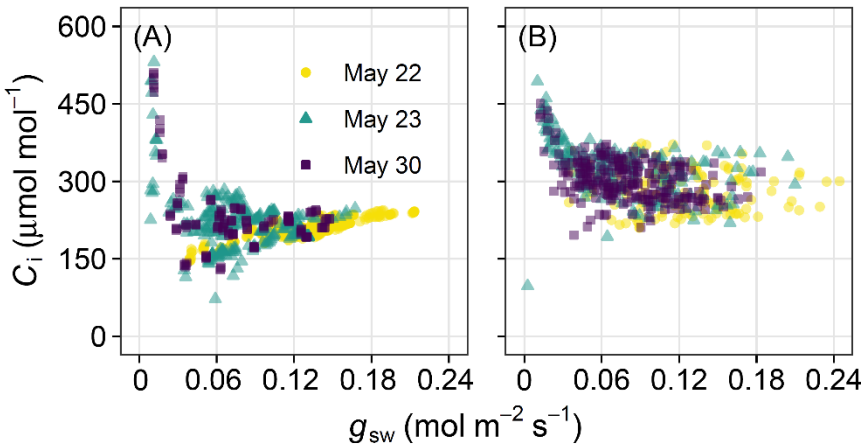

Figure 1.3 Relationships between stomatal conductance to water vapor (g_{sw}) and intercellular CO_2 concentration (C_i) measured by a portable gas exchange system (LI-6400, LI-COR, Lincoln, NE, USA) equipped with a leaf chamber fluorometer (A) and clear top chamber (B) on the day when gas exchange measurements were conducted (*i.e.,* yellow circle: May 22; blue triangle: May 23; purple square: May 30).

1.2.4. Calculation of mesophyll conductance and biochemical capacity parameters

From the method proposed by Harley *et al*. (1992), g_m was calculated as follows:

$$g_m = {A_{nmax}} \Big/ {C_i - \frac{\Gamma^*[ETR + 8\,(A_{nmax} + R_d)]}{ETR - 4\,(A_{nmax} + R_d)}}, \quad (1.3)$$

where A_{nmax} and C_i are taken from gas exchange measurements at saturating light, and ETR is calculated by Eq. 1.2. R_d is the mitochondrial respiration rate in the light, estimated by multiplying the maximum carboxylation rate on intercellular CO_2 concentration by 0.015, and Γ^* is the CO_2 compensation point in the absence of mitochondrial respiration (Bernacchi *et al*., 2001).

From the transport equation for CO_2 diffusion into the leaf, the CO_2 concentration at the carboxylation site (C_c) was calculated as follows:

$$C_c = C_i - P_{Nmax}/g_m\,. \quad (1.4)$$

Also, from the measurement of gas exchange under light-saturated conditions, I calculated the maximum carboxylation rate based on CO_2 concentration at the carboxylation site at the respective T_{leaf} [$V_{cmax}(C_c,T_{leaf})$] by the one-point method (De Kauwe *et al*., 2016), as follows:

$$V_{cmax}(C_c, T_{leaf}) = A_{nmax}\left(\frac{C_c + K_m}{C_c - \Gamma^*} - 0.015\right), \quad (1.5)$$

where K_m is the Michaelis–Menten constant defined by Bernacchi *et al*. (2001). Other Rubisco kinetics and their temperature dependencies were also taken from Bernacchi *et al*. (2001). Moreover, I used the following Arrhenius function to standardize $V_{cmax}(C_c,T_{leaf})$ to 25°C:

$$V_{cmax}(C_c, T_{leaf}) = V_{cmax}(C_c)\,\exp\left[\frac{E_a\,(T_{leaf,K} - 298.15)}{298.15\,R\,T_{leaf,K}}\right], \quad (1.6)$$

where $V_{cmax}(C_c)$ is the maximum carboxylation rate based on CO_2 concentration at the carboxylation site at 25°C, R is the universal gas constant (8.314 J mol^{-1} K^{-1}), and E_a is the activation energy obtained by fitting Eq. 1.6 to the relationship between $V_{cmax}(C_c,T_{leaf})$ and T_{leaf}

(61.00 kJ mol^{-1}; Fig. 1.4).

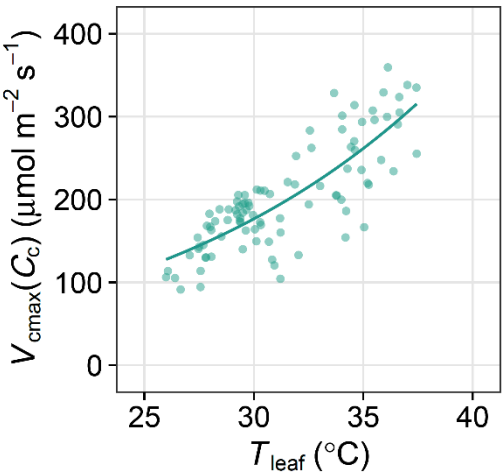

Figure 1.4 Relationships between leaf temperature (T_{leaf}) and maximum carboxylation rate based on the CO_2 concentration at the carboxylation site at T_{leaf} [$V_{cmax}(C_c,T_{leaf})$]. The solid line was calculated from the fitting curve using the Arrhenius function. Linear regression was conducted with R (version 4.0.2; R Development Core Team, Vienna, Austria).

1.2.5. Quantitative limitation analysis

To evaluate the contributions of stomatal, mesophyll, and biochemical limitations on the midday depression of photosynthesis in strawberry plants, quantitative limitation analysis proposed by Jones (1985) and further extended by Wilson *et al*. (2000) and Grassi and Magnani (2005) was performed. According to Grassi and Magnani (2005), relative changes in A_{nmax} can be expressed in terms of parallel relative changes in stomatal conductance, mesophyll conductance, and biochemical capacity [*i.e.*, $V_{cmax}(C_c)$]:

$$\frac{dA_{nmax}}{A_{nmax}} = S_L + MC_L + B_L = l_s\frac{dg_{sc}}{g_{sc}} + l_{mc}\frac{dg_m}{g_m} + l_b\frac{dV_{cmax}(C_c)}{V_{cmax}(C_c)}, \quad (1.7)$$

$$l_s = \frac{g_{tot}/g_{sc}\cdot\partial A_{nmax}/\partial C_c}{g_{tot}+\partial A_{nmax}/\partial C_c}, \quad (1.8)$$

$$l_{mc} = \frac{g_{tot}/g_m\cdot\partial A_{nmax}/\partial C_c}{g_{tot}+\partial A_{nmax}/\partial C_c}, \quad (1.9)$$

$$l_b = \frac{g_{tot}}{g_{tot}+\partial A_{nmax}/\partial C_c}, \quad (1.10)$$

where g_{sc} is stomatal conductance to CO_2 (*i.e.*, g_{sw}/1.6); g_{tot} is total conductance to CO_2 between

the leaf surface and carboxylation site (*i.e.*, $1/g_{tot} = 1/g_{sc} + 1/g_m$); S_L, MC_L, and B_L are the contributions of g_{sc}, g_m, and $V_{cmax}(C_c)$ to relative change in photosynthetic rate (*i.e.*, dA_{nmax}/A_{nmax}), respectively; l_s, l_{mc}, and l_b are the corresponding relative limitations ($0 < l_i < 1$, i = s, mc, b). Then, dA_{nmax}/A_{nmax} was defined as follows:

$$\frac{dA_{nmax}}{A_{nmax}} \approx \frac{A_{nmax,ref} - A_{nmax}}{A_{nmax,ref}}, \tag{1.11}$$

$$A_{nmax,ref} = \frac{V_{cmax,ref} \cdot \left[C_a - A_{nmax,ref} \cdot \left(1/g_{sc,ref} + 1/g_{m,ref}\right) - \Gamma^*\right]}{\left[C_a - A_{nmax,ref}\left(1/g_{sc,ref} + 1/g_{m,ref}\right) + K_c \cdot (1 + O/K_o)\right]} - R_d, \tag{1.12}$$

where $g_{sc,ref}$, $g_{m,ref}$, and $V_{cmax,ref}$ are the reference values of g_{sc}, g_m, and $V_{cmax}(C_c)$ defined as the maximum measured values; $A_{nmax,ref}$ is the reference photosynthetic rate assuming $g_{sc,ref}$, $g_{m,ref}$, and $V_{cmax,ref}$ are reached simultaneously; O is the O_2 concentration; K_c and K_o are the Michaelis constants for carboxylation and oxygenation defined by Chen *et al*. (2014), respectively; R_d is the day respiration rate. In addition, $\partial A_{nmax}/\partial C_c$ in Eqs. 1.8−1.10 was calculated as follows:

$$\partial A_{nmax}/\partial C_c = V_{cmax} \cdot [\Gamma^* + K_c(1 + O/K_o)]/[C_c + K_c \cdot (1 + O/K_o)]^2 . \tag{1.13}$$

1.2.6. Statistical analysis

Descriptive statistics [determination of means and standard error of all parameters, *i.e.,* Ψ_w, A_{nmax}, g_{sc}, g_m, $V_{cmax}(C_c)$, *ETR*, and respective limitations] was done using the R software (version 4.0.2, R Development Core Team, Vienna Austria). Linear regression was used to analyze the relationship between A_{nmax} and respective parameters [g_{sc}, g_m, $V_{cmax}(C_c)$, *ETR*, C_i, C_c]. The significance of the correlations between A_{nmax} and respective parameters was checked with Pearson's correlation test using R software.

1.3. Results

1.3.1. Diurnal changes in environmental conditions in the greenhouse

Although all days were relatively sunny, with a maximum PPFD around 1800 µmol m^{-2} s^{-1}, differences in environments were observed each day (Fig. 1.5). The lowest average PPFD of 631.1 µmol m^{-2} s^{-1}, T_a of 20.8°C, and *VPD* of 0.79 kPa were observed on May 22, whereas the highest average PPFD of 717.7 µmol m^{-2} s^{-1}, T_a of 25.5°C, and *VPD* of 1.72 kPa were observed on May 30. On May 23, the average PPFD, T_a, and *VPD* were 698.3 µmol m^{-2} s^{-1}, 24.6°C, and 1.31 kPa, respectively, which were intermediate between May 22 and 30.

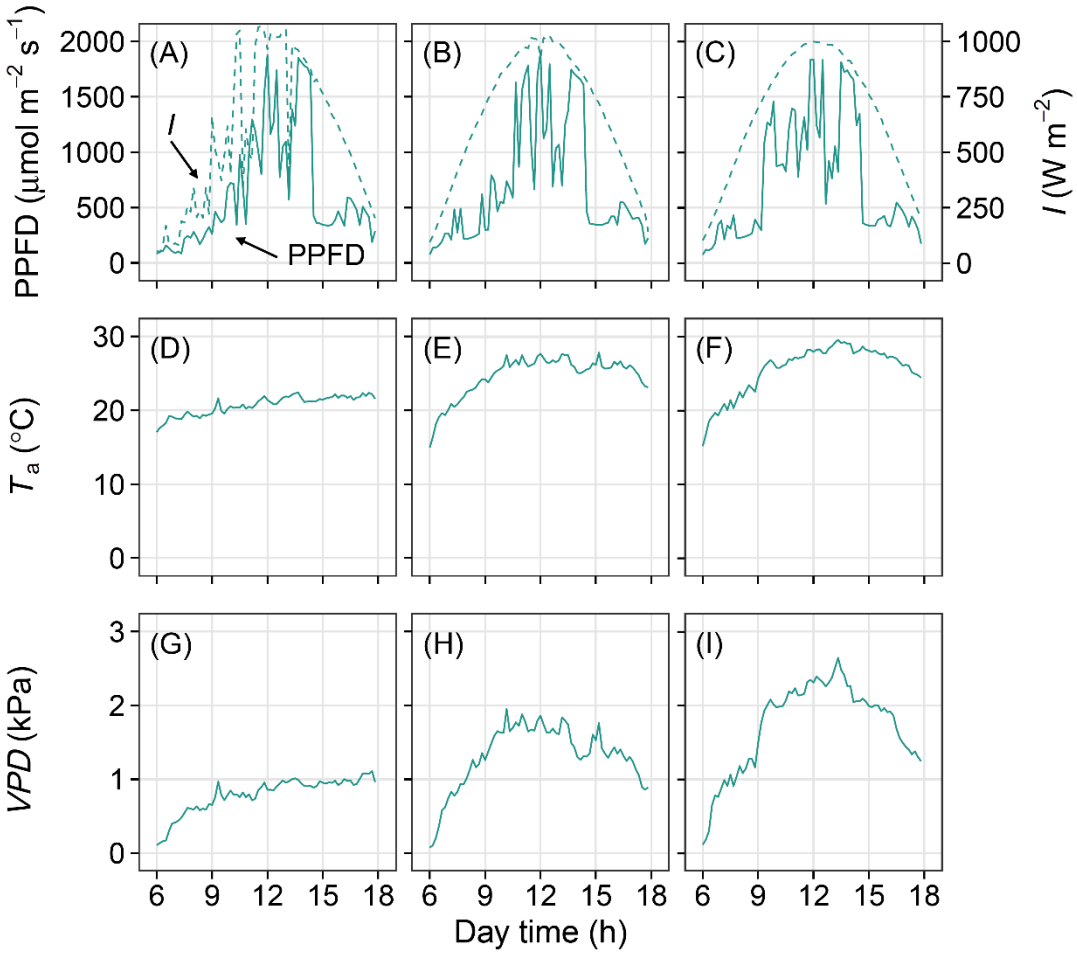

Figure 1.5 Diurnal changes in outside solar radiation (*I*; dashed line) and PPFD (solid line; A, B, C), temperature (T_a; D, E, F), and vapor pressure deficit (*VPD*; G, H, I) inside the greenhouse. The respective rows indicate the day when gas exchange measurements were conducted (*i.e.,* A, D, G: May 22; B, E, H: May 23; C, F, I: May 30).

1.3.2. Diurnal changes in leaf water potential and photosynthetic parameters

The diurnal changes in Ψ_w were similar among the measurement days, which decreased during the morning periods and then increased in the afternoon periods (Fig. 1.6). Ψ_w at 6:00 was −0.08, −0.09, and −0.07 MPa on May 22, 23, and 30, respectively, showing that strawberry plants had an appropriate water status in the early morning. During the morning periods, Ψ_w on May 30 was relatively lower than those on May 22 and 23. The lowest Ψ_w value was observed between 12:00 and 14:00, which was −0.65, −0.90, and −0.91 MPa on May 22, 23, and 30, respectively. Ψ_w tended to increase from 14:00 to 18:00.

Midday depression was observed depending on the environmental stress on each measurement day (Figs. 1.7 and 1.8). Owing to the severe environmental stress around midday (10:00 to 14:00) on May 30, g_{sw} was lower than 0.05 mol m^{-2} s^{-1}, which resulted in an unreliable C_i value (Fig. 1.3). Therefore, most data between 10:00 and 14:00 were discarded, and fewer data points were shown (Fig. 1.8C, F, I, L).

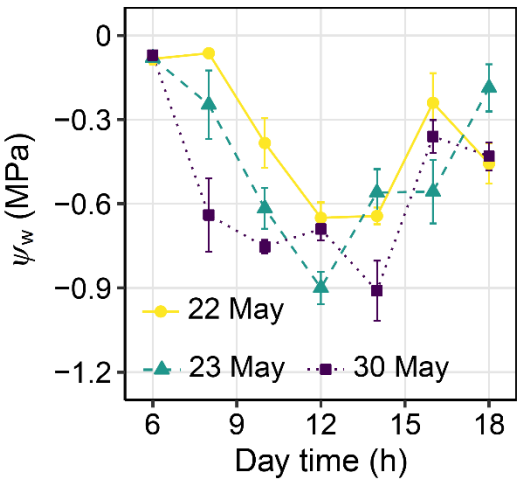

Figure 1.6 Diurnal changes in leaf water potential (Ψ_w) on the day when gas exchange measurements were conducted (May 22, 23, and 30). Means ± *SE* (n = 3) are shown.

On May 22, A_{nmax} was maintained at around 15 μmol m^{-2} s^{-1} until around 13:30 and then sharply decreased to 12.2 μmol m^{-2} s^{-1} by 14:30 (Fig. 1.8). g_m exceeded g_{sc} throughout the day. g_m peaked (0.27 mol m^{-2} s^{-1}) at around 8:30 and decreased to 0.17 mol m^{-2} s^{-1} by 13:30, whereas g_{sc} showed a relatively constant value of 0.09 mol m^{-2} s^{-1} from 8:30 to 13:30 and decreased to 0.06 mol m^{-2} s^{-1} by 14:30. V_{cmax}(C_c) gradually increased during the morning period and showed a relatively constant value of around 130 μmol m^{-2} s^{-1} and then decreased after 14:45. On May 23, A_{nmax} peaked (13.7 μmol m^{-2} s^{-1}) at around 7:30 and then decreased to about half of the maximum value by 12:00. In addition, g_m was almost constant around 0.20 mol m^{-2} s^{-1} during the morning periods and then decreased to 0.10 mol m^{-2} s^{-1} in the afternoon, whereas g_{sc} peaked (0.07 mol m^{-2} s^{-1}) at 7:30 and then decreased to 0.04 by 14:00. g_m and g_{sc} were almost the same value in the afternoon period compared with those in the morning period. V_{cmax}(C_c) tended to increase from 6:30, peaking (136.4 μmol m^{-2} s^{-1}) at around 10:50 and then decreasing thereafter. On May 30, A_{nmax} peaked (13.4 μmol m^{-2} s^{-1}) at 8:30 and then constantly decreased to 7.8 μmol m^{-2} s^{-1} by 15:00. g_m peaked (0.33 mol m^{-2} s^{-1}) at 8:30 and then sharply decreased to 0.16 mol m^{-2} s^{-1} by 10:00. g_m gradually decreased to 0.10 mol m^{-2} s^{-1} by 15:00. g_{sc} peaked (0.07 mol m^{-2} s^{-1}) at 8:30 and decreased to 0.05 mol m^{-2} s^{-1} by 13:30. V_{cmax}(C_c) increased in the early morning and varied between 146.1 μmol m^{-2} s^{-1} and 92.7 μmol m^{-2} s^{-1}.

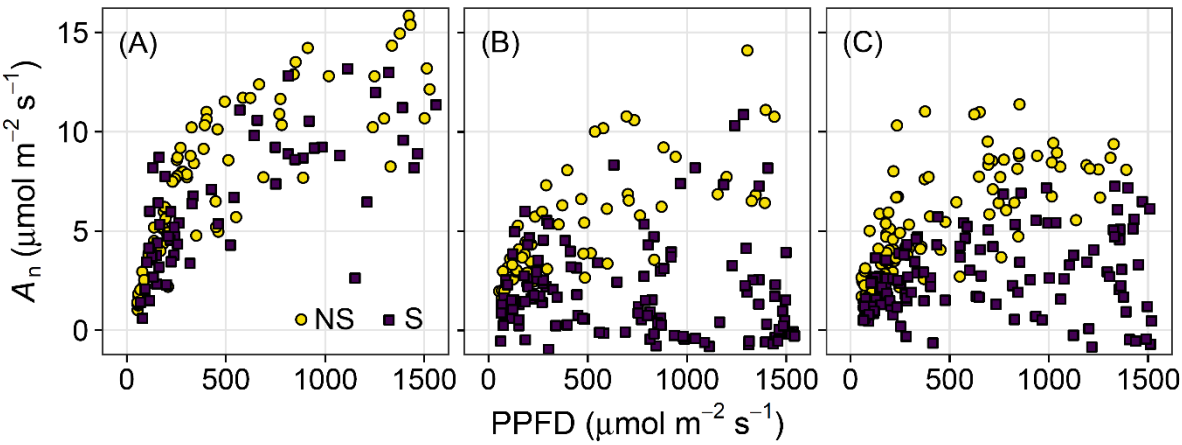

Figure 1.7 Relationships among PPFD and leaf photosynthetic rate (A_n) on the day when gas exchange measurements were conducted (*i.e.,* A: 22 May; B: 23 May; C: 30 May). NS and S indicate A_n before (yellow circle) and after (purple square) decrease, respectively.

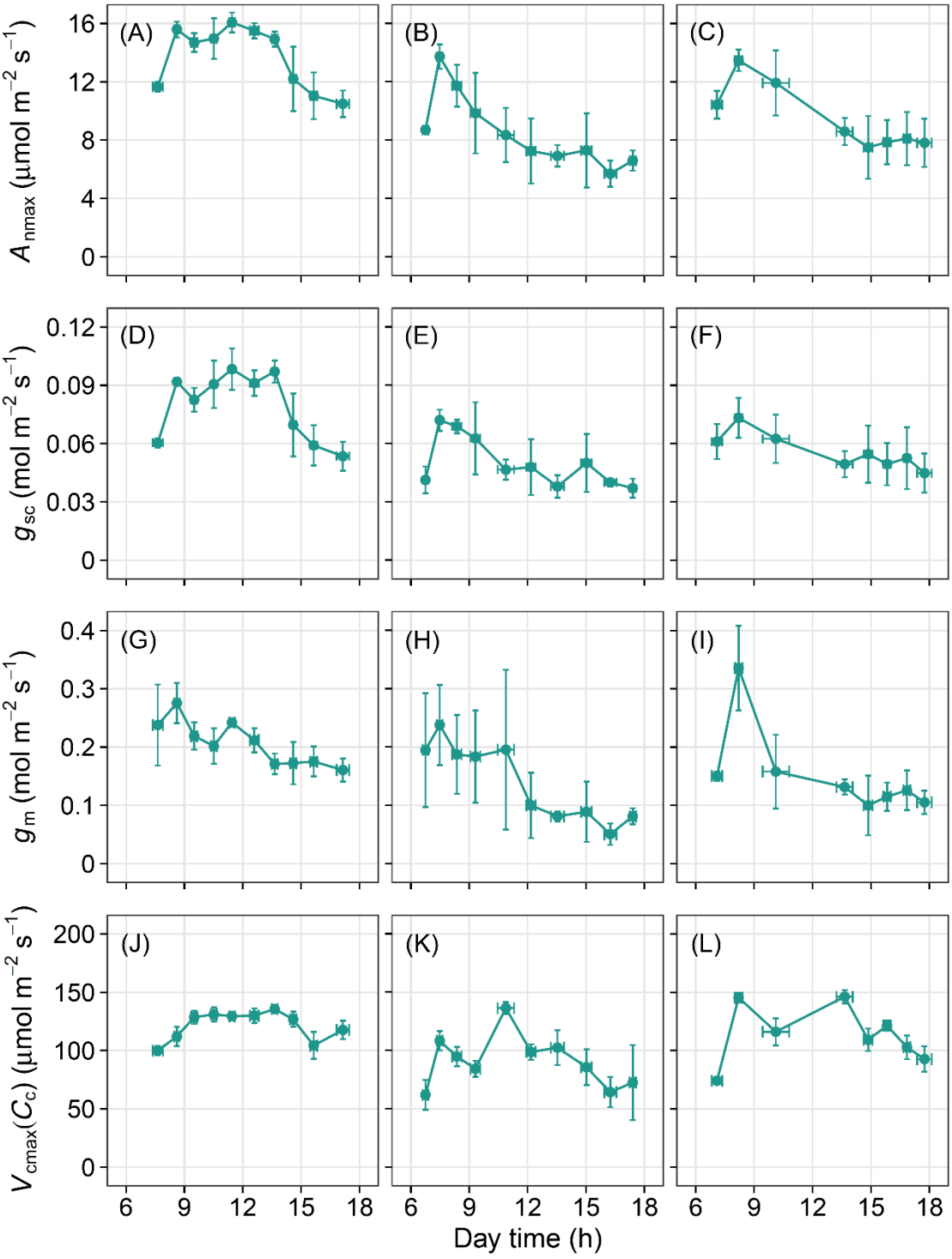

Figure 1.8 Diurnal changes in light-saturated photosynthetic rate (A_{nmax}; A, B, C), stomatal conductance to CO_2 (g_{sc}; D, E, F), mesophyll conductance (g_m; G, H, I), and maximum carboxylation rate based on the CO_2 concentration at the carboxylation site [$V_{cmax}(C_c)$; J, K, L]. The respective rows indicate the day when gas exchange measurements were conducted (*i.e.,* A, D, G, J: May 22; B, E, H, K: May 23; C, F, I, L: May 30). The measurements were conducted from 6:30 am to 18:00 pm (Japan standard time). Means ± *SE* (n = about 3) are shown.

1.3.3. Relationship between photosynthetic rate and parameters

The relationships among A_{nmax} and g_{sc}, g_m, $V_{cmax}(C_c)$, C_i, and C_c are shown in Fig. 1.9. A_{nmax} and diffusion conductance (*i.e.,* g_{sc} and g_m) were significantly positively correlated on all three measurement days (Fig. 1.9A, D, G). No significant correlation was found between A_{nmax} and $V_{cmax}(C_c)$ (Fig. 1.9B, E, H). A significant positive correlation existed between A_{nmax} and C_i on May 22 but was negligible on May 23 and 30 (Fig. 1.9C, F, I). However, A_{nmax} and C_c were significantly positively correlated on all three measurement days (Fig. 1.9C, F, I).

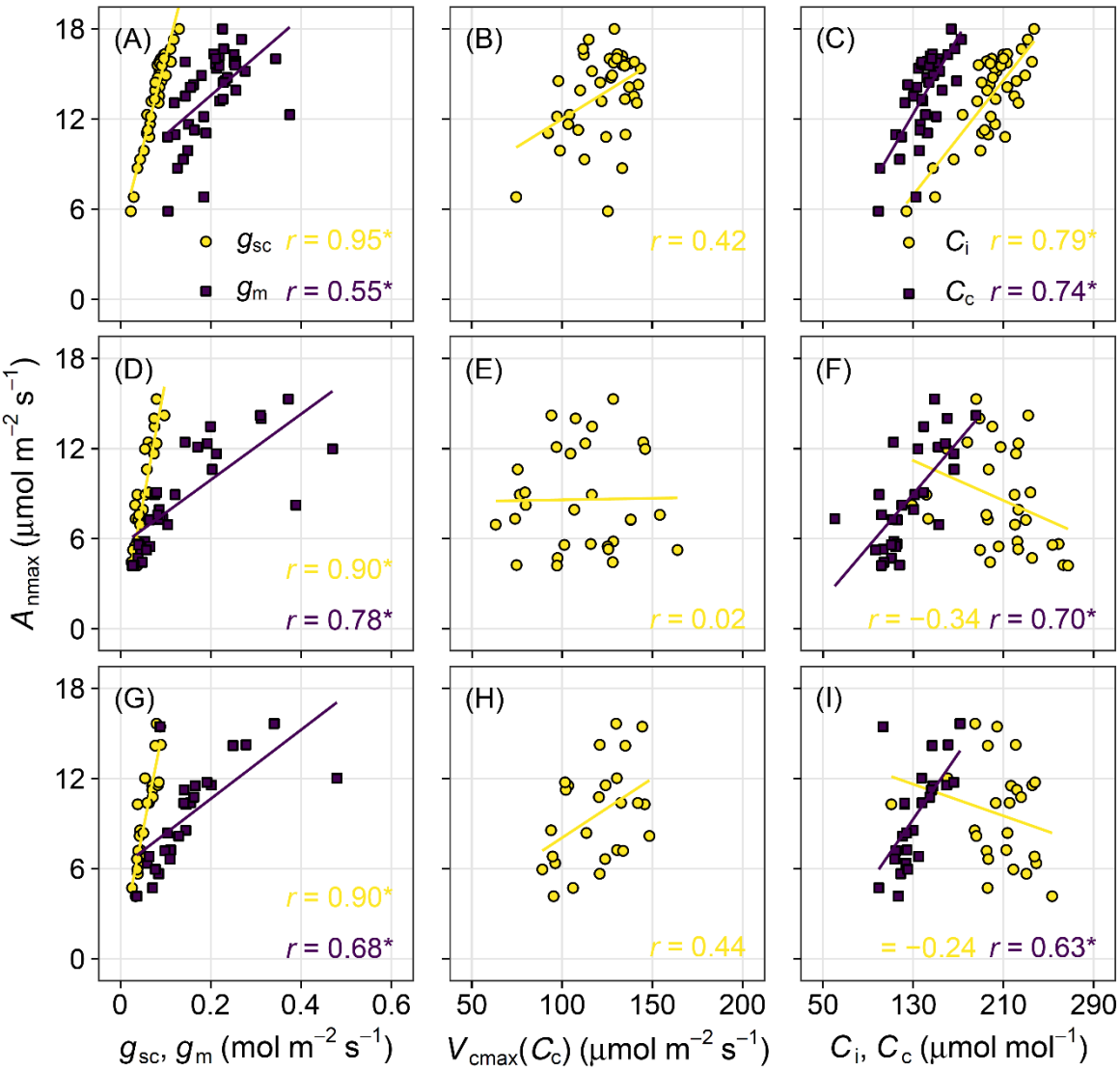

Figure 1.9 Relationships among light-saturated photosynthetic rate (A_{nmax}) and stomatal conductance to CO_2 (g_{sc}; yellow circle) and mesophyll conductance (g_m; purple square; A, D, G), maximum carboxylation rate based on CO_2 concentration at the carboxylation site [V_{cmax}(C_c); yellow circle; B, E, H], and intercellular CO_2 concentration (C_i; yellow circle) and the leaf CO_2 concentration at the carboxylation site (C_c; purple square; C, F, I). The respective columns indicate the day when gas exchange measurements were conducted (*i.e.*, A, B, C: May 22; D, E, F: May 23; G, H, I: May 30). The solid lines indicate respective linear regression. The Pearson correlation coefficients (r) and statistical significance are also shown (*: $p < 0.001$).

1.3.4. Diurnal changes in photosynthetic limitations

The respective limitation dynamically varied throughout each day (Fig. 1.10). On May 22, the A_{nmax} was limited by 44.8% in total (*i.e.,* $S_L + MC_L + B_L$), largely due to S_L (26.5%) and B_L (11.8%) at around 7:30. From 8:30 to 13:30, the limitation sum varied between 21.1% and 28.9%. During this period, S_L and MC_L were the main limiting factors for photosynthesis, whereas B_L was relatively lower, varying between 1.6% and 4.4%. The limitation sum sharply increased at around 14:30 mainly due to an increase in S_L. On May 23, the limitation sum was 59% at around 6:45 and then sharply decreased to 31% at around 7:30 mainly due to S_L. From 7:30 to 9:20, B_L increased from 9.7% to 18.9%, thereby increasing the limitation sum from 31.5% to 47.2%. While B_L decreased and had a relatively lower value than S_L and MC_L after 9:20, S_L and MC_L tended to increase, thereby increasing the total limitation sum. On May 30, the limitation sum decreased from 43.2% to 23% at around 8:10 and then increased thereafter. S_L and MC_L were relatively higher than B_L throughout most of the day.

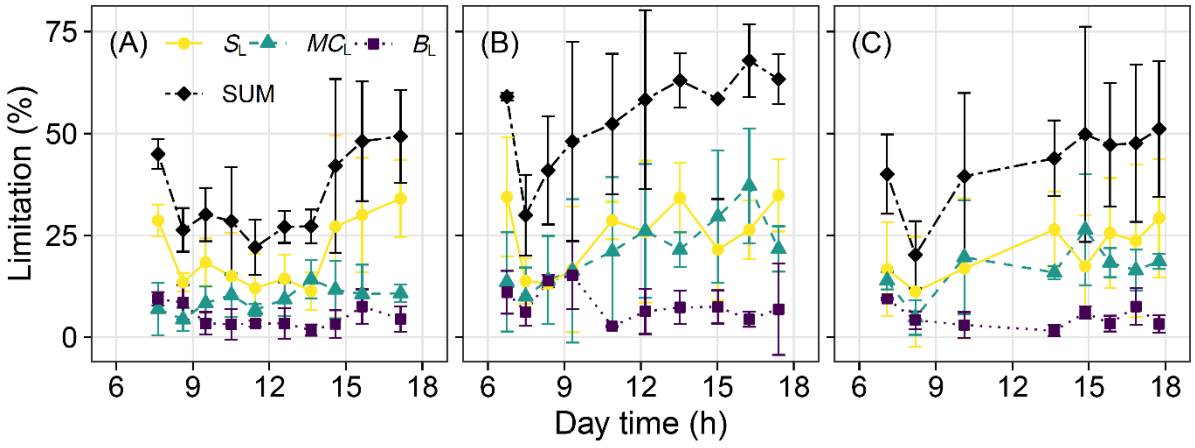

Figure 1.10 Diurnal changes in the limitations to light-saturated photosynthetic rate on the day when gas exchange measurements were conducted (*i.e.,* A: May 22; B: May 23; C: May 30). S_L, MC_L, B_L, and SUM indicate stomatal limitation (yellow circle), mesophyll conductance limitation (blue triangle), biochemical limitation (purple square), and the sum of each limitation (black rhombus), respectively. The measurements were conducted from 6:30 am to 18:00 pm (Japan standard time). Means ± *SE* (n = 3−5) are shown.

1.4. Discussion

1.4.1. Diurnal variations in photosynthetic limiting factors

In the present study, diurnal changes in photosynthetic limitations were investigated in well-watered greenhouse-grown strawberries. A diurnal variation in the proportion of photosynthetic limitation was observed, varying between measurement days under different environmental conditions (Fig. 1.10). While S_L accounted for a large proportion of the photosynthetic limitation on all three measurement days, MC_L also accounted for a large proportion of the photosynthetic limitation under severe environmental conditions (*i.e.,* May 23 and 30). Contrary to my hypothesis, B_L was relatively lower than S_L and MC_L on all three measurement days. This finding was unexpected because previous studies have reported that diffusional limitation is larger under water stress conditions, while the relative importance of B_L increases when water stress is less pronounced (Grassi *et al*., 2009). Strawberry plants' stomatal sensitivity to plant water status may account for the higher proportion of S_L. Jensen *et al*. (2009) reported that the soil moisture at which a decrease in g_{sw} was observed surpassed that at which a decrease in leaf water potential was observed, suggesting conservative stomatal behavior in strawberry plants. In my study, the observed Ψ_w when g_{sc} decreased was between −0.6 and −0.7 MPa on all measurement days, which was insufficient to induce stomatal closure for most crops (West and Gaff 1976; Syvertsen, 1982; Wankmüller and Carminati 2022). This result suggests that strawberry plants conserve plant water status by closing their stomata at an early stage of water stress, thereby preventing a decrease in biochemical activity caused by severe water stress. In addition, Klamkowski and Treder (2006) reported that g_{sw} of 0.05 mol m^{-2} s^{-1} was the threshold of stomatal and non-stomatal limitations in strawberry plants. Because g_{sw} below 0.05 mol m^{-2} s^{-1} was not used in my analysis to ensure photosynthetic parameter accuracy, S_L was expected to be one of the dominant limiting factors for photosynthesis.

In addition to S_L, MC_L accounted for a large proportion of photosynthetic limitations

under severe environmental conditions (*i.e.,* May 23 and 30). While A_{nmax} showed significant positive correlations with both C_i and C_c when the environmental condition was less severe, it showed a significant positive correlation with only C_c (Fig. 1.9C, F, I) under severe environmental conditions. This result suggests that A_{nmax} was limited by the supply of CO_2 from intercellular air spaces to chloroplasts, which in turn caused g_m to be the main limiting factor of A_{nmax}. Although recent studies have shown the effect of g_m on photosynthetic limitation (*e.g.,* Flexas *et al.,* 2009), studies on photosynthetic limitations in horticultural crops have been investigated in terms of stomatal and non-stomatal limitations (Ayari *et al*., 2000; Fan *et al*., 2010; Yuan *et al*., 2016; Rodrigues *et al*., 2018; Sarabi *et al*., 2019), with only a few studies considering g_m (Chen *et al*., 2014; Zhang *et al*., 2021). In my study, g_m was almost constant or increased during the early morning and then decreased toward the afternoon (Fig. 1.8D, E, F). g_m can respond to several environmental and physiological factors, such as light intensity (Douthe *et al*., 2011; Xiong *et al*., 2015), ambient CO_2 concentration (Düring, 2003; Rho *et al*., 2011), leaf temperature (von Caemmerer and Evans; 2015, Xiong *et al*., 2020), and water stress (Grassi and Magnani 2005i Galle *et al*., 2009; Flexas *et al*., 2009). A decrease in g_m was observed when PPFD exceeded 1000 μmol m^{-2} s^{-1} in the current study. Because g_m increases with increasing light intensity (Flexas *et al*., 2007b) and ambient CO_2 concentration inside the studied greenhouse was relatively constant due to ventilation, changes in leaf temperature and plant water status might have affected the changes in g_m in my study. von Caemmerer and Evans (2015) reported that g_m increased when the leaf temperature was 15°C–40°C in *Oryza sativa*, *Nicotiana tabacum*, *Gossypium hirsutum*, *Glycine max*, and *Eucalyptus pauciflora*, whereas the g_m values of *Triticum aestivum*, *Lophostemon confertus*, and *Quercus engelmannii* were relatively constant or decreased for leaf temperature exceeding 30°C. In my study, the leaf temperature was between 30°C and 36°C when a decrease in g_m was observed, suggesting that high leaf temperature might decrease g_m in strawberry plants. In addition to high leaf temperatures, a decrease in g_m has been extensively reported under water stress conditions

(Grassi and Magnani 2005; Galle *et al*., 2009; Flexas *et al*., 2009). The overall trends of g_m and Ψ_w were relatively similar in my study. For example, sharp decreases in g_m and Ψ_w were observed in the morning periods on May 30, whereas decreases in g_m and Ψ_w were observed around noon on May 22 and 23. Therefore, a decrease in Ψ_w might be involved in g_m reduction.

1.4.2. Implications for future research

Although many studies have applied quantitative limitation analysis to investigate the relative proportion of photosynthetic limitations (*e.g.,* Grassi and Magnani 2005; Galle *et al*., 2009; Flexas *et al*., 2009; Varone *et al*., 2012; Chen *et al*., 2014; Xiong *et al*., 2017; Zhang *et al*., 2021), to the best of my knowledge, none of these studies, including this study, have considered limitation by boundary layer conductance, which is an important factor for heat and mass exchange processes of leaves. The limitation of photosynthesis by boundary layer conductance might be negligible if the wind speed is high. However, the influence of boundary layer conductance is important under calm wind conditions, which are often observed inside greenhouses (Boulard *et al*., 2002). Kitaya *et al*. (2003) reported that gas exchange in sweet potato leaves was strongly limited by boundary layer conductance when the wind speed was less than 0.2 m s^{-1}. In addition, as lower boundary layer conductance limits heat exchange of the leaf surface, leaf-to-air temperature difference would be larger when boundary layer conductance is small (Kimura *et al*., 2017). These findings show that if the boundary layer conductance is low during the daytime, it would affect photosynthesis, both directly and indirectly, by acting as resistance to gas exchange and by increasing leaf temperature. Therefore, incorporating boundary layer conductance into quantitative limitation analysis will provide more insights into how diffusional and non-diffusional limitations affect photosynthetic rates. Moreover, quantitative limitation analysis stems from the biochemical model of C_3 photosynthesis, which is defined as the photosynthetic rate limited by the carboxylation of

RuBP (ribulose-1,5-bisphosphate) or by RuBP regeneration (Farquhar *et al*., 1980). In my study, photosynthetic rate was assumed to always limited by RuBP carboxylation. However, light intensity inside greenhouses frequently fluctuates mainly due to a greenhouse structure (Cabrera-Bosquet *et al*., 2016; Fig. 1.4A, B, C), thereby fluctuating the limiting step of photosynthetic rate. Kimura *et al*. (2022) reported that PPFD inside the greenhouse varied spatiotemporally due to changes in sun position and greenhouse structures (*i.e*., the spatial variability of the daily integral of PPFD was 40%). In other words, because the light-receiving conditions of leaves change frequently, the limiting factor of the photosynthetic rate would also often change (*i.e.,* when leaves receive adequate light, the photosynthetic rate is limited by RuBP carboxylation; when the light is interrupted by a greenhouse structure, the photosynthetic rate is limited by RuBP regeneration). Therefore, to more accurately assess the limiting factors of leaf photosynthetic rate in greenhouse-grown plants, the limitation by *ETR* and maximal electron transport rate should also be evaluated based on the light-receiving conditions of leaf surfaces (Chen *et al*., 2014).

1.5. Conclusion

In this chapter, quantitative limitation analysis, which distinguishes the factors of photosynthesis reduction into the three photosynthetic limitations (S_L, MC_L, and B_L), revealed a decrease in A_{nmax} even under well-watered greenhouse conditions. The respective limitations also showed different diurnal changes depending on the environmental stress on each measurement day. Under relatively moderate environmental stress, S_L was the primary limitation of A_{nmax}, whereas S_L and MC_L were the primary limitations under relatively severe stress, suggesting that stomatal closure was the main photosynthetic limitation and that the decline in mesophyll conductance was not negligible, especially under strong environmental stress and even under well-watered greenhouse conditions. The above results suggest that when

estimating leaf photosynthetic rate by using model, it is necessary to consider environmental stress. In the next chapter, I analyzed and discussed the cumulative leaf photosynthetic rate, which was estimated by model with considering the environmental stresses, from flowering as a predictive index for days from flowering to harvest.

Chapter 2

Is cumulative leaf photosynthetic rate suitable for an index to predict the harvest timing?

2.1. Introduction

Environmental factors have a significant impact on strawberry reproductive growth dynamics such as flowering, fruit setting, and harvesting. (Sønsteby *et al*., 2016; Twitchen *et al*., 2021). In particular, light intensity is especially important (Konsin *et al*., 2001; Cervantes *et al*., 2019; Wang *et al*., 2020). Hidaka *et al*. (2013) reported that supplemental lighting using a high irradiance light-emitting diode for 12 h increased fruit weight by 8 g and the number of fruits per plant 1.5-fold. Growth is also affected by temperature (Ariza *et al*., 2015; Sønsteby *et al*., 2016; Cui *et al*., 2021). Ledesma *et al*. (2008) found that high temperatures (30°C/25°C) during fruit growth shortened the time to harvest by 7 days and reduced fruit set by 20%. To date, the responses of growth to the environment have been investigated on a daily to weekly basis using 10 to 60 plants with a 1 to 7-month cultivation period. However, high-resolution (daily) longitudinal data on days from flowering to harvest are necessary to model the timing of flowering, fruit set, and harvesting and to develop efficient management strategies for maximizing strawberry production.

Cumulative values of light intensity and temperature from flowering are conventionally used as harvest indices in strawberry farming (Kawanobu *et al*., 2010; Opstad *et al*., 2011; Krüger *et al*., 2012). However, several studies suggested the relationship between the reproductive growth and photosynthesis. For example, Hidaka *et al*. (2019) reported a close relationship between fruit enlargement and the translocation of photosynthates from leaves to fruits. Furthermore, Nakai *et al*. (2022) reported a role for translocation rate and cumulative

leaf photosynthetic rate. Additionally, photosynthesis is affected by multiple environmental factors, such as light, temperature, and CO_2 concentration, and eco-physiological functions (Farquhar *et al*., 1980). Thus, cumulative photosynthesis from flowering may be a superior index for predicting the time of harvest better than cumulative light intensity and temperature.

In this chapter, I tested whether photosynthesis could describe strawberry HD better than conventional indices. To do this, I monitored the daily dynamics of flowering, fruit setting, and harvesting in 144 strawberry plants (> 2,700 fruits) over 9 month cultivation period and monitored the growth dynamics of each inflorescence and fruit position. Furthermore, I estimated single-leaf photosynthetic rate using a biochemical photosynthesis model with considering the environmental stresses. Finally, I statistically compared the appropriateness of cumulative leaf photosynthetic rate, light intensity, and temperature from flowering to predict the time of harvest.

2.2. Materials and methods

2.2.1. Plant materials and growth conditions

Similar to chapter 1, June-bearing strawberry plants (*Fragaria* × *ananassa* Duch. cv. Fukuoka S6) were used as the experimental crop. The nursery plants were grown in a greenhouse at the National Agriculture and Food Research Organization, Kyushu Okinawa Agricultural Research Center, Japan on June 6, 2019, and 288 plants were transplanted to beds filled with culture soil (Good Soil; Kaneya Co., Ltd., Aichi Japan) in a greenhouse at the Ito Plant Experiment Fields & Facilities, Faculty of Agriculture, Kyushu University, Fukuoka, Japan (Fig. 1.1) on October 3, 2019. The other growth condition is similar to that in chapter 1. In total, one hundred and forty-four of the original two hundred and eighty-eight plants were used.

2.2.2. Measurement of environmental conditions

Photosynthetic photon flux density (PPFD), temperature, relative humidity, CO_2 concentration, and wind speed inside the greenhouse were measured at a height of 1.2 m. The sensors included a quantum sensor (PAR-02D; Prede Co., Ltd., Tokyo, Japan), a temperature/humidity sensor (HMP60; Vaisala, Helsinki, Finland), an infrared CO_2-gas analyzer (GMP252; Vaisala, Helsinki, Finland), and an ultrasonic anemometer (model 81000; R.M Young Company, Traverse City, Michigan, USA). Data were measured every 5 seconds and 5 minutes means logged in a programmable data logger (CR-1000; Campbell Scientific Inc., Logan, Utah, USA).

2.2.3. Simulation of the single-leaf photosynthetic rate

2.2.3.1. Model description

In this study, I estimated the leaf photosynthetic rate (A) in strawberry plants using a combination of the biochemical photosynthesis model (Farquhar *et al*., 1980), the stomatal model (Medlyn *et al*., 2011), and an energy balance equation. In the photosynthesis model, A is limited by the smaller values of the Rubisco-limited rate (A_c) and RuBP-limited rate (A_j):

$$A = \min(A_c, A_j), \tag{2.1}$$

$$A_c = f\frac{V_{cmax}(C_i - \Gamma^*)}{C_i + K_c(1 + O/K_o)} - R_L, \tag{2.2}$$

$$A_j = \frac{J(C_i - \Gamma^*)}{4C_i + 8\Gamma^*} - R_L, \tag{2.3}$$

where V_{cmax} is the maximal carboxylation rate based on intercellular CO_2 concentration, C_i is the intercellular CO_2 concentration, Γ^* is the CO_2 compensation point without the mitochondrial respiration rate, K_c and K_o are the Michaelis–Menten constants for carboxylation and oxygenation, respectively, and O is the O_2 concentration. Also, f is the attenuating function, which represents the effects of environmental stresses on leaf photosynthetic rate, and it is

described in 2.2.3.2. In Eq. 2.3, J is the electron transport rate:

$$J = \frac{\phi I + J_{\max} - \{(\phi I + J_{\max})^2 - 4\phi I J_{\max}\theta\}^{1/2}}{2\theta}, \quad (2.4)$$

where Φ is the initial slope of the curve, I is the PPFD, J_{max} is the maximal electron transport rate, and θ is the convexity of the curve. In Eqs. 2.2 and 2.3, R_L is the mitochondrial respiration rate and is estimated using the relationship between the day respiration rate (R_d) and night respiration rate (R_n) (Villar *et al*., 1995):

$$R_L = R_n \ (if\ I = 0\ \mu mol\ m^{-2}s^{-1}), \quad (2.5)$$

$$R_L = R_d = 0.4\ R_n \ (if\ I > 0\ \mu mol\ m^{-2}s^{-1}). \quad (2.6)$$

The photosynthesis model parameters, *i.e.*, Γ^*, K_c, K_o, R_n, V_{cmax}, and J_{max}, depend on leaf temperature (T_{leaf}), and the temperature dependency of Γ^*, K_c, K_o, and R_n can be described using the following Arrhenius function:

$$k = k_{25} \exp\left[\frac{E_a\left(T_{leaf,K} - 298.15\right)}{298.15\ R\ T_{leaf,K}}\right], \quad (2.7)$$

where k and k_{25} represent the parameter values at T_{leaf} in K and 25°C, respectively, E_a is the activation energy, and R is the universal gas constant (8.314 J mol^{-1} K^{-1}). The temperature dependency of V_{cmax} and J_{max} is expressed as a peaked Arrhenius function describing enzyme deactivation at high temperatures (Johnson *et al*., 1942):

$$k = k_{25} \exp\left[\frac{E_a\left(T_{leaf,K} - 298.15\right)}{298.15\ R\ T_{leaf,K}}\right] \frac{1 + \exp\left(\frac{298.15\ \Delta S - H_d}{298.15\ R}\right)}{1 + \exp\left(\frac{T_{leaf}\ \Delta S - H_d}{T_{leaf}\ R}\right)}, \quad (2.8)$$

where ΔS is the entropy factor and H_d is the deactivation energy.

Following Medlyn *et al*. (2011), stomatal conductance for water vapor (g_{sw}) was given by the following equation:

$$g_{sw} = g_0 + 1.6\left(1 + \frac{g_1}{\sqrt{VPDL}}\right)\frac{A}{C_s}, \quad (2.9)$$

where g_0 and g_1 represent the residual conductance and empirical constant of stomatal conductance, respectively, $VPDL$ is the leaf-to-air vapor pressure deficit in kPa, and C_s is the CO_2 concentration at the leaf surface.

2.2.3.2. Considering the environmental stress

Since a decrease in leaf photosynthetic rate due to environmental stress has been measured in Chapter 1, the following attenuating function f representing the effects of environmental stresses by daily cumulative evapotranspiration E_{accum} from leaves was defined and multiplied by Eq. 2.2:

$$f = \frac{1 + \exp(aE_{ref})}{1 + \exp\left(a(E_{ref} - E_{accum})\right)}, \tag{2.10}$$

where a and E_{ref} are the slope at the inflection point of attenuating function f and the threshold, respectively. Then, E_{accum} was calculated as follows (simplification of the Penman-Monteith equation):

$$E_{accum} = \sum E = \sum \frac{g'_{ah}\rho_a c_p D_a + \Delta R_{ni}}{l\left(\Delta + \left(1 + g'_{ah}/g'_{sw,max}\right)A_\gamma\right)}, \tag{2.11}$$

where g'_{ah} is the leaf boundary layer conductance to heat (m s^{-1}), ρ_a is the mean air density at constant pressure (kg m^{-3}), c_p is the specific heat of the air (1.004 kJ kg^{-1} K^{-1}), D_a is the vapor pressure deficit of the air (hPa), Δ is the slope of the saturation vapor pressure temperature relationship (hPa $°C^{-1}$), R_{ni} is the isothermal net radiation (W m^{-2}), l is the latent heat of vaporization (kJ kg^{-1}) $g'_{sw,max}$ is the daily maximum stomatal conductance to water vapor (m s^{-1}), and A_γ is the psychrometric constant (hPa $°C^{-1}$). Then, g'_{ah} in Eq. 2.11 was the calculated as follow (Kimura *et al.*, 2020b):

$$g'_{ah} = \frac{1}{41.4} 0.21(u/d_{leaf})^{0.5}, \tag{2.11}$$

where a value of 41.4 is the amount of substance per unit volume of air (mol m^{-3}), u is the wind speed (m s^{-1}), and d_{leaf} is the leaf characteristic dimension (0.064 m). Δ in Eq. 2.11 was calculated as follow (Allen *et al.*, 1998):

$$\Delta = \frac{40980\left[0.6108\exp\left({}^{17.27T_{air}}/_{(T_{air}+237.3)}\right)\right]}{(T_{air}+237.3)^2}, \tag{2.13}$$

where T_{air} is the air temperature (°C). Furthermore, $A\gamma$ in Eq. 2.11 is calculated as follow:

$$A_\gamma = \frac{c_p P}{\varepsilon l}, \tag{2.14}$$

where P is the atmospheric pressure (1,013 hPa), and ε is the ratio molecular weight of water vapor/dry air (0.622; Allen *et al*., 1998). Also, R_{ni} in Eq. 2.11 is calculated as follow:

$$R_{ni} = R_{s,abs} + R_{l,abs} - \varepsilon_{l,leaf}\sigma(T_{air} + 273.15)^4, \tag{2.15}$$

$R_{s,abs}$ and $R_{l,abs}$ are the absorbed shortwave and longwave radiation, respectively, $\varepsilon_{l,leaf}$ is the leaf emissivity to longwave radiation (0.97; Gates, 1980), and σ is the Stefan-Boltzmann constant (5.67×10^{-8}; W m^{-2} K^{-4}). $R_{s,abs}$ in Eq. 2.14 was calculated as follow:

$$R_{s,abs} = 0.495\alpha_{s,leaf}\mathrm{PPFD}, \tag{2.16}$$

where 0.495 is the ration of total shortwave energy to photosynthetic photon flux (Mavi and Tupper, 2004), and $\alpha_{s,leaf}$ is the leaf absorptivity of shortwave radiation (0.56; Buckley *et al*., 2014). $R_{l,abs}$ in Eq. 2.14 was calculated as follow (De Boeck *et al*., 2012; Kimura *et al*., 2020b and 2022):

$$R_{l,abs} = \alpha_{l,leaf}\tau_{l,gh}\varepsilon_{l,atm}\sigma(T_{air} + 273.15)^4 + \alpha_{l,leaf}\varepsilon_{l,gh}\sigma\left(T_{gh} + 273.15\right)^4 + \alpha_{l,leaf}\rho_{l,gh}\varepsilon_{l,leaf}\sigma(T_{air} + 273.15)^4, \tag{2.17}$$

where $\alpha_{l,leaf}$ is the leaf absorptivity of longwave radiation (0.97; Gates, 1980); $\varepsilon_{l,atm}$ is the atmospheric emissivity of longwave radiation; T_{gh} is the greenhouse temperature, assumed to equal T_{air} (De Boeck *et al*., 2012); and $\tau_{l,gh}$, $\varepsilon_{l,gh}$, and $\rho_{l,gh}$ are the longwave radiation transmissivity, emissivity, and reflectivity of the greenhouse material, respectively, using typical values for a polyvinyl-chloride greenhouse (0.11, 0.15, 0.74; De Boeck *et al*., 2012). $\varepsilon_{l,atm}$ is calculated as follow (Leuning *et al*., 1995):

$$\varepsilon_{l,atm} = 0.642\left(0.1P\frac{W_a}{T_{air} + 273.15}\right)^{1/7}, \tag{2.18}$$

where W_a is the ambient water vapor concentration (mmol mol^{-1}).

2.2.3.3. Model parameterization

I determined the photosynthetic model parameters [*i.e.*, the maximum carboxylation rate at 25°C ($V_{cmax,25}$) and the maximum electron transport rate at 25°C ($J_{max,25}$; in Eqs. 2.2, 2.4, 2.8)] and stomatal model parameters [*i.e.*, the residual stomatal conductance (g_0) and the empirical constant of stomatal conductance (g_1; in Eq. 2.9)] by gas exchange measurement. To identify $V_{cmax,25}$ and $J_{max,25}$, I conducted the gas exchange using a portable gas exchange system (LI-6400; LI-COR, Lincoln, Nebraska, USA) equipped with a LED light source chamber (6400-02B; LI-COR) and periodically obtained the response curves of the leaf photosynthetic rate (A) to intercellular CO_2 concentrations (C_i; *i.e.*, the A–C_i curve), at different times [*i.e.*, at 309, 310, 317, and 338 days of the year (DOY) in 2019 and 49 and 95 DOY in 2020]. At, this time, I set T_{leaf} and PPFD to 25°C and 1500 μmol m^{-2} s^{-1}, respectively. During all measurements, the vapor pressure deficit in the LI-6400 system was kept at < 2 kPa as much as possible. Curve-fittings for the measured data were performed using the "fitaci" function in the "plantecophys" package (version 1.4.6; Duursma, 2015) in R (version 4.0.2; R Development Core Team, Vienna, Austria), and $V_{cmax,25}$ and $J_{max,25}$ were estimated. To identify g_0 and g_1, I measured diurnal changes in A, g_w, CO_2 concentration, and *VPDL* using the LI-6400 system with a transparent top chamber (standard leaf chamber; LI-COR) under ambient light, temperature, and humidity conditions at different times (at 353 and 360 DOY in 2019 and 92, 97, 133, and 141 DOY in 2020). The stomatal model (Eq. 2.9) was fitted to the measured data using the "fitBB" function in the "plantecophys" package, and g_0 and g_1 were estimated. To identify the dark respiration rate (R_n; Eqs. 2.5, 2.6), I measured the leaf gas exchange rate using the LI-6400 system with a LED chamber in darkness and a chamber reference CO_2 concentration of 400 μmol mol^{-1}. Measurements were repeated at various leaf temperatures to estimate the temperature dependence of R_n. The Arrhenius equation (Eq. 2.7) was fitted to the obtained data and temperature-dependent parameters were determined, *i.e.*, the night respiration rate at 25°C

($R_{n,25}$) and the activation energy for R_n [$E_a(R_n)$].

2.2.3.4. Solving model

To estimate A with an ever-changing T_{leaf}, I followed Nakai *et al*. (2022). Firstly, I set the arbitrary stomatal conductance ($g_{sw,SET}$) as the initial value and estimated T_{leaf} using the "tleaf" in the "tealeaves" package (version 1.0.5; Muir, 2019) in R. This allows users to set leaf and environmental parameters, as well as physical constants. For the environment and leaf parameters, I used the measured environmental conditions and a leaf characteristic dimension of 0.064 m (Kimura *et al*., 2020a), respectively. I used the default values for the other parameters. Secondly, I obtained R_n using $R_{n,25}$, $E_a(R_n)$ in Eq. 2.7, and the estimated T_{leaf}. Thirdly, I estimated A using the "Photosyn" function in the "plantecophys" package with the estimated T_{leaf} and R_n values. I determined $V_{cmax,25}$ and $J_{max,25}$ (in Eqs. 2.2, 2.4, 2.8). Other model parameters related to temperature dependence such as the activation energy for V_{cmax} [$E_a(V_{cmax})$] and J_{max} [$E_a(J_{max})$], entropy factor for V_{cmax} [$\Delta S(V_{cmax})$] and J_{max} [$\Delta S(J_{max})$], and deactivation energy for V_{cmax} [$H_d(V_{cmax})$] and J_{max} [$H_d(J_{max})$] were obtained from Kimura *et al*. (2020b), who took measurements in real cultivation settings using the same cultivar (Table 2.1; in Eq. 2.8). I used measured PPFD, temperature, relative humidity, CO_2 concentration, and wind speed for the environmental parameters, while default values were used for the remaining parameters. Fourthly, I estimated stomatal conductance ($g_{sw,NEW}$) using the stomatal model with the estimated A value, identified g_0 and g_1 (in Eq. 2.9), and measured environmental conditions. This process was repeated until the difference between $g_{sw,SET}$ and $g_{sw,NEW}$ was minimal. Finally, the obtained $g_{sw,NEW}$ was used as the next $g_{sw,SET}$, and A was continuously estimated throughout the cultivation period.

Table 2.1 Physiological parameters used to estimate the photosynthetic rate and stomatal conductance in strawberry leaves each month.

Parameter	Value (month of use)	Unit	Reference
$V_{cmax,25}$	106.59 (Oct. and Nov. 2019)	μmol m^{-2} s^{-1}	This study
	120.47 (Dec. 2019 and Jan. 2020)		
	105.07 (Feb. and Mar. 2020)		
	110.43 (Apr. 2020)		
	109.61 (May and June 2020)		
$E_a(V_{cmax})$	53.20 (whole period)	kJ mol^{-1}	Kimura *et al*. (2020b)
$\Delta S(V_{cmax})$	0.637 (whole period)	kJ K^{-1} mol^{-1}	Kimura *et al*. (2020b)
$H_d(V_{cmax})$	200 (whole period)	kJ mol^{-1}	Kimura *et al*. (2020b)
$J_{max,25}$	203.55 (Oct. and Nov. 2019)	μmol m^{-2} s^{-1}	This study
	233.59 (Dec. 2019 and Jan. 2020)		
	232.16 (Feb. and Mar. 2020)		
	228.00 (Apr. 2020)		
	204.49 (May and June 2020)		
$E_a(J_{max})$	23.74 (whole period)	kJ mol^{-1}	Kimura *et al*. (2020b)
$\Delta S(J_{max})$	0.639 (whole period)	kJ K^{-1} mol^{-1}	Kimura *et al*. (2020b)
$H_d(J_{max})$	200 (whole period)	kJ mol^{-1}	Kimura *et al*. (2020b)
g_0	0.035 (Oct. 2019–Jan. 2020)		This study
	0.019 (Feb. 2020–Apr. 2020)		
	0.017 (May and June 2020)		
g_1	2.75 (Oct. 2019–Jan. 2020)	mol m^{-2} s^{-1}	This study
	2.83 (Feb. 2020–Apr. 2020)		
	1.57 (May and June 2020)		
$R_{n,25}$	1.46 (whole period)	μmol m^{-2} s^{-1}	This study
$E_a(R_n)$	53.50	kJ mol^{-1}	This study

2.2.4. Acquisition of reproductive growth data

All the flowers were tagged daily, and the dates of flowering, fruit setting, and harvesting recorded. The growth stage of the fruit was determined based on specific characteristics (Fig. 2.1). Flowering was defined when the petals were fully unfolded and the receptacle and all anthers were visible. Fruit setting was defined as the falling of petals and the expansion of the achenes on the receptacle. Harvesting was defined as the fruit surface evenly red. The number of flowerings (FL_t), fruit settings (FR_t), and harvestings (H_t) per day and plant were determined by dividing the daily values by the total number of plants (144). The number of flowers (NFL_t), fruit (NFR_t), and cumulative harvests (NH_t) per day and plant were calculated using the following:

$$NFL_t = NFL_{t-1} - FR_t + FL_t, \tag{2.19}$$

$$NFR_t = NFR_{t-1} - H_t + FR_t, \tag{2.20}$$

$$NH_t = NH_{t-1} + H_t, \tag{2.21}$$

where t is any given day after planting (d).

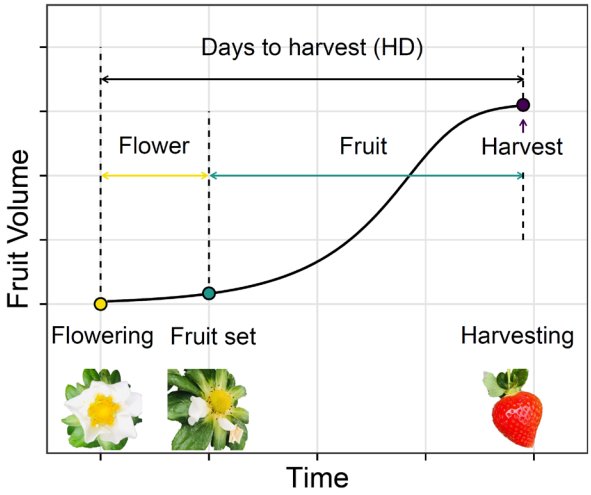

Figure. 2.1 Schematic diagram of the reproductive growth process (flowering, fruit setting, and harvesting) in strawberries. Flowering–fruit setting and fruit setting–harvesting were defined as flower and fruit, respectively. The number of days from flowering to harvesting was defined as HD.

2.2.5. Statistical analysis

To analyze changes in environmental factors and leaf photosynthetic rate, daily cumulative PPFD (I), daily averaged temperature (T_a), daily averaged CO_2 concentration (C_a), and daily cumulative leaf photosynthetic rate (A_n) were calculated. Average and cumulative values during the fruit growing period for light, temperature, and leaf photosynthetic rate were calculated using the averaged and cumulative I, T_a, and A_n from flowering to harvest denoted as I_A, $T_{a,A}$, $A_{n,A}$ and I_C, $T_{a,C}$, $A_{n,C}$, respectively. The root mean square error (RMSE) was used to evaluate the accuracy of simulating A.

A suitable analysis method was needed to evaluate and compare the appropriateness of each index. Although the multiple regression analysis is used to compare the influence of each index (Doan and Tanaka, 2022), it was not suitable for this study since the aim was not to investigate the degree of influence. It was better to compare the coefficient of variation that represents variations in I_C, $T_{a,C}$, and $A_{n,C}$. However, since there was only one sample for each index, statistical comparison was not possible. Therefore, the determining degree (D) was newly defined here as a dimensionless quantity and calculated using the following equation:

$$D = |x_i - \bar{x}|/\bar{x}, \tag{2.22}$$

where x_i is the ith data point (*i.e.*, I_C, $T_{a,C}$, or $A_{n,C}$ of the ith fruit) and $\bar{x}$ is the mean value for each index. The index with the smallest average D has the smallest variance (*i.e.*, the highest appropriateness). Significant differences in D between the indices were determined using the Steel–Dwass test in R.

2.3. Results

2.3.1. Environmental conditions and leaf photosynthetic rate

The environmental conditions inside the greenhouse exhibited seasonal variations (Fig. 2.2). *I* gradually decreased from 0 to 90 days and then increased to 230 days, after which *I* decreased because the shade curtains were activated (Fig. 2.2A). T_a changed with *I*: it gradually decreased from 0 to 50 days as *I* decreased but was constant at 13°C from 50 to 200 days (Fig. 2.2B). Thereafter, T_a increased as *I* increased. C_a increased from 0 to 80 days and then decreased (Fig. 2.2C). Furthermore, to assess the accuracy of leaf photosynthetic rate estimation, I investigated the relationship between the diurnal variations of measured *A* over three days in each season and the estimated *A* (Fig. 2.3). The use of *f* allowed for a successful reproduction of the decline in the leaf photosynthetic rate, especially in the afternoon on each experimental date. Also, estimated *A* showed reasonable values, and it was observed that considering environment stresses led to a significant reduction in RMSE (= 2.87 and 1.61 μmol m^{-2} s^{-1} respectively; Fig. 2.4). A_n changed seasonally, with large fluctuations in response to change in *I* (Figs. 2.2 and 2.5). On sunny days, A_n gradually decreased from 0 to 90 days, increased from 90 to 230 days, and then decreased to 200 mmol m^{-2} d^{-1}.

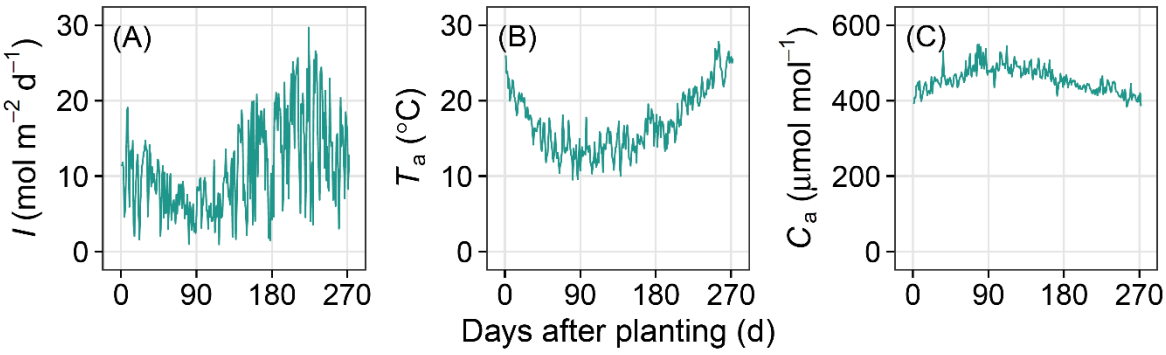

Figure 2.2 Changes in daily cumulative photosynthetic photon flux density *I* (A), daily average temperature T_a (B), and daily average CO_2 concentration (C) measured at a fixed point in the center of a greenhouse throughout the experimental period (October 3, 2019–June 30, 2020).

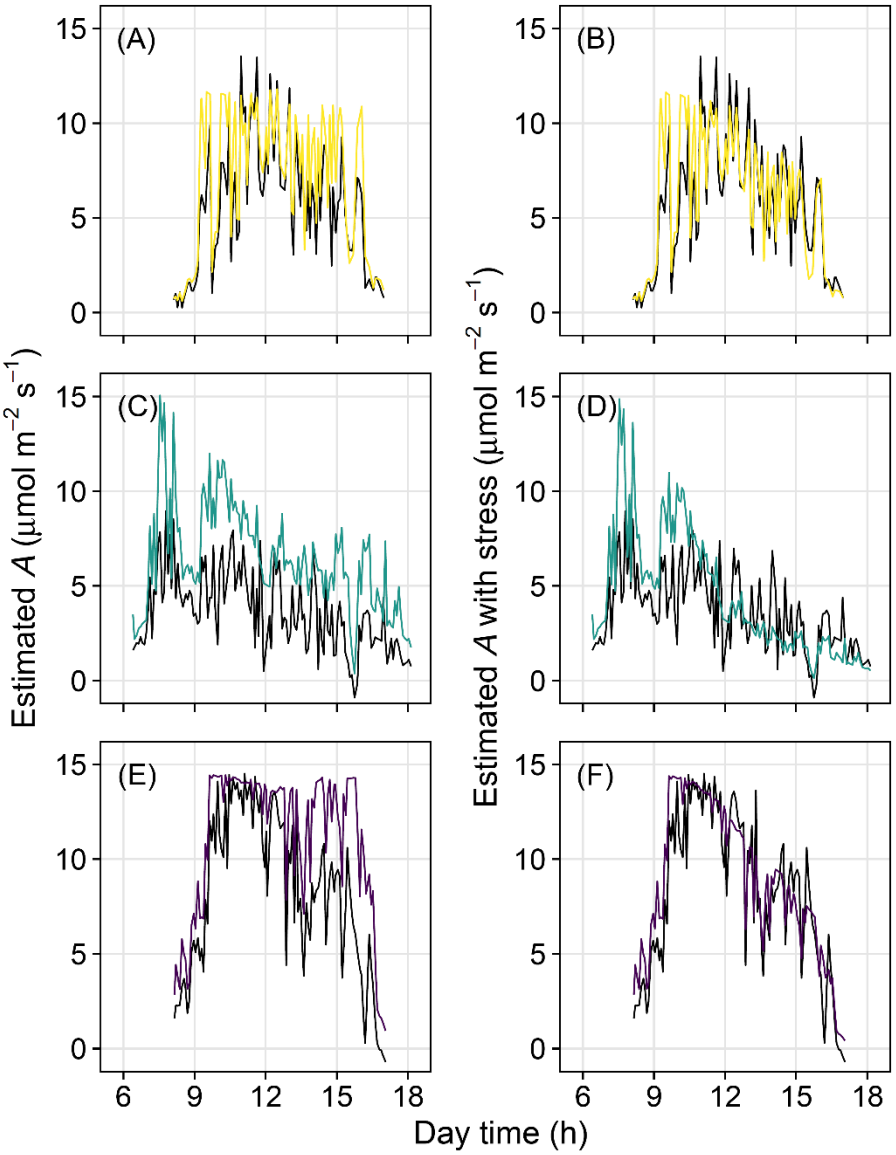

Figure. 2.3 Diurnal changes in measured and estimated photosynthetic rate (*A*) for cased without (A, C, E) and with consideration of environmental stresses (B, D, F) on May 22, 2021, October 28, 2021, and January 12, 2022. The black solid line denotes the measured *A*, and the colored solid line denoted the estimated *A* (yellow: January 12, 2022; blue: May 22, 2021; purple: October 28, 2021).

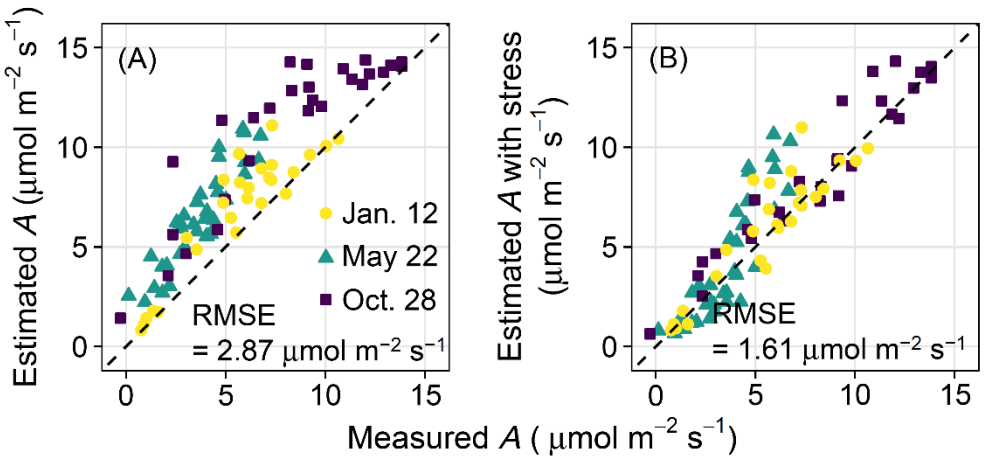

Figure. 2.4 Relationship between the measured and estimated photosynthetic rate (A) for cased without (A) and with consideration of environmental stresses (B) on May 22, 2021, October 28, 2021, and January 12, 2022. The dashed line denotes a one-to-one relationship. The mean values of the photosynthetic capacities ($V_{cmax,25}$ and $J_{max,25}$; n = 5) and stomatal characteristics (g_0 and g_1) estimated using the gas exchange measurements were used.

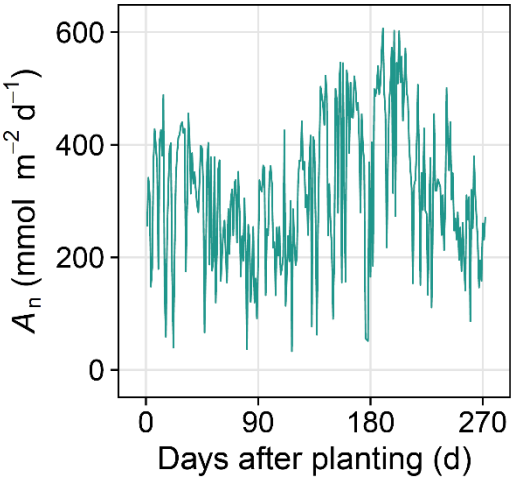

Figure. 2.5 Change in daily cumulative photosynthetic rate (A_n) estimated using biochemical photosynthesis model parameters, including the measured maximum carboxylation rate (V_{cmax}) and maximum electron transport rate (J_{max}), environmental factors inside a greenhouse, and environmental stresses throughout the experimental period (October 3, 2019–June 30, 2020).

2.3.2. Daily dynamics of reproductive growth

A FL_t wave was followed by a FR_t wave and a H_t wave (Fig. 2.6A). These three waves occurred three times during the cultivation period, and these groups were regarded as the first, second, and third inflorescences, respectively. In the first inflorescence, the waves of flowering, fruit setting, and harvesting were close to Gaussian and occurred 45 to 101, 52 to 108, and 89 to 150 days after planting, respectively. The waves of the second inflorescence were skewed to the left compared with the first and occurred at 108 to 180, 119 to 195, and 157 to 213 days, respectively. The waves of the third inflorescence occurred at 183 to 249, 189 to 255, and 215 to 270 days, respectively, and took the form of Gaussian distributions. The maximum values of these waves of the third inflorescence were smaller, and the variation increased compared with those of the first inflorescence. Waves of NFL_t, NFR_t, and NH_t were observed periodically (Fig. 2.6B). In the first inflorescence, maximum values for NFL_t (2.1), NFR_t (6.6), and NH_t (6.7) were recorded of the 70, 92, and 150 days, respectively. The maximum NFL_t was smaller than the maximum NFR_t because the number of days from flowering to fruit set was shorter than that from fruit set to harvest, and fruit set started before all flowers had opened. In the second inflorescence, maximum values for NFL_t (1.8), NFR_t (6.1), and NH_t (6.4) were recorded of the 161, 175, and 213 days. In the third inflorescence, maximum values for NFL_t (1.0), NFR_t (4.4), and NH_t (6.1) were recorded of the 217, 232, and 270 days, respectively.

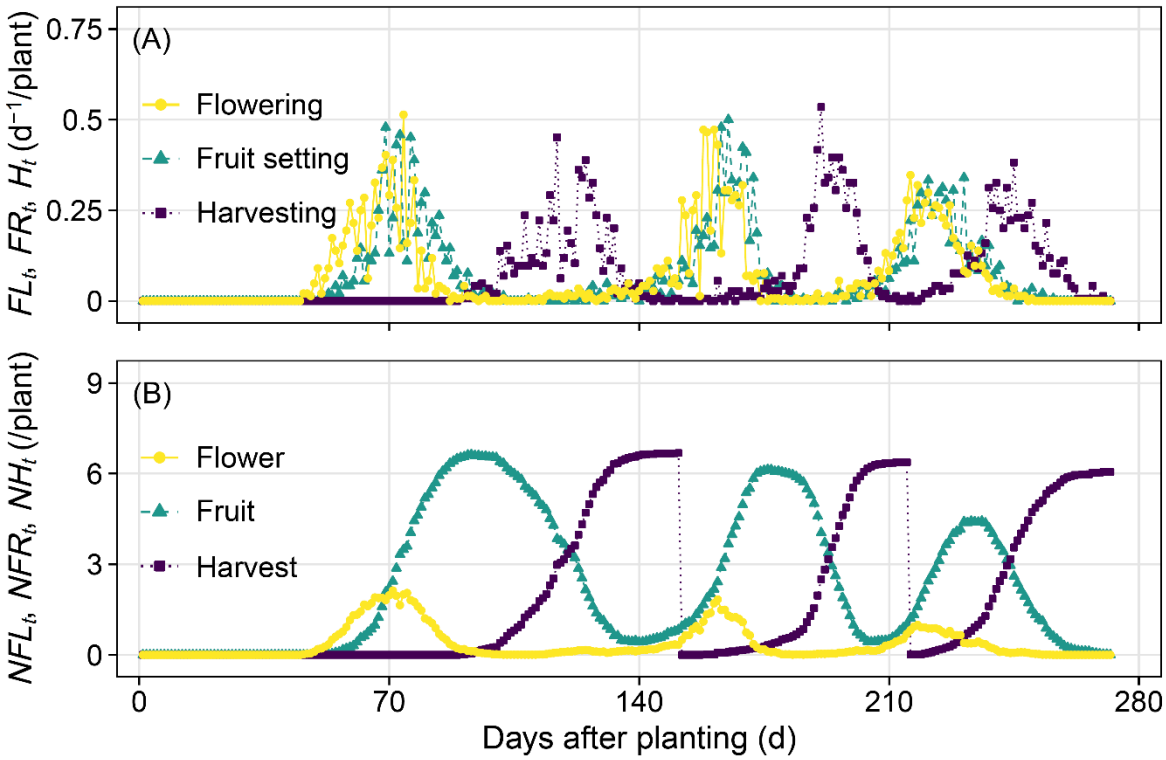

Figure. 2.6 Daily dynamics of the rate of flowering (FL_t; yellow circle), fruit set (FR_t; blue circle), and harvesting (H_t; purple circle) (A), and the daily dynamics of the number of flowers (NFL_t; yellow circle), fruits (NFR_t; blue circle), and harvests (NH_t; purple circle) in each inflorescence (B) per plant throughout the cultivation period (October 3, 2019–June 30, 2020). The number of flowers, number of fruits, and cumulative harvest at each date was estimated using Eqs. 2.19–2.21.

2.3.3. Days to harvesting, light, temperature, and photosynthesis for each inflorescence and fruit position

The mean days to harvesting (HD) in the first, second, and third inflorescences was 51.75, 34.91, and 23.2 days, respectively. Thus, HD shortened with as inflorescence advanced (Fig. 2.7). The mean HD changed among the primary, secondary, and tertiary fruit positions in the first (48.7, 50.8, and 53.0 days, respectively), second (40.1, 35.7, and 33.3 days, respectively), and third (22.8, 22.9, and 23.5 days, respectively) inflorescence. However, the distribution of HD in the primary and secondary fruit positions in the second inflorescence was

wider than that in the other inflorescences. I_A increased from 6.2 to 16.4 mol m^{-2} d^{-1} as growth progressed (Figs. 2.8A to C). Although the mean I_A changed among the primary, secondary, and tertiary fruit positions in the first (6.3, 6.1, and 6.2 mol m^{-2} d^{-1}, respectively) and second inflorescence (12.6, 13.0, and 13.4 mol m^{-2} d^{-1}, respectively), no significant difference was detected in third inflorescence (16.6, 16.6, and 16.2 mol m^{-2} d^{-1}, respectively). $T_{a,A}$ of each fruit in the first, second, and third inflorescence increased as I_A increased (13.2°C, 16.0°C, and 21.1°C, respectively; Figs. 2.8D to F). The mean $T_{a,A}$ also changed among the fruit positions in the first (13.3°C, 13.1°C, and 13.2°C, respectively), second (15.6°C, 15.9°C, and 16.2°C, respectively), and third (20.2°C, 20.7°C, and 21.5°C, respectively) inflorescence. I_C increased in the order of the second, third, and first inflorescence, and the mean values were 458.9, 380.6, and 322.0 mol m^{-2}, respectively (Figs. 2.8G to I). Although the mean I_C changed among the fruit positions in the first (306.1, 311.8, and 331.5 mol m^{-2}, respectively) and second inflorescence (500.1, 462.7, and 447.4 mol m^{-2}, respectively), no difference was detected in the third inflorescence (378.5, 380.2, and 381.4 mol m^{-2}, respectively). The I_C distribution in the primary and secondary fruit position in the second inflorescence was wider than that in the other inflorescences. Unlike I_C, $T_{a,C}$ decreased as growth progressed, and the mean values in the first, second, and third inflorescence were 682.8, 557.9, and 488.0°C d, respectively (Figs. 2.8J to L). The mean $T_{a,C}$ also changed among the fruit positions in the first (645.5, 665.8, and 701.4°C d, respectively), second (619.9, 564.3, and 540.3°C d, respectively), and third (458.5, 474.4, and 503.8°C d, respectively) inflorescence. Similar to I_C, the distribution of $T_{a,C}$ in the primary and secondary fruit position in the second inflorescence was wider than that in the others.

$A_{n,A}$ increased from 195.1 to 358.7 mmol m^{-2} d^{-1} as growth progressed, and the same trend was detected for I_A and $T_{a,A}$ (Figs. 2.9A to C). In contrast, mean $A_{n,A}$ in the fruit position was similar within the first (198.0, 195.1, and 195.9 mmol m^{-2} d^{-1}, respectively), second (304.9, 313.1, and 323.4 mmol m^{-2} d^{-1}, respectively), and third (358.7, 358.6, and 354.7 mmol m^{-2} d^{-1}, respectively) inflorescence. $A_{n,C}$ was stable among different inflorescences and fruit, with means values of 10.14, 11.05, and 8.28 kmol m^{-2} for the first, second, and third inflorescences respectively (Figs. 2.9D to F). Similar to I_C and $T_{a,C}$ (Fig. 2.8), the distribution of $A_{n,C}$ in the primary and secondary fruit position in the second inflorescence was wider than that in the others.

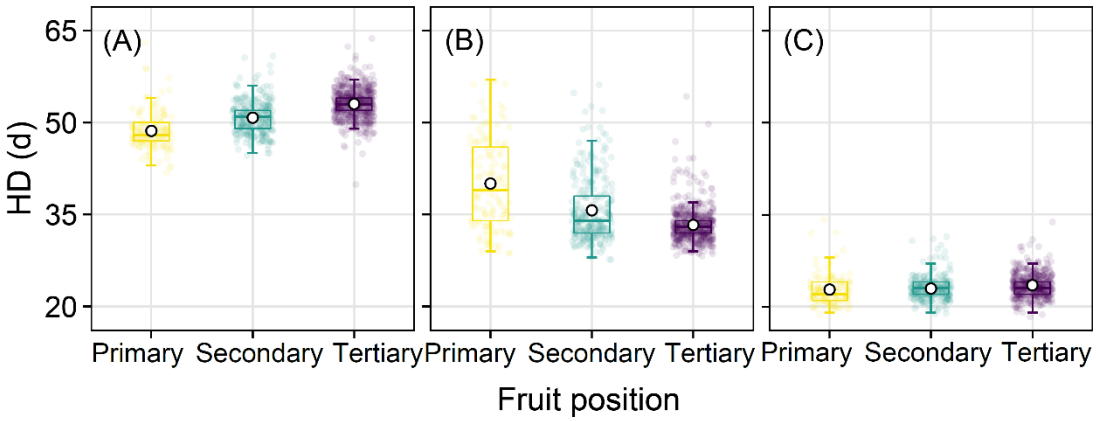

Figure. 2.7 Days to harvest (HD) in each inflorescence and each fruit position. Each row indicates inflorescence (A: 1st; B: 2nd; C: 3rd). In the boxplots, the boxes indicate the 25th percentile to the 75th percentile, and the median is shown by a line within the box. The whiskers extend to 1.5 times the interquartile range from the 25th and 75th percentiles. Mean values are represented by white circles.

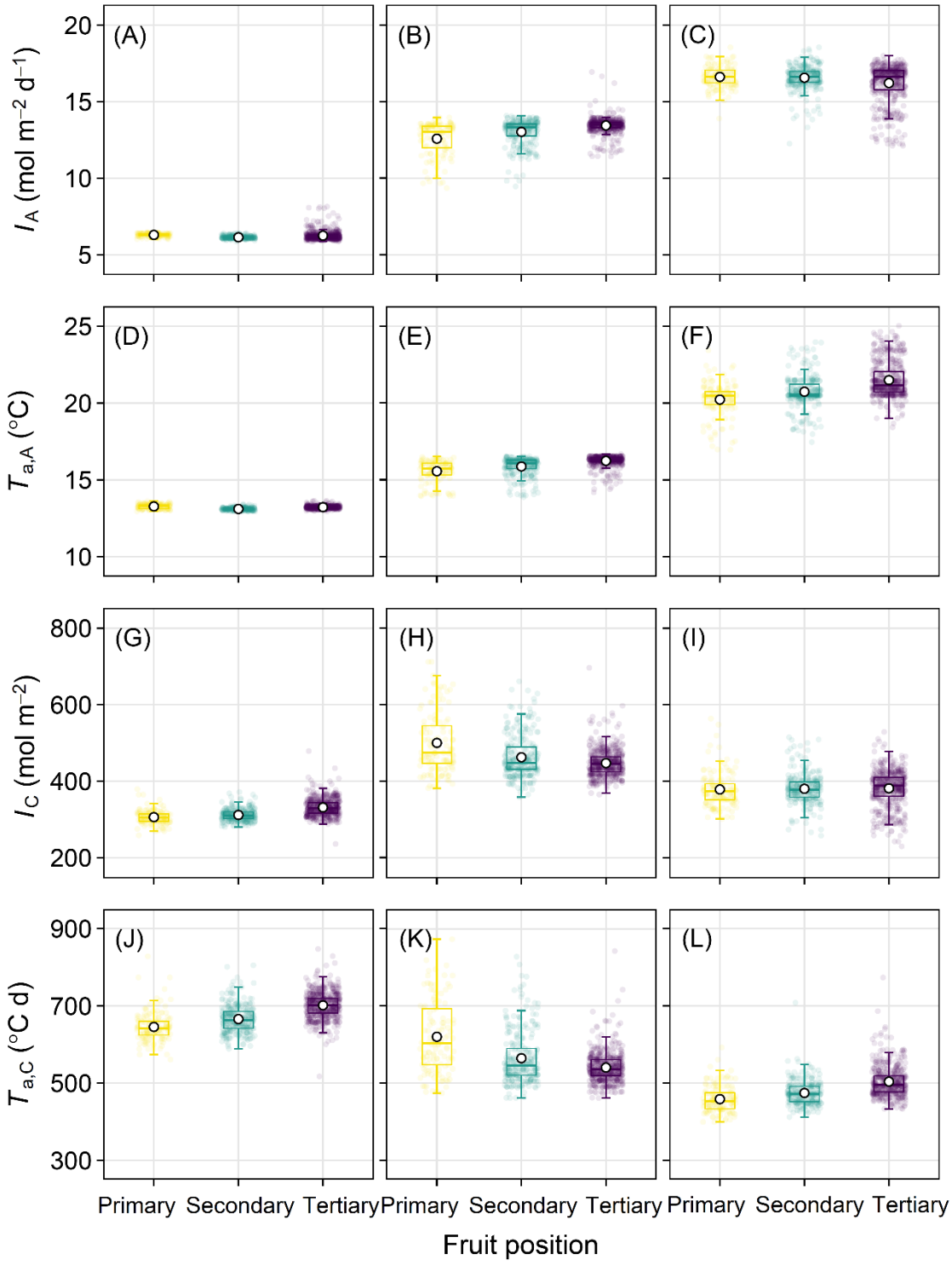

Figure. 2.8 Average and cumulative values of daily cumulative PPFD and daily average temperature from flowering to harvesting in each inflorescence and each fruit position (I_A, I_C, $T_{a,A}$, and $T_{a,C}$, respectively). Each row indicates inflorescence (A, D, G, J: 1st; B, E, H, K: 2nd; C, F, I, L: 3rd). In the boxplots, the boxes indicate the 25th percentile to the 75th percentile, and the median is shown by a line within the box. The whiskers extend to 1.5 times the interquartile range from the 25th and 75th percentiles. Mean values are represented by white circles.

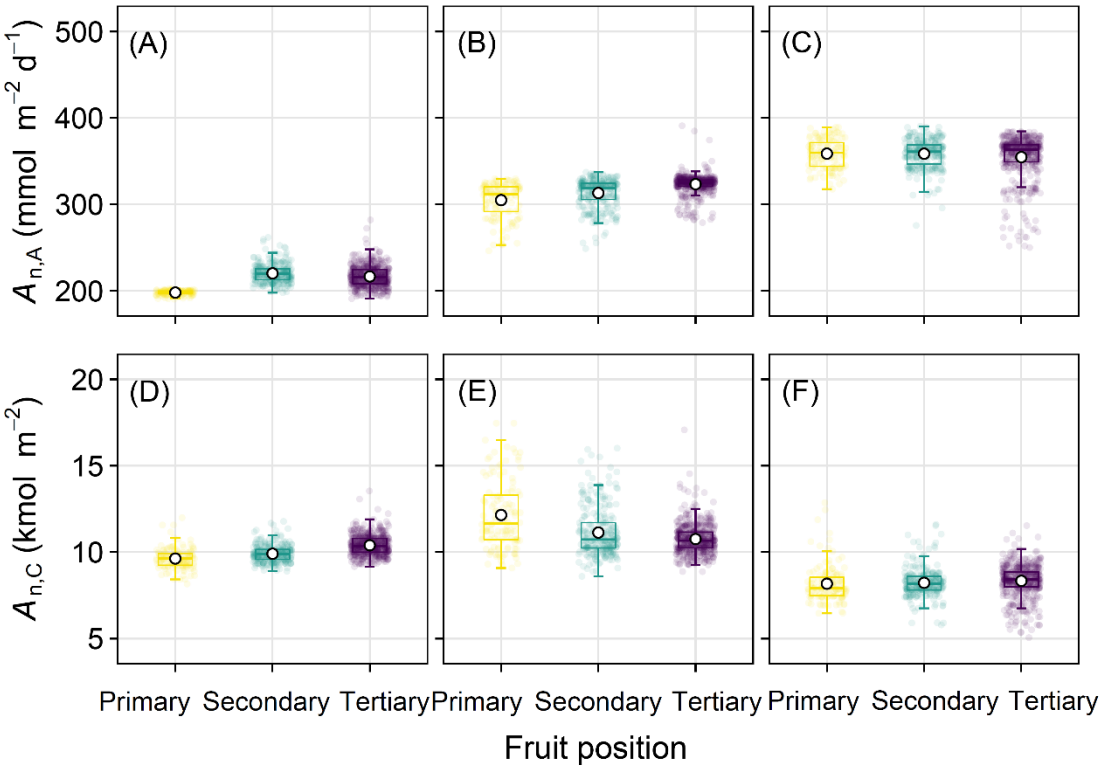

Figure. 2.9 Average and cumulative values of the daily integral of leaf photosynthesis from flowering to harvesting per fruit per inflorescence ($A_{n,A}$ and $A_{n,C}$, respectively). Each row indicates inflorescence (A, D: 1st; B, E: 2nd; C, F: 3rd). In the boxplots, the boxes indicate the 25th percentile to the 75th percentile, and the median is shown by a line within the box. The whiskers extend to 1.5 times the interquartile range from the 25th and 75th percentiles. Mean values are represented by white circles. Mean values are represented by white circles.

2.3.4. Comparison of determining degrees among each predictive index on fruit harvest

The D values of I_C, $T_{a,C}$, and $A_{n,C}$ were 0.149, 0.145, and 0.139, respectively, and the D value of $A_{n,C}$ was significantly smaller than that for others (Table 2.2). As shown in the third and fourth rows of panels in Fig. 2.8 and in the second row of panels in Fig. 2.9, the average values of each index were 386.2 mol m^{-2}, 579.4°C d, and 9.9 kmol m^{-2}, respectively, and the standard deviations were 70.2 mol m^{-2}, 94.8°C d, and 1.5 kmol m^{-2}, respectively.

Table 2.2 Determining degree (D) among each predictive index [*i.e.*, cumulative values of daily integral of PPFD, daily average of temperature, and daily integral of leaf photosynthesis (I_C, $T_{a,C}$, and $A_{n,C}$, respectively)] in all inflorescences. Different letters indicate significant differences ($p < 0.001$) as determined by a Steel–Dwass test.

	I_C	$T_{a,C}$	$A_{n,C}$
D value	0.149^b	0.145^b	0.139^a

2.4. Discussion

2.4.1. Relationships of light intensity, temperature, and leaf photosynthesis with strawberry reproductive growth

In this study, all environmental factors inside the greenhouse, leaf photosynthetic rate, and the dynamics of flowering, fruit setting, and harvesting changed markedly throughout the cultivation period (Figs. 2.2, 2.5, and 2.6). The increases in I_A, $T_{a,A}$, and $A_{n,A}$ with growth progression accelerated fruit harvest timing (Figs. 2.7–2.9). Although several studies have shown that using such relationships to control the environment inside a greenhouse can effectively promote reproductive growth (Hidaka *et al*., 2014, 2016, 2022; Yoneda *et al*., 2020), some studies have reported that extremely low or high temperatures adversely affect strawberry reproductive growth (Ledesma *et al*., 2008; Ledesma and Kawabata, 2016; Ariza *et al*., 2015). For example, Cui *et al*. (2021) found that short periods of high (35°C) and low temperatures (2°C) decreased strawberry pollen viability and germination rate, increasing the rate of malformed strawberry fruits. My results are generally consistent with these studies (*i.e.*, the change in temperature within the appropriate range reduced HD), whereas an extremely low temperature suppressed reproductive growth (100 to 150 days after planting; Fig. 2.6). Thus, the distributions of HD, I_C, $T_{a,C}$, and $A_{n,C}$ in the primary and secondary fruit positions in the second inflorescence were likely wider due to differences in reproductive growth activity.

Photosynthesis is a fundamental biochemical process in crop production (Long *et al*.,

2006), and its relationship with reproductive growth has been previously reported (Choi *et al*., 2016; Hidaka *et al*., 2019). For example, Hidaka *et al*. (2016) found that the use of supplemental lighting increased the photosynthetic rate, number of flowers per inflorescence, and flowering, and these effects were further increased by elevated CO_2 concentration and temperature. Miyoshi *et al*. (2021) divided strawberry fruit growth into different developmental stages and revealed that white-ripening strawberry fruits, the developmental stage during which fruits begin to expand rapidly and increase greatly in size, had the highest translocation rate as well as the highest accumulation of photosynthates. Furthermore, I have discovered that the fruits respiration rate varies according to their developmental stages (Fig. 2.10; Ono *et al*., 2022). These studies and my findings suggest that eco-physiological functions, including photosynthesis, also affect strawberry reproductive growth. Additionally, the fruit-bearing history after the second inflorescence varied among plants due to different first inflorescence timings in fruit harvesting. Hence, individual fruit's photosynthate accumulation offers a more accurate description of harvest timing throughout cultivation, compared to light intensity or temperature as indices.

I examined various predictive HD indices in 2,752 strawberry fruits harvests and found that $A_{n,C}$ demonstrated superior accuracy while maintaining simplicity of sampling when compared to cumulative light and temperature, conventional indices. This is due to $A_{n,A}$ significantly changing in each inflorescence, whereas $A_{n,C}$ remained almost stable throughout the experimental period (Fig. 2.9). Although similar trends were observed for I_C and $T_{a,C}$ (Fig. 2.8), the D value of $A_{n,C}$ was significantly lower than that of other indices (Teble 2.2). Thus, when $A_{n,C}$ reaches a specific value, it would be possible to consistently determine whether strawberry fruits can be harvested. Describing the time from flowering to harvesting is essential in forecasting yield dynamics. Therefore, several studies have reported the cumulative values of light intensity or temperature from flowering as indices of harvest timing (Opstad *et al*., 2011; Krüger *et al*., 2012). Kawanobu *et al*. (2010) reported that the strawberry fruits were

harvested when cumulative solar irradiance and temperature from flowering to harvesting reached about 400 MJ m^{-2} d and 630°C d, respectively. Although my study is generally consistent with that of Kawanobu *et al*. (2010), they did not statistically compare and discuss the suitability of indices in terms of the variability of each cumulative value. Doan and Tanaka (2022) showed that mathematical models including cumulative solar radiation and temperature could accurately predict the reproductive growth of tomato clusters. However, their study differed from mine because solar radiation was used as an index of photosynthesis, and reproductive growth was not directly evaluated using photosynthesis. Hernandes-Santana *et al*. (2021) found that leaf turgor pressure was more linked to fruit development stage of olive fruits than photosynthesis. They also emphasized that photosynthesis is crucial in early fruit enlargement, while turgor pressure affects fruit ripeness. However, the cumulative leaf photosynthetic rate, which can be estimated continuously by models, can be a more useful index for predicting the harvest period than turgor pressure, which is continuously difficult to measure. Therefore, although my study does not necessarily support that photosynthesis drives fruit ripeness, I have demonstrated for the first time that $A_{n,C}$ can accurately predict the harvest timing of strawberry fruits as well as or even better than I_C and $T_{a,C}$.

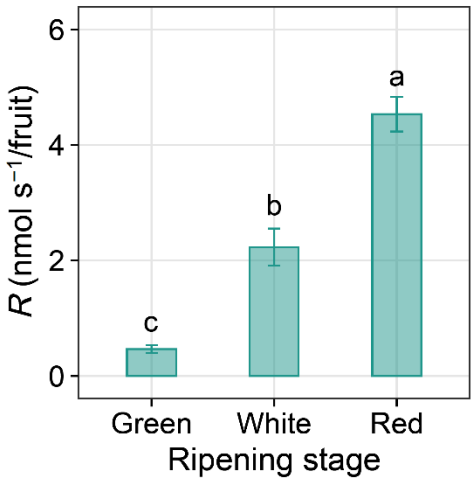

Figure. 2.10 Respiration rate per fruit (*R*) of intact strawberry fruits at different growth stages. Growth stage classified as green, white, and red stages: average fruit volume at each ripening stage was 2.22, 15.27, and 21.32 cm^3, respectively. The means ± *SE* ($n = 7$) are shown. Different letters indicate significant differences among different ripening stages with the Tukey–Kramer test ($p < 0.05$).

2.4.2. Implications for future research

I believe that the findings of this study can be applied to change strawberry production practices. In recent years, with the advent of image analysis technology, it is now possible to measure the number of flowers and fruits consistently over an extended period, even in large-scale cultivation (Chen *et al*., 2019; Abd-Elrahman *et al*., 2021). This is a promising development that will improve the data acquisition while reducing labor and costs. Furthermore, Kaneko *et al*. (2022) and Nomura *et al*. (2022) have shown that a hybrid ANN model, combining process-based and empirical models can accurately estimate the leaf photosynthetic rate. This model can be used to predict the leaf photosynthetic rate based on environmental factors, which are available from forecasts, without the need for periodic parameter measurements using expensive equipment. Given these advancements, in the near future, it will be possible to optimize fruit harvest timing and improve greenhouse management. For example, using a camera to acquire images and the hybrid ANN model to estimate the leaf photosynthetic

rate, it is possible to predict HD and optimize harvest timing by controlling the environment. This approach can be used to develop more efficient strawberry cultivation plans based on the photosynthesis and fruit-bearing histories of individual plants.

Although this study demonstrated that $A_{n,C}$ can be used as an accurate index for strawberry harvest timing, this study has a limitation. The reproductive growth dynamics were examined in strawberries grown under normal CO_2 concentrations. However, CO_2 enrichment can enhance crop growth, flowering, and yield by promoting photosynthesis (Hidaka *et al*., 2016; Miyoshi *et al*., 2017; Nomura *et al*., 2021). In this study, the dynamics of A_n showed the same tendency as I throughout the experimental period (Figs. 2.2 and 2.5) because the photosynthesis was largely dependent on light intensity; thus, there was little difference in the D values between I_C and $A_{n,C}$. Therefore, the usefulness of $A_{n,C}$ as a predictive index should be examined also under CO_2 enrichment conditions. Despite the limitation, my study represents progress toward realizing accurate forecasting and optimizing the reproductive growth dynamics required for efficient strawberry production.

2.5. Conclusion

In this chapter, I investigated the daily responses of strawberry fruit reproductive growth to the environmental factors inside a greenhouse and to leaf photosynthetic rate, which was simulated considering the environmental stresses, using a high number of samples throughout the entire cultivation period. Furthermore, I evaluated statistically whether leaf photosynthetic rate, in comparison to light intensity and temperature, was an appropriate index for the number of days from flowering to harvesting using determining degree values. In conclusion, determining degree analysis in each index showed that the D of $A_{n,C}$ was the lowest, suggesting that cumulative leaf photosynthetic rate from flowering could be a suitable index for predicting the days to harvest. The use of this method can contribute to more accurate

forecasting and optimization of fruit yield dynamics, which will in turn improve the efficiency of strawberry production. The above results will be used when extending from the flowering dynamics model to the harvest dynamics model.

Chapter 3

How the history of environmental factors and leaf photosynthetic rate influences the flowering dynamics?

3.1. Introduction

Strawberry fruits are usually harvested every 3 to 4 days throughout the cultivation period. Also, there are multiple high yield waves occurring throughout cultivation period (MacKenzie and Chandler, 2009; Fig. 2.5) and the unit price fluctuates significantly depending on the timing (Wu *et al*., 2015). Furthermore, it is known that delays in harvesting the strawberry fruits of the first inflorescence, which typically occurs in late November to December, can result in losses amounting to several million yen in Japan (personal communication). Therefore, to achieve the stable and planned production of strawberry fruits, it is essential to accurately predict and optimize the peak timing and extent of harvesting throughout the cultivation period. However, there are no examples of constructing predictive models focusing on environment and eco-physiological functions, especially in relation to the peak dynamics of yield. Hence, there is a need to develop predictive models for the flowering dynamics, which serve as crucial foundational information for harvest prediction.

Flowering represents the transition from vegetative growth to reproductive growth in a life cycle of plants and is a highly significant trait that influences fruit yield and quality through processes like pollination. It has been extensively reviewed in various crop species, *e.g*., tomato: Lozano *et al*. (2009); strawberry: Stewart and Folta (2010); Maize: Xu *et al*. (2012); citrus: Agusti *et al*. (2022). However, while modeling of flowering dynamics is actively pursued within the field of tree phenology (Pope *et al*., 2014; Sperling *et al*., 2019), there are no existing examples of modeling throughout the cultivation period, especially in the case of greenhouse-grown strawberries. This is believed to be due to the fact that the peak of strawberry

flowering dynamics not only occurs multiple times throughout the cultivation period but also is intricately controlled by environment and eco-physiological functions. Therefore, in order to construct predictive models for flowering dynamics, it is essential to thoroughly investigate how environment and eco-physiological functions influence the shape of these fluctuations.

In this chapter, I fitted the existing exponential sine equation to the flowering dynamics of greenhouse-grown strawberries obtained throughout the three cultivation periods and analyzed the relationship between the parameters, which represent the shape of the flowering dynamics, and the history of environmental factors and leaf photosynthetic rate.

3.2. Materials and methods

3.2.1. Plant materials and growth conditions

Similar to chapters 1 and 2, June-bearing strawberry plants (*Fragaria* × *ananassa* Duch. cv. Fukuoka S6) were used as the experimental crop for the three cultivation years. The nursery plants were grown in a greenhouse at the National Agriculture and Food Research Organization, Kyushu Okinawa Agricultural Research Center, Japan on June 6, 2019, June 11, 2020, and June 14, 2021. Two hundred and eighty-eight plants were transplanted to beds filled with culture soil (Good Soil; Kaneya Co., Ltd., Aichi Japan) in a greenhouse at the Ito Plant Experiment Fields & Facilities, Faculty of Agriculture, Kyushu University, Fukuoka, Japan (Fig. 1.1) on October 3, 2019, October 1, 2020, and September 24, 2021. The other growth conditions were like that in chapter 1.

3.2.2. Acquisition of environment, photosynthesis, and flowering dynamics

Similar to chapter 2, the environmental conditions (*i.e.*, photosynthetic photon flux density PPFD, temperature, relative humidity, CO_2 concentration, and wind speed) inside the greenhouse were measured and recorded at the same time intervals throughout the three cultivation periods using the same set of sensors and data logger. The obtaining of leaf photosynthetic rate and reproductive growth dynamics was also carried out throughout the cultivation periods using the methods described in chapter 2. The model parameters used for leaf photosynthetic rate estimation are listed in Tables 2.1, 3.1, 3.2 and Figs. 3.1, 3.2. Additionally, the flowering dynamics of the first inflorescence (FL_t) was daily obtained using a methodology similar to that described in Chapter 2.

Table 3.1 Physiological parameters used to estimate the leaf photosynthetic rate and stomatal conductance in strawberry leaves each month and year for 2020.

Parameter	Value	Unit	Reference
$V_{cmax,25}$	93.08	μmol m^{-2} s^{-1}	This study; Fig. 3.1A
$E_a(V_{cmax})$	85.17	kJ mol^{-1}	This study; Fig. 3.1A
$\Delta S(V_{cmax})$	0.65	kJ K^{-1} mol^{-1}	This study; Fig. 3.1A
$H_d(V_{cmax})$	200	kJ mol^{-1}	This study; Fig. 3.1A
$J_{max,25}$	221.60	μmol m^{-2} s^{-1}	This study; Fig. 3.1B
$E_a(J_{max})$	45.47	kJ mol^{-1}	This study; Fig. 3.1B
$\Delta S(J_{max})$	0.65	kJ K^{-1} mol^{-1}	This study; Fig. 3.1B
$H_d(J_{max})$	200	kJ mol^{-1}	This study; Fig. 3.1B
$K_{c,25}$	404.90	μmol mol^{-1}	Bernacchi *et al.* (2001)
$E_a(K_c)$	79.43	kJ mol^{-1}	Bernacchi *et al.* (2001)
$K_{o,25}$	278.40	mmol mol^{-1}	Bernacchi *et al.* (2001)
$E_a(K_o)$	36.38	kJ mol^{-1}	Bernacchi *et al.* (2001)
Γ^*_{25}	42.75	μmol mol^{-1}	Bernacchi *et al.* (2001)
$E_a(\Gamma^*)$	37.83	kJ mol^{-1}	Bernacchi *et al.* (2001)
$R_{n,25}$	1.46	μmol m^{-2} s^{-1}	This study
$E_a(R_n)$	53.50	kJ mol^{-1}	This study
g_0	0.03	mol m^{-2} s^{-1}	This study
g_1	3.15		This study

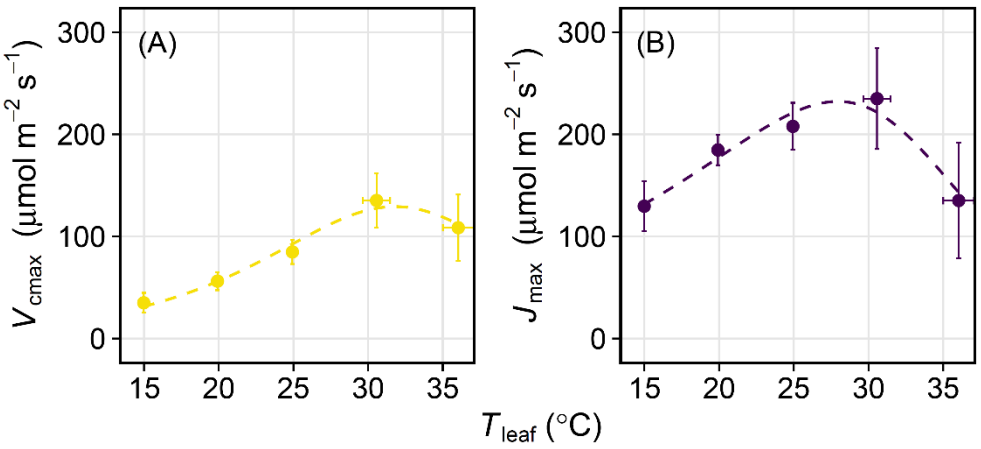

Figure 3.1 Relationships of the maximum carboxylation rate (V_{cmax}; A) and the maximum electron transport rate based on intercellular CO_2 concentration (J_{max}; B) with leaf temperature (T_{leaf}) for 2020. The dushed line is calculated from the fitting curve using Arrhenius function (Eq. 2.8). For, the parameters concerning the temperature dependencies of each variable, please refer to Table 3.1. Means ± *SD* (n = 7) are shown.

Table 3.2 Physiological parameters used to estimate the leaf photosynthetic rate and stomatal conductance in strawberry leaves each month and year for 2021.

Parameter	Value	Unit	Reference
$V_{cmax,25}$	80.72	μmol m^{-2} s^{-1}	This study; Fig. 3.2A
$E_a(V_{cmax})$	75.18	kJ mol^{-1}	This study; Fig. 3.2A
$\Delta S(V_{cmax})$	0.65	kJ K^{-1} mol^{-1}	This study; Fig. 3.2A
$H_d(V_{cmax})$	200	kJ mol^{-1}	This study; Fig. 3.2A
$J_{max,25}$	201.24	μmol m^{-2} s^{-1}	This study; Fig. 3.2B
$E_a(J_{max})$	65.37	kJ mol^{-1}	This study; Fig. 3.2B
$\Delta S(J_{max})$	0.66	kJ K^{-1} mol^{-1}	This study; Fig. 3.2B
$H_d(J_{max})$	200	kJ mol^{-1}	This study; Fig. 3.2B
$K_{c,25}$	404.90	μmol mol^{-1}	Bernacchi *et al.* (2001)
$E_a(K_c)$	79.43	kJ mol^{-1}	Bernacchi *et al.* (2001)
$K_{o,25}$	278.40	mmol mol^{-1}	Bernacchi *et al.* (2001)
$E_a(K_o)$	36.38	kJ mol^{-1}	Bernacchi *et al.* (2001)
Γ^*_{25}	42.75	μmol mol^{-1}	Bernacchi *et al.* (2001)
$E_a(\Gamma^*)$	37.83	kJ mol^{-1}	Bernacchi *et al.* (2001)
$R_{n,25}$	1.46	μmol m^{-2} s^{-1}	This study
$E_a(R_n)$	53.50	kJ mol^{-1}	This study
g_0	0.04	mol m^{-2} s^{-1}	This study
g_1	2.93		This study

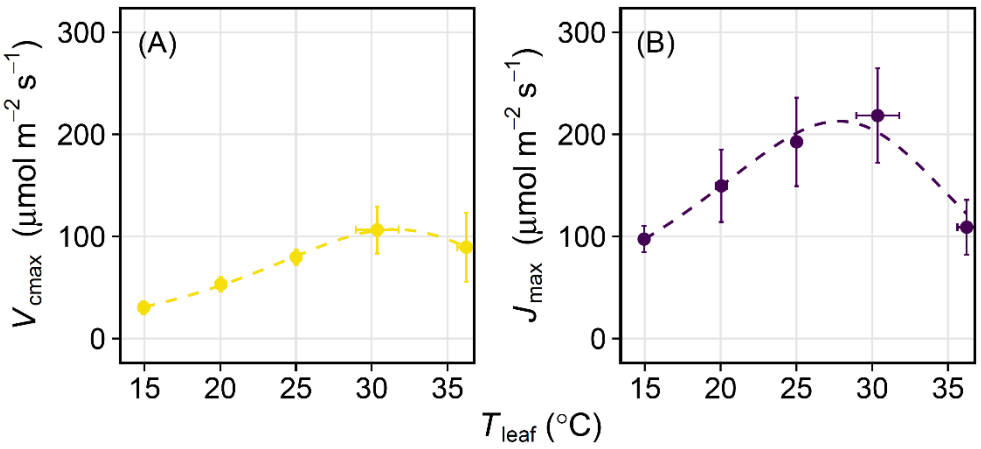

Figure 3.2 Relationships of the maximum carboxylation rate (V_{cmax}; A) and the maximum electron transport rate based on intercellular CO_2 concentration (J_{max}; B) with leaf temperature (T_{leaf}) for 2021. The dushed line is calculated from the fitting curve using Arrhenius function (Eq. 2.8). For, the parameters concerning the temperature dependencies of each variable, please refer to Table 3.1. Means ± *SD* (n = 7) are shown.

3.2.3. Applying exponential sine equation to flowering dynamics

The exponential sine equation (Malo, 2002; referred to as the Malo model) was employed to describe the flowering dynamics:

$$FL_t = a\{\sin[\pi((t-b)/c)^d]\}^e. \quad (3.2)$$

The Malo model has five parameters (*i.e.*, a, b, c, d, and e) and these parameters represent the peak height of FL_t, the start date of FL_t, the duration of the flowering period, the peak skewness of FL_t, and the peak kurtosis of FL_t, respectively (Fig. 3.3). The Malo model allows for characterizing FL_t with the minimal number of parameters. The model parameters a, b, and c for each cultivation period and fruit position could be determined from the observed data, while d and e could not be directly observed. Therefore, I fitted the Malo model to the observed FL_t in order to numerically characterize them. In this study, Bayesian optimization was conducted using GPyOpt package (version 1.2.6) in Python (version 3.10.11). This method employs a probabilistic model to guide the search for optimal parameters. It iteratively selects parameter sets, evaluates them, and updates the model to find the best configuration with minimum experimental effort. The optimization of the model parameters was carried out by treating the unfolding dynamics as a probability distribution.

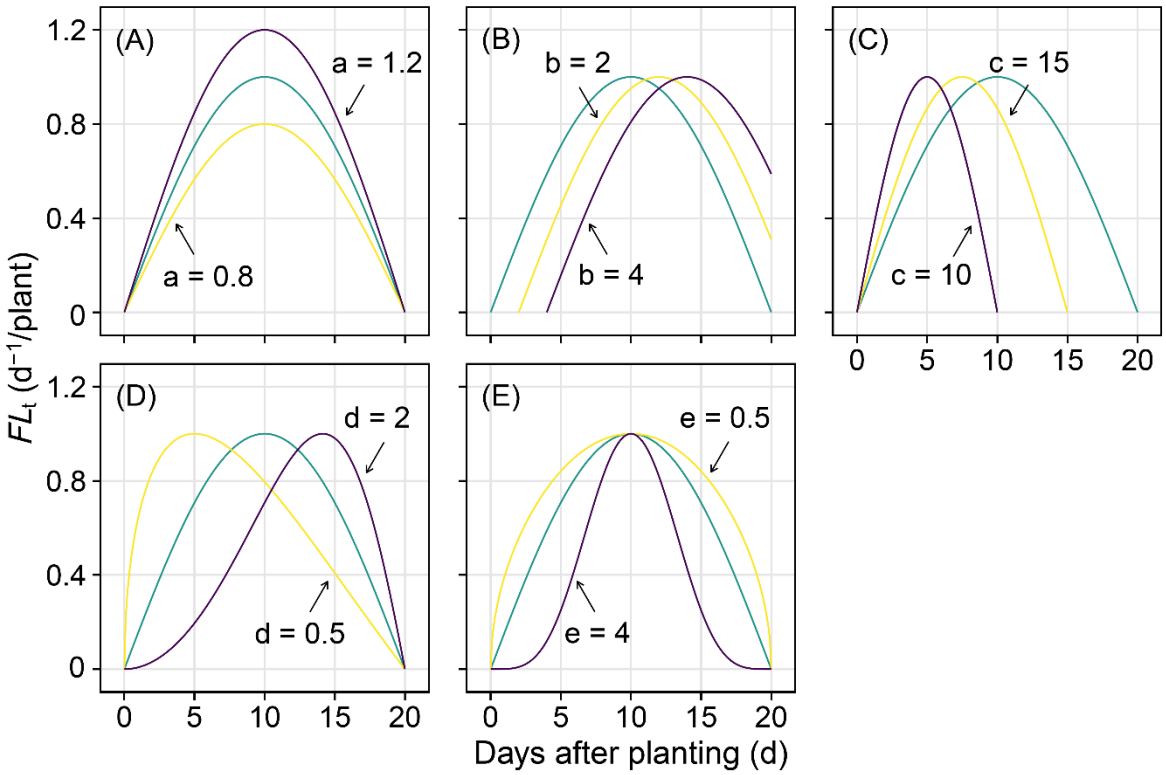

Figure 3.3 The influence of changes in each parameter (*a*, *b*, *c*, *d*, and *e*) of the Malo model on curve shape. Respective panels indicate the change in the shape of the curve when only one parameter is varied: only *a* (A), *b* (B), *c* (C), *d* (D), and *e* (E), respectively. The parameters in the blue curves in respective panels are set as follows: 1 for *a*, 0 for *b*, 20 for *c*, 1 for *d*, and 1 for *e*, respectively.

3.2.4. Analyzing the relationship of the shape of flowering dynamics with environment and photosynthesis

The reproductive growth dynamics of crops are significantly influenced by environment and eco-physiological functions spanning from past to present. Although various data analysis techniques have been employed in this field, they are not suitable for analyzing how far back in the past, for what duration of data, and in what way they influence the target variables. Therefore, I conducted an analysis using the utility functions to investigate how the historical data of environment and photosynthesis influence various parameters of flowering dynamics (Iwao *et al*., 2023). Illustrate the overview of the utility function analysis in Fig. 3.4.

This method represents the target variable (*i.e.*, each model parameter when fitting the Malo model to FL_t) as the cumulative value of z, which is the product of the utilities of each component (environmental factors and leaf photosynthetic rate) at a specific time, integrated over any desired time period. In this case, each model parameter can be expressed as follows:

$$P_{j,\mathrm{est}} = \sum_{j=1}^{n} z_j = \sum_{j=1}^{n} \prod_{i=1}^{l} f_i\left(x_{j,i,1}, \ldots, x_{j,i,m}\right), \tag{3.3}$$

where, $P_{j,\mathrm{est}}$ is the specific target parameter, j is the specific time (h), z_j is the utility of j, i is the specific factors number, $x_{\mathrm{j,i,m}}$ is the factor m of the i-th element at j, and $f_i(x_{j,i,1}, \ldots, x_{j,i,m})$ is the utility function of each factor. The parameters for the utility function of each factor were determined to make the following equation match:

$$f_i^{(t+1)}\left(X_{j,i}\right) = f_i^{t}\left(X_{j,i}\right) - \frac{\partial loss}{\partial f_i\left(X_{j,i}\right)}, \tag{3.4}$$

where $X_{\mathrm{i,j}}$ represents ($x_{j,i,1}$, …, $x_{j,i,m}$). Then, *loss* is the loss function as follow:

$$loss = \frac{1}{2}\sum_{k}(\hat{y}_k - y_k)^2 . \tag{3.5}$$

In this study, I used PPFD, temperature, air vapor deficit (*VPD*; which was calculated by temperature and relative humidity), and leaf photosynthetic rate as explanatory variables to investigate their impact on each parameter, which was defined by fitting the Malo model to the respective FL_t. Also, each explanatory variable was converted to hourly cumulative PPFD ($I_{\mathrm{C,h}}$), hourly averaged temperature ($T_{\mathrm{a,A,h}}$), hourly averaged *VPD* ($VPD_{\mathrm{,A,h}}$), and hourly cumulative leaf photosynthetic rate ($A_{\mathrm{n,C,h}}$), respectively.

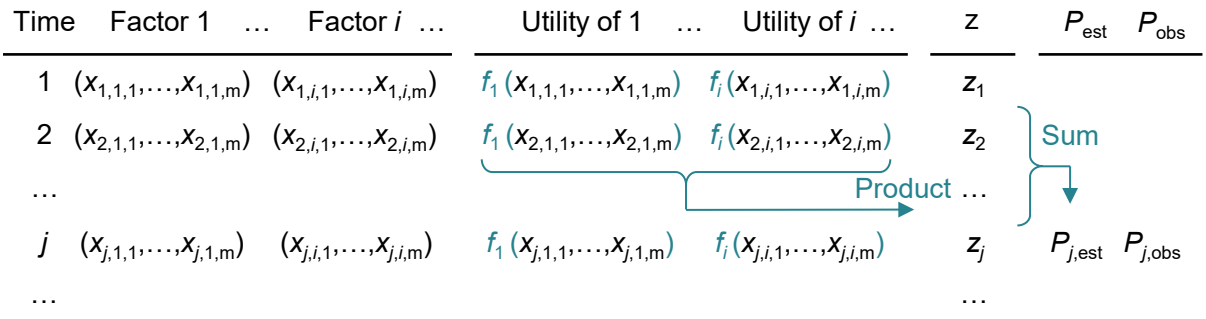

Figure 3.4 Graphical description of the utility function analysis.

3.3. Results

3.3.1. Environmental conditions and leaf photosynthetic rate

Similar to chapter 2, the environmental conditions inside the greenhouse exhibited consistent seasonal variations for 3 years (Fig. 3.5). On sunny days, I gradually decreased to 10 mol m^{-2} d^{-1} from 0 to 90 days and subsequently increased to 30 mol m^{-2} d^{-1} to 230 days, after which I decreased to 15 mol m^{-2} d^{-1} (Fig. 3.5A). T_a changed with I: it gradually decreased from 0 to 0 days as I decreased but was constant at 13°C from 90 to 180 days (Fig. 3.5B). Thereafter, T_a increased to 25°C as I increased. C_a increased to 500 µmol mol^{-1} from 0 to 80 days and then decreased to 400 µmol mol^{-1} (Fig. 3.5C). Similarly, A_n exhibited a consistent trend of change over the 3 cultivation periods (Fig. 3.6). A_n changed seasonally, with large fluctuations in response to change in I (Fig. 3.5A). On sunny days, although A_n gradually decreased from 0 to 90 days in all cultivation periods and reached to 200 mmol m^{-2} d^{-1}, it differently changed in from 90 days after planting. In the cultivation period of 2019, A_n increased to 600 mmol m^{-2} d^{-1} from 90 to 230 days, and then decreased to 300 mmol m^{-2} d^{-1}. In 2020, A_n similarly increased from 90 to 230days, reaching 600 mmol m^{-2} d^{-1}, and then remained relatively stable value. In 2021, it gradually increased from 90 to 230 days, reaching 500 mmol m^{-2} d^{-1}.

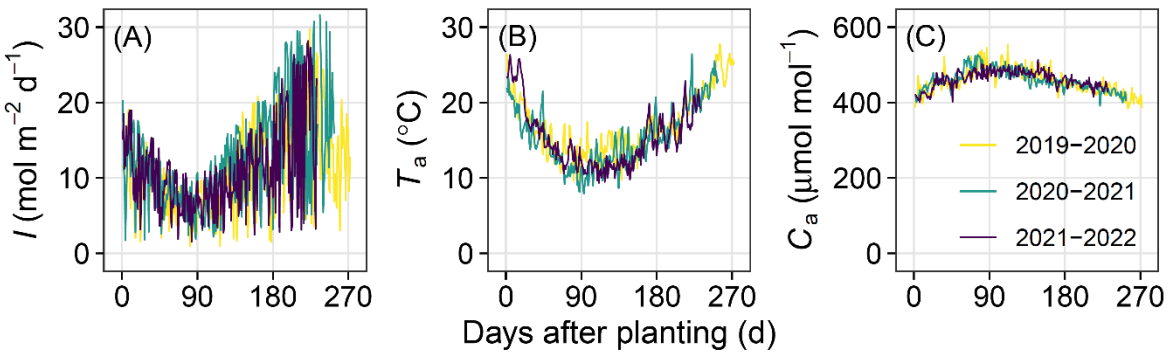

Figure 3.5 Changes in daily cumulative photosynthetic photon flux density I (A), daily average temperature T_a (B), and daily average CO_2 concentration (C) measured at a fixed point in the center of a greenhouse throughout the respective cultivation periods (yellow line: October 3, 2019–June 30, 2020; blue line: October 1, 2020–June 16, 2021; purple line: September 24, 2021–May 14, 2022).

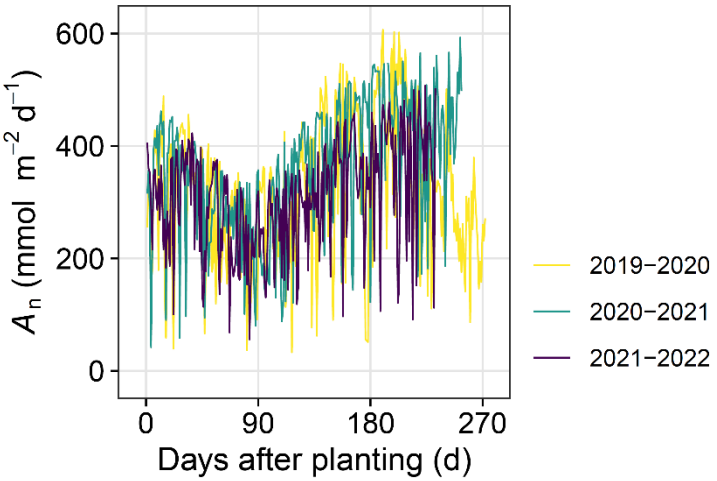

Figure 3.6 Changes in daily cumulative photosynthetic rate (A_n) estimated using biochemical photosynthesis model parameters, including the measured maximum carboxylation rate (V_{cmax}) and maximum electron transport rate (J_{max}), environmental factors inside a greenhouse, and environmental stresses throughout the respective cultivation periods (yellow line: October 3, 2019–June 30, 2020; blue line: October 1, 2020–June 16, 2021; purple line: September 24, 2021–May 14, 2022).

3.3.2. Daily flowering dynamics

FL_t of the first inflorescence exhibited generally similar trends during each cultivation period (2019, 2020, and 2021), and the initiation days were 47, 50, and 58 days after planting, respectively, while the termination days were 110, 106, and 110 days after planting, respectively (Fig. 3.7). In the 2019 cultivation period, FL_t for the primary, secondary, and tertiary fruit position occurred within periods ranging from 47 to 68, 55 to 81, and 62 to 110 days after planting, respectively (Fig. 3.7A). Also, the peak heights of FL_t for the primary, secondary, and tertiary fruit position were 0.19, 0.22 and 0.43 d^{-1}/plant, respectively, increasing in order of fruit position. Similarly, in the 2020 cultivation period, FL_t for the primary, secondary, and tertiary fruit position occurred within periods ranging from 50 to 63, 57 to 77, and 63 to 106 days after planting, respectively (Fig. 3.7B). However, the peak heights of the primary, secondary, and tertiary fruit position in the 2020 cultivation period exhibited a different trend in 2019, with values of 0.20 0.50, and 0.29 d^{-1}/plant, respectively. In this case, the peak heights followed the order of the primary, tertiary, and secondary fruit positions, showing a variation from the typical order. In the 2021 cultivation period, FL_t for the primary, secondary, and tertiary fruit position occurred within periods from 58 to 74, 62 to 93, and 70 to 110 days after planting, respectively (Fig. 3.7C). Additionally, similar to the 2019 cultivation period, the peak heights of the primary, secondary, and tertiary fruit position were 0.13, 0.33, and 0.37, respectively, increasing in order of fruit position.

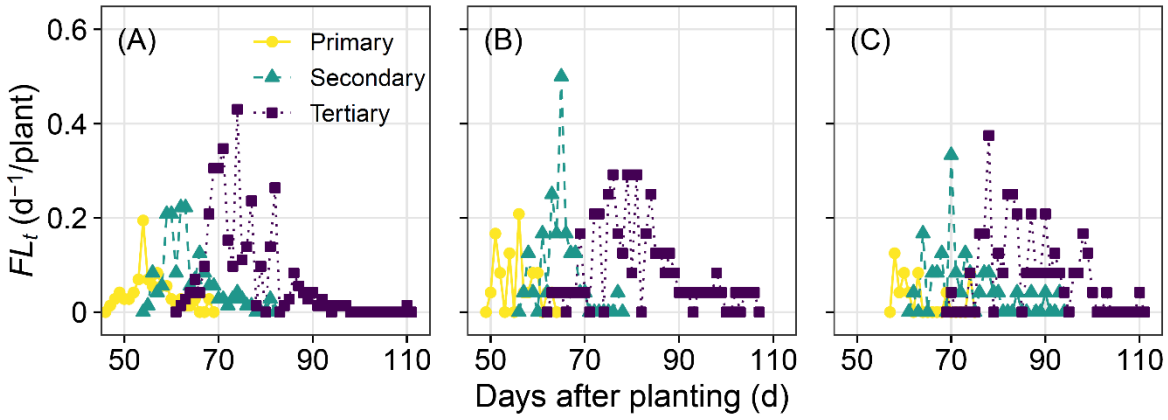

Figure 3.7 Daily dynamics of the flowering rate (FL_t) in first inflorescence and each fruit position for each cultivation period [*i.e.*, 2019 (A), 2020 (B), and 2021 (C), respectively]. The yellow circle, blue triangle, and purple square denote the primary, secondary, and tertiary fruit position, respectively.

3.3.3. Shape of flowering dynamics of each fruit position

The results of fitting the Malo model to FL_t in first inflorescence and each fruit position for the three cultivation periods (2019, 2020, and 2021) are presented in Fig. 3.8. The Malo model successfully reproduced FL_t in each cultivation period and fruit position relatively well. However, it should be noted that the shape of the Malo model, which fitted to FL_t for the primary fruit position in the 2021 cultivation season, differed from the others. Also, the model parameters (*a*, *b*, *c*, *d*, and *e*), which defined by fitted the Malo model to FL_t are presented in Table 3.3. The parameter *a*, *b*, and *c* did not exhibit significant differences based on the fruit position across each cultivation period, showing generally similar increasing trends. In strawberry plants, the primary, secondary, and tertiary fruit position have 1, 2, and 4 fruits, respectively. Thus, it is natural to observe an increase in parameters *a*, *b*, and *c* with the progression of fruit positions since fruits develop in order of their positions. On the contrary, although the parameter *d* for each fruit and cultivation period showed a significantly smaller value only for the primary fruit position in 2021, no notable trends were detected for the other

cases. No clear trend of parameter *e* was also observed in each cultivation period. However, lower values were noted, such as for the primary fruit position in 2021.

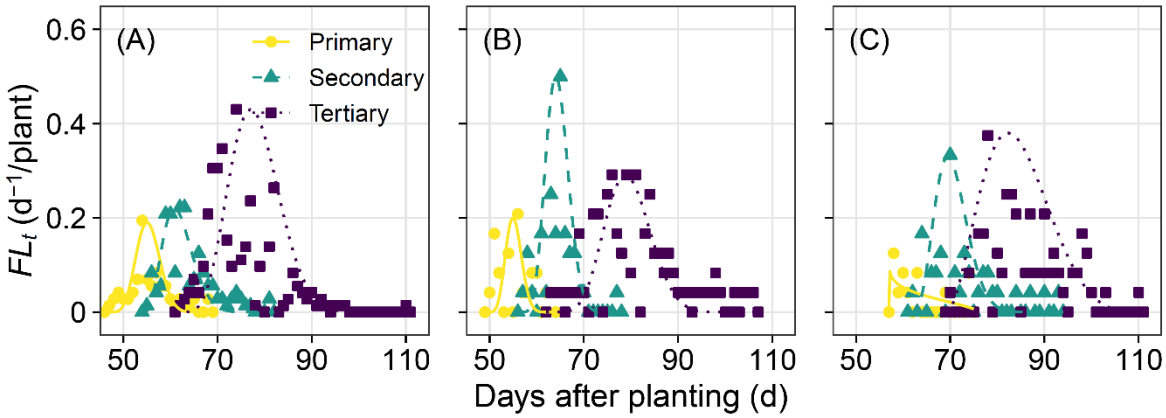

Figure 3.8 Result of fitting the Malo model for the flowering dynamics (FL_t) in first inflorescence and each fruit position for each cultivation period [*i.e.*, 2019 (A), 2020 (B), and 2021 (C), respectively]. The yellow circle, blue triangle, and purple square denote the primary, secondary, and tertiary fruit position, respectively.

Table 3.3 Malo model parameters (*a*, *b*, *c*, *d*, and *e*) fitted to the flowering dynamics in first inflorescence for three cultivation periods (2019, 2020, and 2021).

Year	Parameter	Primary	Secondary	Tertiary
2019	*a*	0.19	0.22	0.43
	b	46.00	54.00	61.00
	c	24.00	29.00	51.00
	d	0.71	0.48	0.60
	e	10.00	8.31	10.00
2020	*a*	0.20	0.50	0.29
	b	49.00	56.00	62.00
	c	16.00	23.00	46.00
	d	0.70	0.66	0.69
	e	10.00	10.00	10.00
2021	*a*	0.13	0.33	0.38
	b	57.00	61.00	69.00
	c	19.00	34.00	43.00
	d	0.04	0.50	0.59
	e	0.60	10.00	3.60

3.3.4. Utility among the history of environmental factors and leaf photosynthetic rate to flowering dynamics

The utility of $I_{C,h}$, $T_{a,A,h}$, $VPD_{A,h}$, and $A_{n,C,h}$ for each parameter (*b*, *c*, *d*, and *e*) changed in intensity in the three cultivation periods (Fig. 3.9). The utility for *b* was mainly influenced by $I_{C,h}$ and $A_{n,C,h}$ (> 0 mmol m^{-2} h^{-1}) emerging as the key determining factors (Figs. 3.9A, E, I, M). The average values for each utility were 0.55, 0.27, 0.11, and 0.21 (0.41 in the case of $A_{n,C,h}$ > 0 mmol m^{-2} h^{-1}), respectively. The utility for *c* was influenced not only by $I_{C,h}$ and $A_{n,C,h}$ (> 0 mmol m^{-2} h^{-1}) but also by $VPD_{A,h}$ (Figs. 3.9B, F, J, N). The average values for each utility were 0.66, 0.35, 0.77, and 0.24 (0.41 in the case of $A_{n,C,h}$ > 0 mmol m^{-2} h^{-1}), respectively. For *d*, in addition to $T_{a,A,h}$, the utility of $VPD_{A,h}$ was also high (Figs. 3.9C, G, K, O). The average values for each utility were 0.03, 0.43, 0.54, and 0.15 (0.32 in the case of $A_{n,C,h}$ > 0 mmol m^{-2} h^{-1}), respectively. Moreover, in this context, the utility of $VPD_{A,h}$ increased with higher $VPD_{A,h}$ values. For *e*, the utility was high for $T_{a,A,h}$, $VPD_{A,h}$, and $A_{n,C,h}$ (> 0 mmol m^{-2} h^{-1}) (Figs. 3.9D, H, L, P). The average values for each utility were 0.30, 0.59, 0.86, and 0.29 (0.57 in the case of $A_{n,C,h}$ > 0 mmol m^{-2} h^{-1}), respectively. Additionally, in contrast to the case of *d*, the utility increased with lower $VPD_{A,h}$ values.

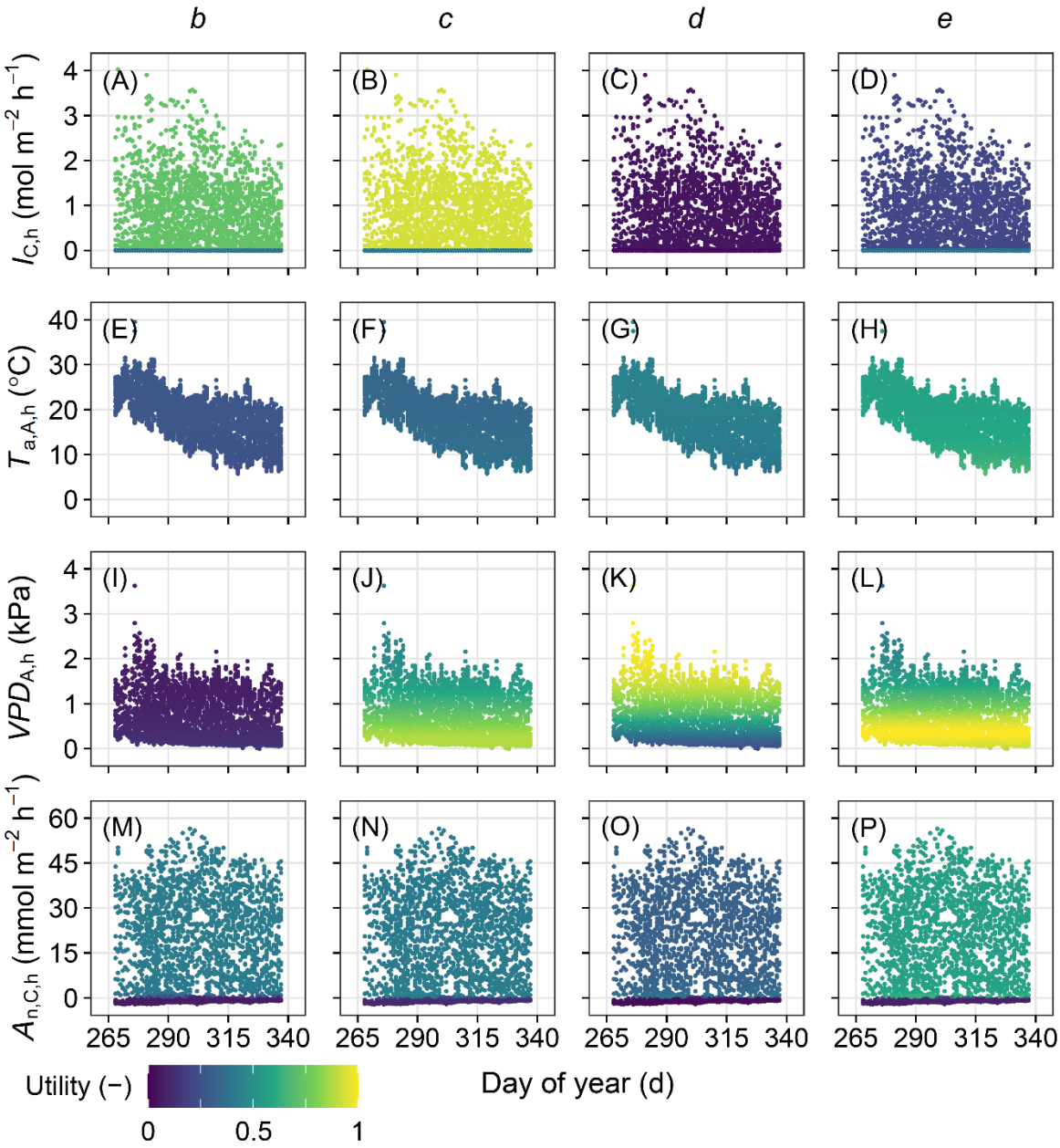

Figure 3.9 Changes in the utility of hourly cumulated photosynthetic photon flux density ($I_{C,h}$; A, B, C, D), hourly averaged temperature ($T_{a,A,h}$; E, F, G, H), hourly average vapor pressure deficit ($VPD_{A,h}$; I, J, K, L), and hourly cumulated photosynthetic rate ($A_{n,C,h}$; M, N, O, P) on the flowering dynamics of the first inflorescence across three cultivation period s. Each column represents the utility associated with various parameters when fitting the flowering dynamics with the exponential sine equation (Malo, 2002), denoted by the parameters: start date (*b*; A, E, I, M), duration (*c*; B, F, J, N), skewness (*d*; C, G, K, O), and kurtosis (*e*, D, H, L, P). The color of each plot indicates the magnitude of utility for the respective parameters.

3.4. Discussion

3.4.1. Influences of environmental factors and leaf photosynthetic rate on the flowering dynamics

In this study, I obtained daily data of environmental conditions inside the greenhouse and photosynthesis over the three cultivation periods (Figs. 3.5, 3.6). Throughout each cultivation period, FL_t of the first inflorescence exhibited generally similar trends during each cultivation period (Fig. 3.7). In addition, FL_t observed in each year and fruit position were quantified by fitting the Malo model, and this allowed me to numerically characterize the shape of flowering dynamics, which dynamically varies, influenced by various factors (Figs. 3.8 and 3.9; Table 3.3). In general, although the model fitting was successful for almost all flowering dynamics, there were cases where the accuracy in representing the actual flowering dynamics was notably low (Fig. 3.8C). This result is considered to be due to a small number of measured fruits and the significant deviation of flowering dynamics from a normal distribution shape.

The start date and rate of flowering in many crops are known to be influenced by various environmental factors in a complex manner. For example, Hidaka *et al*. (2016) reported that the flowering initiation of each inflorescence was accelerated through supplement light treatment with elevated CO_2 concentration and temperature in strawberries. Additionally, Kobayashi *et al*. (2010) revealed, through analysis using a generalized linear model in rise, that solar radiation, temperature, and vapor pressure deficit significantly impact the onset of flowering. Furthermore, Bakker (1989) observed a positive correlation between nighttime vapor pressure deficit (< 1 kPa) and the number of flowers in bell peppers. The above results suggest similar trends for the influence of each environment ($I_{C,h}$, $T_{a,A,h}$, and $VPD_{A,h}$) and eco-physiological function ($A_{n,C,h}$) obtained in this study on the parameters b (start date) and c (duration) of the Malo model fitting to FL_t at each cultivation period and fruit position (Fig. 3.9A, B, E, F, I, J, M, N). In other words, the environmental condition, which does not impose

drought stress on the gas exchange of strawberry leaves, likely led to the promotion of photosynthetic products accumulation, and in turn, this would have resulted in the increased development of terminal flowers and a higher flowering rate. Furthermore, regarding the parameter *d* (skewness) influencing the characteristics of the peak in FL_t, a significant impact was observed from both $T_{a,A,h}$, and high values of $VPD_{A,h}$ (Fig 3.9C, G, K, O). The influence on parameter *d* with $VPD_{A,h}$ exhibited opposite behavior compared to the case of parameter *c*. It is suggested that drought stress, by hindered flowering and acted to synchronize the flowering of many plants during the same timing. Similarly, for the parameter *e* (kurtosis) influencing the peak, it was dominantly impacted by $T_{a,A,h}$, low lebel of $VPD_{A,h}$, and $A_{n,C,h}$ (Fig. 3.9D, H, L, P). The influence of $VPD_{A,h}$ on parameter *e* showed a similar trend to that of parameter *c* (Fig. 3.9J). It is suggested that the relatively low environmental stress influenced uniform flowering distribution. In summary, analyzing the influence of the history of environment and eco-physiological functions as a foundation for the yield predictive model on the FL_t of the first inflorescence based on the utility functions revealed that *VPD* strongly impact the characteristics of the flowering peak.

3.4.2. Implications for future research

In this study, I focused on the flowering dynamics of only the first inflorescence during the three cultivation periods and analyzing its relationship with the history of environment and eco-physiological functions. However, for the modeling of flowering dynamics and, consequently, the construction of predictive models for yield dynamics, a more comprehensive analysis is necessary. In strawberries, flowering and harvesting occur alternately and periodically throughout the cultivation period (Fig. 2.6; MacKenzie and Chandler, 2009). During this consideration, one crucial factor to take into account is the variation in fruit load. Fruit load, indicating how much fruits the plant holds at given point, is crucial index that

significantly influences the distribution dynamics of photosynthates from leaves to fruits (Edwards *et al*., 2010). Since strawberries undergo a cycle of (1) an increase in fruit load due to flowering and fruit growth, (2) a decrease in fruit load due to harvesting, and (3) triggering of the flowering of next inflorescence as a result of decrease in fruit load, repeating in a continuous cycle throughout the cultivation period, and it is considered that fruit load significantly influences on the shape of flowering dynamics. Fruit load can be assessed as the total fruit volume per plant, and fruit volume can be non-destructively and continuously evaluated based on the fruit dimensions (Hidaka *et al*., 2017). Furthermore, it is also essential to consider the transition between reproductive growth and vegetative growth throughout the cultivation period. Indeed, flowering reflects the transition from vegetative growth to reproductive growth in a life cycle of crops, and it is a crucial trait that significantly influences both fruit yield and quality (Lozano *et al*., 2009; Stewart and Folta, 2010; Xu *et al*., 2012; Agusti *et al*., 2022). thus, it is necessary to also considered the interactions between these factors. Leaf area index (*LAI*) is commonly used as an index of vegetative growth, and in recent years, several methods for measuring *LAI* have been developed [*e.g*., using the spectral analysis of light wavelength transmitting through the canopy (Yamaguchi *et al*., 2023); utilizing image analysis (Nomura *et al*., 2022)]. Therefore, it is believed that these methods allowed me to non-destructively and continuously measure fruit load and vegetative growth dynamics in strawberries as well.

Additionally, in this study, I estimated leaf photosynthetic rate (Figs. 2.3; 2.4; 2.5; 3.6); however, it is conceivable that by gaining a more detailed understanding of vegetative growth, I can extend the estimation of photosynthetic rate to the plant/canopy level, enabling more meaningful analysis in terms of reproductive growth. In fact, Parry *et al*. (2011) suggested a relationship between canopy photosynthesis and crop reproductive growth or yield. Also, Kaneko *et al*. (2022) and Nomura *et al*. (2022) have shown that a hybrid ANN model, combining process-based and empirical models can accurately estimate the photosynthetic rate.

This model can be used to estimate the canopy photosynthetic rate based on environmental factors and *LAI*. By utilizing the mentioned methods and continuously obtaining data on the environment, canopy photosynthesis, fruit load, vegetative growth, and reproductive growth, I believe that not only can I conduct a more detailed analysis of flowering dynamics but also pave the way for modeling flowering dynamics and yield dynamics.

3.5. Conclusion

In this chapter, I obtained daily data on environmental conditions inside the greenhouse, leaf photosynthetic rate, and flowering dynamics of first inflorescence throughout the three cultivation periods of strawberries. Furthermore, I fitted the existing exponential sine equation to characterize the shape of the flowering dynamics in each fruit position, while conducting a detailed analysis of how the history of environment (PPFD, temperature, and *VPD*) and eco-physiological functions (leaf photosynthetic rate) influenced these parameters. As a result, it became evident that each historical record had varying degrees of impact on the flowering dynamics of the first inflorescences and each fruit position. These findings have the potential to contribute to the construction of predictive models for flowering dynamics and would be applied to the development of the yield model when combined with the results from chapter 2.

General conclusion

In this study, for the purpose of constructing a universal and accurate predictive model for the reproductive growth dynamics of strawberry plants, I aimed to elucidate the relationship between various environmental factors and leaf photosynthetic rate with the reproductive growth dynamics.

Firstly, for accurately estimating leaf photosynthetic rate, I investigated the necessity of considering the environmental stresses during photosynthesis estimation by analyzing the diurnal variation of photosynthetic limiting factors (*i.e.*, stomatal conductance, mesophyll conductance, and maximum carboxylation rate). As a result, even under well-watered conditions, it became evident that leaf photosynthetic rate was limited by a decrease in stomatal conductance due to environmental stresses (*e.g.*, strong solar radiation, high temperature, and drought). Also, mesophyll conductance, which has often been disregarded in the past, was highlighted as a potential limiting factor under strong environmental stress. Moreover, it was observed that the stomatal response of strawberry plants to environmental stress was more sensitive compared to the other crops, emphasizing the necessity of considering environmental stresses when estimating leaf photosynthetic rate.

Secondary, using data obtained throughout the cultivation period for various environmental factors (*e.g.*, photosynthetic photon flux density PPFD, temperature, humidity, CO_2 concentration, wind speed), leaf photosynthetic rate, and reproductive growth dynamics (flowering, fruit setting, and harvesting), I investigated the utility of the cumulative photosynthetic rate after flowering as a predictive index for the harvesting date. A model combining photosynthetic biochemical model, stomatal model, leaf gas diffusion model, and leaf thermal balance model was developed. This model incorporated stress coefficient estimated from environmental factors, enabling the long-term continuous estimation of leaf

photosynthetic rate while accounting for environmental stresses. Furthermore, the statistical comparison of various indices (cumulative values from flowering to harvesting of PPFD, temperature, and leaf photosynthetic rate) for individual fruits was conducted to assess their usefulness as harvest prediction indices. The results revealed, for the first time, the utility of the cumulative leaf photosynthetic rate was highest compared to the other indices, contributing valuable insights to the construction of a harvest prediction model.

Finally, the impact of the historical records of each environmental factor and leaf photosynthetic rate on the flowering dynamics, which serve as crucial foundational information for harvest prediction, was analyzed. Flowering dynamics for the first inflorescence obtained over the three cultivation periods were subjected to regression analysis using the Malo model, which combines exponential and sine functions. The analysis involved examining the relationships between the obtained model parameters (*i.e.*, representing the start, end skewness, and kurtosis of the flowering dynamics) and the historical records of environmental factors (PPFD, temperature, and vapor pressure deficit *VPD*) as well as leaf photosynthetic rate. As a result, it was revealed for the first time that PPFD and leaf photosynthetic rate strongly influence the start of flowering, PPFD, leaf photosynthetic rate, and *VPD* influence the end of flowering, temperature and *VPD* influence skewness, and temperature, *VPD*, and photosynthetic rate strongly influence kurtosis. These findings contribute valuable insights to the construction of a predictive model for flowering dynamics.

As described above, this thesis established the foundation for the construction of a predictive model for reproductive growth dynamics in greenhouse-grown strawberries through the acquisition and analysis of extensive and accurate long-term continuous data on environment and eco-physiological functions. I believe my research will contribute to improving strawberry production in the near future.

Acknowledgements

This study was supported by many people. Firstly, I would like to express my sincere gratitude to my advisor Associate Prof. Dr. Daisuke Yasutake (Faculty of Agriculture, Kyushu University) for his invaluable guidance, support, encouragement of this study. I am truly thankful for the time and effort he dedicated, despite his very busy schedule, in writing of the paper, handling the peer review process, and assisting with the preparation of the research proposal. Should I have the opportunity to mentor others in the future, I aspire to become a leader like Associate Prof. Dr. Yasutake.

I would also like to appreciate Prof. Dr. Masaharu Kitano (IoP Collaborative Creation Center, Kochi University) and Prof. Dr. Tomoyoshi Hirota (Faculty of Agriculture, Kyushu University). From Prof. Dr. Kitano, who never allowed for easy deception, I received strict yet affectionate guidance. From Prof. Dr. Hirota, I gained insights into the significance and challenges of extending the results to practical cultivation settings.

I extend my grateful thanks to Assistant Prof. Dr. Gaku Yokoyama (Faculty of Agriculture, Kyushu University), who guided me to a researcher, for his devoted support for gas exchange measurement and meaningful discussions of research. I will never forget the two years when we conducted experiments together, sometimes working from early morning to noon, even three days a week at times. Additionally, the experience of co-authoring a paper as co-first authors was a valuable one.

I also thank Prof. Dr. Tadashige Iwao (IoP Collaborative Creation Center, Kochi University) for his lectures on the program language Python and how analysis the parameter fitting and the flowering dynamics. He generously took the time out of his busy schedule to teach me the skills that I could never have acquired through self-study alone.

I would also like to appreciate Dr. Kota Hidaka (National Agriculture and Food

Research Organization) for providing the plant material every year, discussing about this thesis, and supporting the preparation of the research proposal.

I would also like to appreciate Prof. Dr. Takashi Okayasu and Prof. Dr. Yukio Ozaki (Faculty of Agriculture, Kyushu University) for pleasantly accepting a vice chair of my doctoral thesis.

Furthermore, I would like to express my deepest gratitude to people in Laboratory of Agricultural Meteorology, Kyushu University; namely, Dr. Kensuke Kimura (currently, National Agriculture and Food Research Organization), Dr. Koichi Nomura (currently, IoP Collaborative Creation Center, Kochi University), Dr. Shigehiro Kubota, Mr. Kengo I, Mr. Koichiro Yoshida, Ms. Hiromi Nakai, Mr. Takahiro Keneko, Mr. Yoshiya Teruya, Mr. Hiromu Yamaguchi, Ms. Tomoyo Yanagisawa, and Mr. Asaya Takahashi for their support and discuss in the experiment. Of course, I also thank my other lab mates (too many people to list here) for kindly support.

I deeply thank my friends (especially, the members of Kyushu University Volleyball Team and the homies) for their understanding and support. Finally, I thank my family for their warm support throughout my life in general.

All the experiments in this thesis were financially supported by Grants-in-Aid for Scientific Research (JSPS KAKENHI grant number 22KJ2433) from the Japan Society for the Promotion of Science, JST SPRING, Grant Number JPMJSP2136, and the Advanced Next-Generation Greenhouse Horticulture by IoP (Internet of Plants), Japan.

References

Abd-Elrahman, A., Wu, F., Agehara, S., Britt, K., 2021. Improving strawberry yield prediction by integrating ground-based canopy images in modeling approaches. *ISPRS International Journal of Geo-Information*, 10. https://doi.org/10.3390/ijgi10040239.

Agustí, M., Reig, C., Martínez-Fuentes, A., Mesejo, C., 2022. Advances in citrus flowering: A review. *Frontiers in Plant Science*, 13, 868831. https://doi.org/10.3389/fpls.2022.868831.

Allen, R. G., Pereira, L. S., Raes, D., Smith, M., 1998. FAO Irrigation and drainage Paper No. 56, Rome, Italy.

Ariza, M. T., Soria, C., Martínez-Ferri, E., 2015. Developmental stages of cultivated strawberry flowers in relation to chilling sensitivity. *AoB PLANTS*, 7, 419–431. https://doi.org/10.1093/aobpla/plv012.

Ayari O., Dorais M., Gosselin A., 2000. Daily Variations of photosynthetic efficiency of greenhouse tomato plants during winter and spring. *Journal of the American Society for Horticultural Science*, 125, 235-241. https://doi.org/10.21273/JASHS.125.2.235.

Bakker, J. C., 1989. The effects of air humidity on flowering, fruit set, seed set and fruit growth of glasshouse sweet pepper (*Capsicum annuum* L.). *Scientia Horticulturae*, 40, 1–8. https://doi.org/10.1016/0304-4238(89)90002-2.

Bernacchi, C. J., Singsaas, E. L., Pimentel, C., Portis, A. R., Long, S. P., 2001. Improved temperature response functions for models of Rubisco-limited photosynthesis. *Plant, Cell and Environment*, 24, 253–259. https://doi.org/10.1046/j.1365-3040.2001.00668.x.

Boulard, T., Mermier, M., Fargues, J., Smits, N., Rougier, M., Roy, J. C., 2002. Tomato leaf boundary layer climate: Implications for microbiological whitefly control in greenhouses. *Agricultural and Forest Meteorology*, 110, 159–176. https://doi.org/10.1016/S0168-1923(01)00292-1.

Boyer, J. S., Chin Wong, S., Farquhar, G. D., 1997. CO_2 and water vapor exchange across leaf cuticle (epidermis) at various water potentials. *Plant Physiology*, 114, 185–191. https://doi.org/10.1104/pp.114.1.185.

Buckley, T. N., Martorell, S., Diaz-Espejo, A., Tomàs, M., Medrano, H., 2014. Is stomatal conductance optimized over both time and space in plant crowns? A field test in grapevine (*Vitis vinifera*). *Plant, Cell and Environment*, 37(12), 2707–2721. https://doi.org/10.1111/pce.12343.

Cabrera-Bosquet, L., Fournier, C., Brichet, N., Welcker, C., Suard, B., Tardieu, F., 2016. High-throughput estimation of incident light, light interception and radiation-use efficiency of thousands of plants in a phenotyping platform. *New Phytologist*, 212, 269–281. https://doi.org/10.1111/nph.14027.

Cervantes, L., Ariza, M. T., Gómez-Mora, J. A., Miranda, L., Medina, J. J., Soria, C., Martínez-Ferri, E., 2019. Light exposure affects fruit quality in different strawberry cultivars under field conditions. *Scientia Horticulturae*, 252, 291–297. https://doi.org/10.1016/j.scienta.2019.03.058.

Chen, T. W., Henke, M., De Visser, P. H. B., Buck-Sorlin, G., Wiechers, D., Kahlen, K., Stützel, H., 2014. What is the most prominent factor limiting photosynthesis in different layers of a greenhouse cucumber canopy? *Annals of Botany*, 114, 677–688. https://doi.org/10.1093/aob/mcu100.

Chen, Y., Lee, W. S., Gan, H., Peres, N., Fraisse, C., Zhang, Y., He, Y., 2019. Strawberry yield prediction based on a deep neural network using high-resolution aerial orthoimages. *Remote Sensing*, 11, 1–21. https://doi.org/10.3390/rs11131584

Choi, H. G., Moon, B. Y., Kang, N. J., 2016. Correlation between strawberry (*Fragaria ananassa* Duch.) productivity and photosynthesis-related parameters under various growth conditions. *Frontiers in Plant Science*, 7, 1–13. https://doi.org/10.3389/fpls.2016.01607.

Cui, M., Pham, M. D., Hwang, H., Chun, C., 2021. Flower development and fruit malformation in strawberries after short-term exposure to high or low temperature. *Scientia Horticulturae*, 288, 110308. https://doi.org/10.1016/j.scienta.2021.110308.

De Boeck, H. J., De Groote, T., Nijs, I., 2012. Leaf temperatures in glasshouses and open-top chambers. *New Phytologist*, 194, 1155–1164. https://doi.org/10.1111/j.1469-8137.2012.04117.x.

De Kauwe, M. G., Lin, Y. S., Wright, I. J., Medlyn, B. E., Crous, K. Y., Ellsworth, D. S., Maire, V., Prentice, I. C., Atkin, O. K., Rogers, A., Niinemets, Ü., Serbin, S. P., Meir, P., Uddling, J., Togashi, H. F., Tarvainen, L., Weerasinghe, L. K., Evans, B. J., Ishida, F. Y., Domingues, T. F., 2016. A test of the "one-point method" for estimating maximum carboxylation capacity from field-measured, light-saturated photosynthesis. *New Phytologist*, 210, 1130–1144. https://doi.org/10.1111/nph.13815.

Doan, C. C., Tanaka, M., 2022. Relationships between tomato cluster growth indices and cumulative environmental factors during greenhouse cultivation. *Scientia Horticulturae*, 295, 110803. https://doi.org/10.1016/j.scienta.2021.110803.

Douthe, C., Dreyer, E., Epron, D., Warren, C. R., 2011. Mesophyll conductance to CO_2, assessed from online TDL-AS records of $^{13}CO_2$ discrimination, displays small but significant short-term responses to CO_2 and irradiance in *Eucalyptus* seedlings. *Journal of Experimental Botany*, 62, 5335–5346. https://doi.org/10.1093/jxb/err141.

Düring H., 2003. Stomatal and mesophyll conductances control CO_2 transfer to chloroplasts in leaves of grapevine (*Vitis vinifera* L.). *Vitis*, 42, 65-68.

Duursma, R. A., 2015. Plantecophys - An R package for analysing and modelling leaf gas exchange data. PLoS One, 10, e0143346. https://doi.org/10.1371/journal.pone.0143346.

Edwards, D., Jolliffe, P., Ehret, D., 2010. Canopy profiles of starch and leaf mass per area in greenhouse tomato and the relationship with leaf area and fruit growth. *Scientia Horticulturae*, 125, 637–647. https://doi.org/10.1016/j.scienta.2010.05.019.

Egea, G., González-Real, M. M., Baille, A., Nortes, P. A., Diaz-Espejo, A, 2011. Disentangling the contributions of ontogeny and water stress to photosynthetic limitations in almond trees. *Plant, Cell and Environment*, 34, 962–979. https://doi.org/10.1111/j.1365-3040.2011.02297.x.

Evans J.R., Loreto F., 2000. Acquisition and diffusion of CO_2 in higher plant leaves. – In: Leegood R.C., Sharkey T.D., von Caemmerer S (eds.): Photosynthesis: physiology and metabolism Pp. 321-351. Kluwer Academic Publishers, Dordrecht. https://doi.org/10.1007/0-306-48137-5_14.

Fan, P. G., Li, L. S., Duan, W., Li, W. D., Li, S. H., 2010. Photosynthesis of young apple trees in response to low sink demand under different air temperatures. *Tree Physiology*, 30, 313–325. https://doi.org/10.1093/treephys/tpp114.

Farquhar, G. D., Caemmerer, S., Berry, J. A., 1980. A biochemical model of photosynthetic CO_2 assimilation in leaves of C_3 species. *Planta*, 149, 78–90. http://dx.doi.org/10.1007/BF00386231.

Flexas, J., Díaz-Espejo, A., Berry, J. A., Cifre, J., Galmés, J., Kaldenhoff, R., Medrano, H., Ribas-Carbó, M., 2007a. Analysis of leakage in IRGA's leaf chambers of open gas exchange systems: Quantification and its effects in photosynthesis parameterization. *Journal of Experimental Botany*, 58, 1533–1543. https://doi.org/10.1093/jxb/erm027.

Flexas, J., Diaz-Espejo, A., Galmés, J., Kaldenhoff, R., Medrano, H., Ribas-Carbo, M., 2007b. Rapid variations of mesophyll conductance in response to changes in CO_2 concentration around leaves. *Plant, Cell and Environment*, 30, 1284–1298. https://doi.org/10.1111/j.1365-3040.2007.01700.x.

Flexas, J., Barón, M., Bota, J., Ducruet, J. M., Gallé, A., Galmés, J., Jiménez, M., Pou, A., Ribas-Carbó, M., Sajnani, C., Tomàs, M., Medrano, H., 2009. Photosynthesis limitations during water stress acclimation and recovery in the drought-adapted *Vitis* hybrid Richter-110 (*V. berlandieri*×*V. rupestris*). *Journal of Experimental Botany*, 60, 2361–2377. https://doi.org/10.1093/jxb/erp069.

Galle, A., Florez-Sarasa, I., Tomas, M., Pou, A., Medrano, H., Ribas-Carbo, M., Flexas, J., 2009. The role of mesophyll conductance during water stress and recovery in tobacco (*Nicotiana sylvestris*): Acclimation or limitation? *Journal of Experimental Botany*, 60, 2379–2390. https://doi.org/10.1093/jxb/erp071.

Gates, D. M., 1980. *Biophysical ecology*. Springer Verlag. https://doi.org/10.1007/978-1-4612-6024-0.

Grassi, G., Ripullone, F., Borghetti, M., Raddi, S., Magnani, F., 2009. Contribution of diffusional and non-diffusional limitations to midday depression of photosynthesis in *Arbutus unedo* L. *Trees*, 23, 1149–1161. https://doi.org/10.1007/s00468-009-0355-7.

Grassi, G., Magnani, F., 2005. Stomatal, mesophyll conductance and biochemical limitations to photosynthesis as affected by drought and leaf ontogeny in ash and oak trees. *Plant, Cell and Environment*, 28, 834–849. https://doi.org/10.1111/j.1365-3040.2005.01333.x.

Harley, P. C., Loreto, F., Marco, G. Di, Sharkey, T. D., 1992. Theoretical considerations when estimating the mesophyll conductance to CO_2 flux by analysis of the response of photosynthesis to CO_2. *Plant Physiology*, 98, 1429–1436. https://doi.org/10.1104/pp.98.4.1429.

He, J., Austin, P. T., Nichols, M. A., Lee, S. K., 2007. Elevated root-zone CO_2 protects lettuce plants from midday depression of photosynthesis. *Environmental and Experimental Botany*, 61, 94–101. https://doi.org/10.1016/j.envexpbot.2007.04.001.

Hernandez-Santana, V., Perez-Arcoiza, A., Gomez-Jimenez, M. C., Diaz-Espejo, A., 2021. Disentangling the link between leaf photosynthesis and turgor in fruit growth. *Plant Journal*, 107, 1788–1801. https://doi.org/10.1111/tpj.15418.

Hidaka, K., Dan, K., Imamura, H. Miyoshi, Y., Takayama, T., Sameshima, K., Kitano, M., Okimura, M., 2013. Effect of supplemental lighting from different light sources on growth and yield of strawberry. *Environmental Control in Biology*, 51, 41–47. http://doi.org/10.2525/ecb.51.41.

Hidaka, K., Okamoto, A., Araki, T., Miyoshi, Y., Dan, K., Imamura, H., Kitano, M., Sameshima, K., Okimura, M., 2014. Effect of photoperiod of supplemental lighting with light-emitting diodes on growth and yield of strawberry. *Environmental Control in Biology*, 52, 63–71. https://doi.org/10.2525/ecb.52.63.

Hidaka, K., Dan, K., Miyoshi, Y., Imamura, H., Takayama, T., Kitano, M., Sameshima, K., Okimura, M., 2016. Twofold increase in strawberry productivity by integration of environmental control and movable beds in a large-scale greenhouse. *Environmental Control in Biology*, 54, 79–92. https://doi.org/10.2525/ecb.54.79.

Hidaka, K., Miyoshi, Y., Okamoto, A., Dan, K., Imamura, H., Takayama, T., Yasutake, D., Kitano, M., 2017. Effect of fruit gas exchange on photosynthate accumulation and fruit growth of strawberries. *Acta Horticulturae*, 1156, 509–515. https://doi.org/10.17660/ActaHortic.2017.1156.76.

Hidaka, K., Miyoshi, Y., Ishii, S., Suzui, N., Yin, Y. G., Kurita, K., Nagao, K., Araki, T., Yasutake, D., Kitano, M., Kawachi, N., 2019. Dynamic analysis of photosynthate translocation into strawberry fruits using non-invasive ^{11}C-labeling supported with conventional destructive measurements using ^{13}C-labeling. *Frontiers in Plant Science*, 9, 1–12. https://doi.org/10.3389/fpls.2018.01946.

Hidaka, K., Nakahara, S., Yasutake, D., Zhang, Y., Okayasu, T., Dan, K., Kitano, M., Sone, K., 2022. Crop-local CO_2 enrichment improves strawberry yield and fuel use efficiency in protected cultivations. *Scientia Horticulturae*, 301, 111104. https://doi.org/10.1016/j.scienta.2022.111104.

Hu, M. J., Guo, Y. P., Shen, Y. G., Guo, D. P., Li, D. Y., 2009. Midday depression of photosynthesis and effects of mist spray in citrus. *Annals of Applied Biology*, 154, 143–155. https://doi.org/10.1111/j.1744-7348.2008.00282.x.

Iwao, T., Kitano, M., Nomura, K., Saito, M., Tada, I., Yamazaki, T., 2023. [Utilization of AI in the IoP (Internet of Plants) and challenges] IoP (Internet of Plants) deno AI riyou to kadai ni tuite (in Japanese). *Proceedings of Annual Meeting of Society of Agricultural Meteorology of Japan 2023 (SAMJ2023)*, 52.

Jensen, N. L., Jensen, C. R., Liu, F., Petersen, K. K., 2009. Water relations and abscisic acid in pot-grown strawberry plants under limited irrigation. *Journal of the American Society for Horticultural Science*, 134, 574–580. https://doi.org/10.21273/jashs.134.5.574.

Jones, H. G., 1985. Partitioning stomatal and non-stomatal limitations to photosynthesis. *Plant, Cell and Environment*, 8, 95–104. https://doi.org/10.1111/j.1365-3040.1985.tb01227.x.

Kaneko, T., Nomura, K., Yasutake, D., Iwao, T., Okayasu, T., Ozaki, Y., Mori, M., Hirota, T., Kitano, M., 2022. A canopy photosynthesis model based on a highly generalizable artificial neural network incorporated with a mechanistic understanding of single-leaf photosynthesis. *Agricultural and Forest Meteorology*, 323, 109036. https://doi.org/10.1016/j.agrformet.2022.109036.

Kawanobu, S., Waiima, T., Zushi, K., Mori, T., Matsuzoe, N., 2010. Seasonal variations in the maturation period, anthocyanin content, and ascorbic acid content in strawberry fruits. *Environmental Control in Biology*, 48, 175–184. https://doi.org/10.2525/ecb.48.175.

Khoshnevisan, B., Rafiee, S., Mousazadeh, H., 2014. Application of multi-layer adaptive neuro-fuzzy inference system for estimation of greenhouse strawberry yield. *Measurement*, 47, 903–910. https://doi.org/10.1016/j.measurement.2013.10.018.

Kimura, K., Yasutake, D., Nakazono, K., Kitano, M., 2017. Dynamic distribution of thermal effects of an oscillating frost protective fan in a tea field. *Biosystems Engineering*, 164, 98–109. https://doi.org/10.1016/j.biosystemseng.2017.09.010.

Kimura, K., Yasutake, D., Yamanami, A., Kitano, M., 2020a. Spatial examination of leaf-boundary-layer conductance using artificial leaves for assessment of light airflow within a plant canopy under different controlled greenhouse conditions. *Agricultural and Forest Meteorology*, 280, 107773. https://doi.org/10.1016/j.agrformet.2019.107773.

Kimura, K., Yasutake, D., Koikawa, K., Kitano, M., 2020b. Spatiotemporal variability of leaf photosynthesis and its linkage with microclimates across an environment-controlled greenhouse. *Biosystems Engineering*, 195, 97–115. https://doi.org/10.1016/j.biosystemseng.2020.05.003.

Kimura, K., Yasutake, D., Koikawa, K., Kitano, M., 2022. Spatiotemporally variable incident light, leaf photosynthesis, and yield across a greenhouse: fine-scale hemispherical photography and a photosynthesis model. *Precision Agriculture*. https://doi.org/10.1007/s11119-022-09933-z.

Kitaya, Y., Tsuruyama, J., Shibuya, T., Yoshida, M., Kiyota, M., 2003. Effects of air current speed on gas exchange in plant leaves and plant canopies. *Advances in Space Research*, 31, 177–182. https://doi.org/10.1016/S0273-1177(02)00747-0.

Klamkowski, K., Treder, W., 2006. Morphological and physiological responses of strawberry plants to water stress. *Agriculturae Conspectus Scientificus*, 71, 159–165.

Kobayasi, K., Matsui, T., Yoshimoto, M., Hasegawa, T., 2009. Effects of temperature, solar radiation, and vapor-pressure deficit on flower opening time in rice. *Plant Production Science*, 13, 21–28. https://doi.org/10.1626/pps.13.21.

Konsin, M., Voipio, I., Palonen, P., 2001. Influence of photoperiod and duration of short-day treatment on vegetative growth and flowering of strawberry (*Fragaria* × *ananassa* Duch). *The Journal of Horticultural Science and Biotechnology*, 76, 77–82. https://doi.org/10.1080/14620316.2001.11511330.

Krüger, E., Josuttis, M., Nestby, R., Toldam-Andersen, T. B., Carlen, C., Mezzetti, B., 2012. Influence of growing conditions at different latitudes of Europe on strawberry growth performance, yield and quality. *Journal of Berry Research*, 2, 143–157. https://doi.org/10.3233/JBR-2012-036.

Laisk, A., Loreto, F., 1996. Determining photosynthetic parameters from leaf CO_2 exchange and chlorophyll fluorescence: ribulose-1,5-bisphosphate carboxylase/oxygenase specificity factor, dark respiration in the light, excitation distribution between photosystems, alternative electron transport rate, and mesophyll diffusion resistance. *Plant Physiology*, 110, 903–912. https://doi.org/10.1104/pp.110.3.903.

Ledesma, N. A., Nakata, M., Sugiyama, N., 2008. Effect of high temperature stress on the reproductive growth of strawberry cvs. “Nyoho” and “Toyonoka”. *Scientia Horticulturae*, 116, 186–193. https://doi.org/10.1016/j.scienta.2007.12.010.

Ledesma, N. A., Kawabata, S., 2016. Responses of two strawberry cultivars to severe high temperature stress at different flower development stages. *Scientia Horticulturae*, 211, 319–327. https://doi.org/10.1016/j.scienta.2016.09.007.

Legard, D. E., Xiao, C. L., Mertely, J. C., Chandler, C. K., 2000. Effects of plant spacing and cultivar on incidence of Botrytis fruit rot in annual strawberry. *Plant Disease*, 84, 531–538. https://doi.org/10.1094/PDIS.2000.84.5.531.

Leuning, R., Kelliher, F. M., De Pury, D. G. G., Schulze, E. D., 1995. Leaf nitrogen, photosynthesis, conductance and transpiration: Scaling from leaves to canopies. *Plant, Cell & Environment*, 18, 1183–1200. https://doi.org/10.1111/j.1365-3040.1995.tb00628.x.

Lobell, D. B., Cahill, K. N., Field, C. B. 2006. Weather-based yield forecasts developed for 12 California crops. *California Agriculture*, 60, 211–215. https://doi.org/10.3733/ca.v060n04p211.

Long, S. P., Zhu, X. G., Naidu, S. L., Ort, D. R., 2006. Can improvement in photosynthesis increase crop yields? *Plant, Cell and Environment*, 29, 315–330. https://doi.org/10.1111/j.1365-3040.2005.01493.x.

López, A., Valera, D. L., Molina-Aiz, F. D., Peña, A., 2012. Sonic anemometry to evaluate airflow characteristics and temperature distribution in empty Mediterranean greenhouses equipped with pad-fan and fog systems. *Biosystems Engineering*, 113, 334–350. https://doi.org/10.1016/j.biosystemseng.2012.09.006.

Lozano, R., Giménez, E., Cara, B., Capel, J., Angosto, T., 2009. Genetic analysis of reproductive development in tomato. *International Journal of Developmental Biology*, 53, 1635–1648. https://doi.org/10.1387/ijdb.072440rl.

Lu, N., Nukaya, T., Kamimura, T., Zhang, D., Kurimoto, I., Takagaki, M., Maruo, T., Kozai, T., Yamori, W., 2015. Control of vapor pressure deficit (VPD) in greenhouse enhanced tomato growth and productivity during the winter season. *Scientia Horticulturae*, 197, 17–23. https://doi.org/10.1016/j.scienta.2015.11.001.

Lu, T., Meng, Z., Zhang, G., Qi, M., Sun, Z., Liu, Y., Li, T., 2017. Sub-high temperature and high light intensity induced irreversible inhibition on photosynthesis system of tomato plant (*Solanum lycopersicum* L.). *Frontiers in Plant Science*, 8, 1–16. https://doi.org/10.3389/fpls.2017.00365.

MacKenzie, S. J., Chandler, C. K., 2009. A method to predict weekly strawberry fruit yields from extended season production systems. *Agronomy Journal*, 101, 278–287. https://doi.org/10.2134/agronj2008.0208.

Malo, J. E., 2002. Modelling unimodal flowering phenology with exponential sine equations. *Functional Ecology,* 16, 413–418. https://doi.org/10.1046/j.1365-2435.2002.00629.x.

Márquez D. A., Stuart-Williams H., Farquhar G. D., 2021. An improved theory for calculating leaf gas exchange more precisely accounting for small fluxes. *Nature Plants*, 7, 317-326. https://doi.org/10.1038/s41477-021-00861-w.

Mavi, H. S., Tupper, G. J., 2004. *Agrometeorology: Principles and applications of climate studies in agriculture.* Food Products Press. https://doi.org/10.1201/9781482277999.

Medlyn, B. E., Duursma, R. A., Eamus, D., Ellsworth, D. S., Prentice, I. C., Barton, C. V. M., Crous, K. Y., De Angelis, P., Freeman, M., Wingate, L., 2011. Reconciling the optimal and empirical approaches to modelling stomatal conductance. *Global Change Biology*, 17, 2134–2144. https://doi.org/10.1111/j.1365-2486.2010.02375.x.

Menzel, C. M., 2021. A review of productivity in strawberries: marketable yield has a linear, but inconsistent relationship with total yield, and cannot be predicted from total yield. *The Journal of Horticultural Science and Biotechnology*, 96, 135–144. https://doi.org/10.1080/14620316.2020.1808086.

Miyoshi, Y., Hidaka, K., Okayasu, T., Yasutake, D., Kitano, M., 2017. Effects of local CO_2 enrichment on strawberry cultivation during the winter season. *Environmental Control in Biology*, 55, 165–170. https://doi.org/10.2525/ecb.55.165.

Miyoshi, Y., Hidaka, K., Yin, Y.-G., Suzui, N., Kurita, K., Kawachi, N., 2021. Non-invasive ^{11}C-Imaging revealed the spatiotemporal variability in the translocation of photosynthates into strawberry fruits in response to increasing daylight integrals at leaf surface. *Frontiers in Plant Science*, 12. https://doi.org/10.3389/fpls.2021.688887.

Muir, C. D., 2019. Tealeaves: An R package for modelling leaf temperature using energy budgets. *AoB Plants*, 11, 1–10. https://doi.org/10.1093/aobpla/plz054.

Muraoka, H., Tang, Y., Terashima, I., Koizumi, H., Washitani, I., 2000. Contributions of diffusional limitation, photoinhibition and photorespiration to midday depression of photosynthesis in *Arisaema heterophyllum* in natural high light. *Plant, Cell and Environment*, 23, 235–250. https://doi.org/10.1046/j.1365-3040.2000.00547.x.

Nakai, H., Yasutake, D., Kimura, K., I, K., Hidaka, K., Eguchi, T., Hirota, T., Okayasu, T., Ozaki, Y., Kitano, M., 2022. Dynamics of carbon export from leaves as translocation affected by the coordination of carbohydrate availability in field strawberry. *Environmental and Experimental Botany*, 196, 104806. https://doi.org/10.1016/j.envexpbot.2022.104806.

Neri, D., Baruzzi, G., Massetani, F., Faedi, W., 2012. Strawberry production in forced and protected culture in Europe as a response to climate change. *Canadian Journal of Plant Science*, 92, 1021–1036. https://doi.org/10.4141/CJPS2011-276.

Nomura, K., Yasutake, D., Kaneko, T., Takada, A., Okayasu, T., Ozaki, Y., Mori, M., Kitano, M., 2021. Long-term compound interest effect of CO_2 enrichment on the carbon balance and growth of a leafy vegetable canopy. *Scientia Horticulturae*, 283, 110060. https://doi.org/10.1016/j.scienta.2021.110060.

Nomura, K., Saito, M., Kitayama, M., Goto, Y., Nagao, K., Yamasaki, H., Iwao, T., Yamazaki, T., Tada, I., Kitano, M., 2022. Leaf area index estimation of a row-planted eggplant canopy using wide-angle time-lapse photography divided according to view-zenith-angle contours. *Agricultural and Forest Meteorology*, 319, 108930. https://doi.org/10.1016/j.agrformet.2022.108930.

Nomura, K., Kaneko, T., Iwao, T., Kitayama, M., Goto, Y., Kitano, M., 2023. Hybrid AI model for estimating the canopy photosynthesis of eggplants. *Photosynthesis Research*, 155, 77–92. https://doi.org/10.1007/s11120-022-00974-z.

Ono, S., Yasutake, D., Yokoyama, G., Teruya, Y., Hidaka, K., Okayasu, T., Nomura, K., Kitano, M., 2022. Closed chamber system for easily measuring the respiration rate of intact fruits. *Environment Control in Biology*, 60, 33–37. https://doi.org/10.2525/ecb.60.33.

Ono, S., Yasutake, D., Kimura, K., Kengo, I., Teruya, Y., Hidaka, K., Yokoyama, G., Hirota, T., Kitano, M., Ozaki, Y. 2023. Effect of microclimate and photosynthesis on strawberry reproductive growth in a greenhouse : using cumulative leaf photosynthesis as an index to predict the time of harvest. *The Journal of Horticultural Science and Biotechnology*, 1–10. https://doi.org/10.1080/14620316.2023.2254759.

Opstad, N., Sønsteby, A., Myrheim, U., Heide, O. M., 2011. Seasonal timing of floral initiation in strawberry: Effects of cultivar and geographic location. *Scientia Horticulturae*, 129, 127–134. https://doi.org/10.1016/j.scienta.2011.03.022.

Parry, M. A. J., Reynolds, M., Salvucci, M. E., Raines, C., Andralojc, P. J., Zhu, X. G., Price, G. D., Condon, A. G., Furbank, R. T., 2011. Raising yield potential of wheat. II. Increasing photosynthetic capacity and efficiency. *Journal of Experimental Botany*, 62, 453–467. https://doi.org/10.1093/jxb/erq304.

Pathak, T. B., Dara, S. K., Biscaro, A., 2016. Evaluating correlations and development of meteorology based yield forecasting model for strawberry. *Advances in Meteorology*, 2016, 9525204. https://doi.org/10.1155/2016/9525204.

Pelletier, V., Pepin, S., Gallichand, J., Caron, J., 2016. Reducing cranberry heat stress and midday depression with evaporative cooling. *Scientia Horticulturae*, 198, 445–453. https://doi.org/10.1016/j.scienta.2015.12.028.

Pons, T. L., Flexas, J., Von Caemmerer, S., Evans, J. R., Genty, B., Ribas-Carbo, M., Brugnoli, E., 2009. Estimating mesophyll conductance to CO_2: methodology, potential errors, and recommendations. *Journal of Experimental Botany*, 60, 2217–2234. https://doi.org/10.1093/jxb/erp081.

Pope, K. S., Da Silva, D., Brown, P. H., DeJong, T. M. 2014. A biologically based approach to modeling spring phenology in temperate deciduous trees. *Agricultural and Forest Meteorology*, 198–199, 15–23. https://doi.org/10.1016/j.agrformet.2014.07.009.

Raschke, K., Resemann, A., 1986. The midday depression of CO_2 assimilation in leaves of *Arbutus unedo* L.: diurnal changes in photosynthetic capacity related to changes in temperature and humidity. *Planta*, 168, 546–558. https://doi.org/10.1007/BF00392275.

Rho H., Yu D. J., Kim S. J., Chun C., Lee H. J., 2011. Estimation of carboxylation efficiency from net CO_2 assimilation rate as a function of chloroplastic CO_2 concentration in strawberry (*Fragaria* × *ananassa* cv. Maehyang) leaves. *Horticulture, Environment, and Biotechnology*, 52, 547–552. https://doi.org/10.1007/s13580-011-0035-6.

Robinson, J. C., Bower, J. P., 1988. Transpiration from banana leaves in the subtropics in response to diurnal and seasonal factors and high evaporative demand. *Scientia Horticulturae*, 37, 129–143. https://doi.org/10.1016/0304-4238(88)90156-2.

Rodrigues, W. P., Silva, J. R., Ferreira, L. S., Machado Filho, J. A., Figueiredo, F. A., Ferraz, T. M., Bernado, W. P., Bezerra, L. B., de Abreu, D. P., Cespom, L., 2018. Stomatal and photochemical limitations of photosynthesis in coffee (*Coffea* spp.) plants subjected to elevated temperatures. *Crop and Pasture Science*. 69, 317–325. https://doi.org/10.1071/CP17044.

Roessler, P. G., & Monson, R. K. (1985). Midday depression in net photosynthesis and stomatal conductance in Yucca glauca. *Oecologia*, 67, 380–387. https://doi.org/10.1007/bf00384944.

Sack, L., Cowan, P. D., Jaikumar, N., Holbrook, N. M., 2003. The "hydrology" of leaves: co-ordination of structure and function in temperate woody species. *Plant, Cell and Environment*, 26, 1343–1356. https://doi.org/10.1046/j.0016-8025.2003.01058.x.

Samtani, J. B., Rom, C. R., Friedrich, H., Fennimore, S. A., Finn, C. E., Petran, A., Wallace, R. W., Pritts, M. P., Fernandez, G., Chase, C. A., Kubota, C., Bergefurd, B., 2019. The status and future of the strawberry industry in the United States. *HortTechnology*, 29, 11–24. https://doi.org/10.21273/horttech04135-18.

Sarabi, B., Fresneau, C., Ghaderi, N., Bolandnazar, S., Streb, P., Badeck, F. W., Citerne, S., Tangama, M., David, A., Ghashghaie, J., 2019. Stomatal and non-stomatal limitations are responsible in down-regulation of photosynthesis in melon plants grown under the saline condition: Application of carbon isotope discrimination as a reliable proxy. *Plant Physiology and Biochemistry*, 141, 1–19. https://doi.org/10.1016/j.plaphy.2019.05.010.

Song, X., Zhou, G., He, Q., Zhou, H., 2020. Stomatal limitations to photosynthesis and their critical Water conditions in different growth stages of maize under water stress. *Agricultural Water Management*, 241. https://doi.org/10.1016/j.agwat.2020.106330.

Sønsteby, A., Solhaug, K. A., Heide, O. M., 2016. Functional growth analysis of 'Sonata' strawberry plants grown under controlled temperature and daylength conditions. *Scientia Horticulturae*, 211, 26–33. https://doi.org/10.1016/j.scienta.2016.08.003.

Sperling, O., Kamai, T., Tixier, A., Davidson, A., Jarvis-Shean, K., Raveh, E., DeJong, T. M., Zwieniecki, M. A., 2019. Predicting bloom dates by temperature mediated kinetics of carbohydrate metabolism in deciduous trees. *Agricultural and Forest Meteorology*, 276–277, 107643. https://doi.org/10.1016/j.agrformet.2019.107643.

Stewart, P. J., Folta, K. M., 2010. A review of photoperiodic flowering research in strawberry (*Fragaria spp.*). *Critical Reviews in Plant Sciences*, 29, 1–13. https://doi.org/10.1080/07352680903436259.

Syvertsen J.P., 1982. Minimum leaf water potential and stomatal and stomatal closure in citrus leaves of different ages. *Annals of Botany*, 49, 827-834. https://doi.org/10.1093/oxfordjournals.aob.a086309.

Szymańska, R., Ślesak, I., Orzechowska, A., Kruk, J., 2017. Physiological and biochemical responses to high light and temperature stress in plants. *Environmental and Experimental Botany*, 139, 165–177. https://doi.org/10.1016/j.envexpbot.2017.05.002.

Twitchen, C., Else, M. A., Hadley, P., 2021. The effect of temperature and light intensity on rate of strawberry fruit ripening. *Acta Horticulturae*, 1309, 643–648. https://doi.org/10.17660/ActaHortic.2021.1309.92.

Varone, L., Ribas-Carbo, M., Cardona, C., Gallé, A., Medrano, H., Gratani, L., Flexas, J., 2012. Stomatal and non-stomatal limitations to photosynthesis in seedlings and saplings of Mediterranean species pre-conditioned and aged in nurseries: Different response to water stress. *Environmental and Experimental Botany*, 75, 235–247. https://doi.org/10.1016/j.envexpbot.2011.07.007.

Villar, R., Held, A. A., Merino, J., 1995. Dark leaf respiration in light and darkness of an evergreen and a deciduous plant species. *Plant Physiology*, 107, 421–427. https://doi.org/10.1104/pp.107.2.421.

von Caemmerer, S., Evans, J. R., 2015. Temperature responses of mesophyll conductance differ greatly between species. *Plant, Cell and Environment*, 38, 629–637. https://doi.org/10.1111/pce.12449.

Wang, R., Eguchi, M., Gui, Y., Iwasaki, Y., 2020. Evaluating the effect of light intensity on flower development uniformity in strawberry (*Fragaria ×ananassa*) under early induction conditions in forcing culture. *HortScience*, 55, 670–675. https://doi.org/10.21273/HORTSCI14917-20.

Wankmüller, F. J. P., Carminati, A., 2022. Stomatal regulation prevents plants from critical water potentials during drought: Result of a model linking soil–plant hydraulics to abscisic acid dynamics. *Ecohydrology*, 15, 1–15. https://doi.org/10.1002/eco.2386.

West, D. W., Gaff, D. F., 1976. The effect of leaf water potential, leaf temperature and light intensity on leaf diffusion resistance and the transpiration of leaves of *Malus sylvestris*. *Physiologia Plantarum*, 38, 98–104. https://doi.org/10.1111/j.1399-3054.1976.tb04866.x.

Wilson, K. B., Baldocchi, D. D., Hanson, P. J., 2000. Quantifying stomatal and non-stomatal limitations to carbon assimilation resulting from leaf aging and drought in mature deciduous tree species. *Tree Physiology*, 20, 787–797. https://doi.org/10.1093/treephys/20.12.787.

Wu, F., Guan, Z., Whitaker, V. 2015. Optimizing yield distribution under biological and economic constraints: Florida strawberries as a model for perishable commodities. *Agricultural Systems*, 141, 113–120. https://doi.org/10.1016/j.agsy.2015.10.002.

Xiong, D., Liu, X., Liu, L., Douthe, C., Li, Y., Peng, S., Huang, J., 2015. Rapid responses of mesophyll conductance to changes of CO_2 concentration, temperature and irradiance are affected by N supplements in rice. *Plant, Cell and Environment*, 38, 2541–2550. https://doi.org/10.1111/pce.12558.

Xiong, D., Douthe, C., Flexas, J., 2017. Differential coordination of stomatal conductance, mesophyll conductance, and leaf hydraulic conductance in response to changing light across species. *Plant, Cell and Environment*, 41, 436–450. https://doi.org/10.1111/pce.13111.

Xu, J., Liu, Y., Liu, J., Cao, M., Wang, J., Lan, H., Xu, Y., Lu, Y., Pan, G., Rong, T., 2012. The genetic architecture of flowering time and photoperiod sensitivity in maize as revealed by QTL review and meta analysis. *Journal of Integrative Plant Biology*, 54 358–373. https://doi.org/10.1111/j.1744-7909.2012.01128.x.

Yamaguchi, H., Yasutake, D., Hirota, T., Nomura, K., 2023. Nondestructive measurement method of leaf area index using near-infrared radiation and photosynthetically active radiation transmitted through a leafy vegetable canopy. *HortScience*, 58, 16–22. https://doi.org/10.21273/HORTSCI16761-22.

Yokoyama, G., Ono, S., Yasutake, D., Hidaka, K., Hirota, T., 2023. Diurnal changes in the stomatal, mesophyll, and biochemical limitations of photosynthesis in well-watered greenhouse-grown strawberries. *Photosynthetica*, 61, 12–23. https://doi.org/10.32615/ps.2023.001.

Yoneda, A., Yasutake, D., Hidaka, K., Muztahidin, N. I., Miyoshi, Y., Kitano, M., Okayasu, T., 2020. Effects of supplemental lighting during the period of rapid fruit development on the growth, yield, and energy use efficiency in strawberry plant production. *International Agrophysics*, 34, 233–239. https://doi.org/10.31545/INTAGR/117623.

Yuan, X. K., Yang, Z. Q., Li, Y. X., Liu, Q., Han, W., 2016. Effects of different levels of water stress on leaf photosynthetic characteristics and antioxidant enzyme activities of greenhouse tomato. *Photosynthetica*, 54, 28–39. https://doi.org/10.1007/s11099-015-0122-5.

Zhang, D., Zhang, Z., Li, J., Chang, Y., Du, Q., Pan, T., 2015. Regulation of vapor pressure deficit by greenhouse micro-fog systems improved growth and productivity of tomato via enhancing photosynthesis during summer season. *PLoS One*, 10, e0133919. https://doi.org/10.1371/journal.pone.0133919.

Zhang, Y., Henke, M., Buck-Sorlin, G. H., Li, Y., Xu, H., Liu, X., Li, T., 2021. Estimating canopy leaf physiology of tomato plants grown in a solar greenhouse: Evidence from simulations of light and thermal microclimate using a Functional-Structural Plant Model. *Agricultural and Forest Meteorology*, 307, 108494. https://doi.org/10.1016/j.agrformet.2021.108494.

Zhu, K., Yuan, F. H., Wang, A. Z., Wu, J. B., Guan, D. X., Jin, C. J., Flexas, J., Gong, C. J., Zhang, H. X., Zhang, Y. S., 2021. Stomatal, mesophyll and biochemical limitations to soil drought and rewatering in relation to intrinsic water-use efficiency in Manchurian ash and Mongolian oak. *Photosynthetica*, 59, 49–60. https://doi.org/10.32615/ps.2020.084.